A Metabolomics-Based Analysis of Acyl-Homoserine Lactone Quorum Sensing in Pseudomonas aeruginosa

Peter William Davenport

Downing College

University of Cambridge

December 2017

This dissertation is submitted for the degree of Doctor of Philosophy

Summary

A Metabolomics-Based Analysis of Acyl-Homoserine Lactone Quorum Sensing in *Pseudomonas aeruginosa*

Peter William Davenport

Pseudomonas aeruginosa is a metabolically versatile environmental bacterium that grows in extremely diverse habitats—from sea water to jet fuel—and is able to infect a large variety of organisms. It is a significant cause of human disease and is one of the most frequent healthcare-associated infections. *P. aeruginosa* uses a sophisticated gene regulatory network to adapt its growth strategy to these diverse environmental niches and the fluctuating conditions it encounters therein. The *las* and *rhl* "quorum sensing" (QS) intercellular communication systems play integral roles in this regulatory network and control the expression of factors important to the bacterium's ecological fitness, including many secreted factors involved in nutrient acquisition, microbial competition, and virulence. These QS systems use diffusible acyl-homoserine lactone (AHL) signalling molecules to infer environmental parameters, including bacterial population density, and to coordinate behaviour across bacterial communities.

This dissertation describes an investigation into the relationship between QS and small molecule primary metabolism, using metabolomic methods based on nuclear magnetic resonance spectroscopy and mass spectrometry. Analysis of extracellular metabolic profiles (the bacteria's "metabolic footprint") established that QS can modulate the uptake and excretion of primary metabolites and that this effect was strongest during the transition from exponential to stationary phase cell growth. Analysis of the cellular metabolome and proteome demonstrated that QS affected most major branches of primary metabolism, notably central carbon metabolism, amino acid metabolism and fatty acid metabolism. These data indicate that QS repressed acetogenesis and the oxidative $C0_2$-evolving portion of the TCA cycle, while inducing the glyoxylate bypass and arginine fermentation. QS also induced changes to fatty acid pools associated with lower membrane fluidity and higher chemical stability. Elevated levels of stress-associated polyamines were detected in QS mutants, which may be a consequence of a lack of QS-dependent adaptations. These findings suggest that wild-type QS directs metabolic adaptations to stationary phase stressors, including oxidative stress.

Previous work, including several transcriptomic studies, has suggested that QS can play a role in primary metabolism. However, there has been no previous study of the global impact of AHL QS on the metabolome of *P. aeruginosa*. Research presented here demonstrates that QS induces a global readjustment in the primary metabolism and provides insight into QS-dependent metabolic changes during stationary-phase adaptation.

To my parents

Acknowledgements

First and foremost, I would like to express my gratitude to **Martin Welch** for supervision and encouragement throughout the project. I would also like to thank **Jules Griffin** for supervision and advice, particularly in regard to metabolomic and statistical methodology. My thanks also go to past and present members of the **Welch Laboratory, Griffin Laboratory**, **Salmond Laboratory** and the **Cambridge Centre for Proteomics** (CCP) for all their help and advice, as well as being welcoming, supportive and fun to work with. Thank you to the **BBSRC** for funding the project and to **Downing College**, the **SGM** and the **Cambridge Philosophical Society** for travel grants.

Special thanks to the following people: **Mahon Maguire** and **Reza Salek** for advice and training in NMR spectroscopy; **Oliver Jones**, **Christopher Titman**, **Claire Waterman** and **Helen Atherton** for advice and introduction to GC-MS analysis; **Baljit Ubhi** for fun collaboration and discussion regarding LC-MS analysis; **Kathryn Lilley** and **Svenja Hester** for advice and support regarding proteomic analyses; **Denis Rubtsov** for helpful discussion of statistical methods. Thank you to my **family** and **friends** for their advice, care and support throughout my doctoral training: in particular, **my parents John and Pauline**, **Alan Neal**, my grandmother **Hannah Livesey**, my siblings **Rupert** and **Isobel**, **David Belin**, and **Hilary Fabich** for loving encouragement and inspiration.

Contents

List of Tables

List of Figures

Chapter 1

Introduction

1.1 Pseudomonas aeruginosa

1.1.1 General background and characteristics

Pseudomonas aeruginosa is a Gram-negative bacillus with unipolar motility, about 1-5 μm long and 0.5-1.0 μm wide. It is the type species of the *Pseudomonas* genus and is a member of the fluorescent pseudomonad subgenus, which includes *P. fluorescens*, *P. putida*, *P. chlororaphis*, *P. aureofaciens*, *P. cichorii* and *P. syringae*. The name *Pseudomonas* was given by Walter Migula of the Karlsruhe Institute in Germany at the end of the 19th Century, and seems to have been derived from the Greek *pseudo* ("false") and either *monas* ("unit") or the nanoflagellate *Monas*, i.e. false unit *or* false *Monas* (Migula 1900; Palleroni 2010). The name *aeruginosa* (Latin—"full of verdigris") was given to the species earlier by the German biologist Joseph Schröter in reference to the blue-green colour of colonies grown on certain media. Schröter noted that these colonies could be propagated to form new colonies of the same colour and hence of the same bacteria, a key step in the development of Robert Koch's pure-culture techniques (Schröter 1872). *P. aeruginosa* has subsequently attracted research interest for production of coloured dyes, as a source of antimicrobials, its environmental and metabolic versatility, as a human pathogen, and as a model organism in fields including bacterial antibiotic resistance, biofilm formation and bacterial intercellular signalling.

P. aeruginosa is one of the most prevalent inhabitants of oligotrophic—that is, low nutrient content— aquatic ecosystems and as such is likely among the most abundant organisms on Earth. *P. aeruginosa* has low nutrient requirements—it can survive in deionized or distilled water—but is also successful in high nutrient environments such as sewage. Its optimal growth temperature in rich growth media is 37˚C, but grows at temperatures up to 42˚C. Although it is principally considered a soil and water bacterium it is one of most versatile bacteria in terms of its range of habitats, having been isolated from environments as diverse as plant rhizospheres, dolphin gastric juice, disinfectant solutions and jet plane fuel

(Costerton and Anwar 1994; Grosso-Becerra et al. 2014). Important to its persistence in natural and artificial environments as well as chronic infections is its ability to form biofilms—communities of bacteria encased in complex polysaccharides, rendering the bacteria resistant to removal by mechanical means, detergents, disinfectants, antibiotics, disinfectants, immune response or predation by protozoa. It is able to infect a wide variety of host organisms including nematodes, insects, many vertebrate species and plants (Mahajan-Miklos et al. 2000).

1.1.2 Genomic complexity and metabolic versatility

The first complete *P. aeruginosa* genome to be sequenced was that of the wound isolate strain PAO1, published in 2000 (Stover et al. 2000). This revealed a 6.3 Mbp circular chromosome encoding ~5,570 predicted coding sequences, large for a bacteria and similar in coding capacity to that of simple eukaryotes such as *Saccharomyces cerevisiae* (Kulasekara and Lory 2004). Almost 10% of genes appear to encode regulatory functions including 24 sigma factors, 434 transcriptional regulators and many environmental sensors, an unusually high proportion compared with other bacteria (cf. ~5.8% in *E. coli*, 5.3% in *B. subtilis*). This includes a remarkable number of two-component system (TCS) proteins comprised of 55 sensor-kinases, 89 response regulators and 14 sensor-response regulator hybrids (cf. 39 response regulators in *E. coli* K-12) (Stover et al. 2000; Ashby 2004). A disproportionate 150 genes are predicted to encode Outer Membrane Proteins, including factors involved in environmental sensing, adhesion, motility, antibiotic efflux and secretion of virulence factors. Almost 300 genes encode cytoplasmic membrane transport systems, of which around two thirds are predicted to be involved in uptake of nutrients and other small molecules. These features reflect the remarkable ability of *P. aeruginosa* to adapt to diverse environmental and nutritional challenges.

The genome also contains a large number of genes involved in the catabolism and transport of organic compounds. *P. aeruginosa* possesses a highly branched respiratory chain with at least 17 respiratory dehydrogenases predicted to feed electrons into the quinone pool and five terminal oxidases. The differing properties of these terminal oxidases, such as their affinity for oxygen and resistance to stresses like cyanide and reactive oxygen species presumably allow aerobic respiration to be adapted to various oxygen concentrations and environmental stresses (Arai 2011). The bacterium also possesses a complete denitrification pathway, allowing growth under anaerobic conditions in the presence of nitrate or nitrite (Zumft 1997). In the absence of both molecular oxygen and nitrogen

oxides, *P. aeruginosa* can still grow—slowly—by anaerobic fermentation of arginine to ornithine through the arginine deiminase pathway (Lüthi et al. 1990). *P. aeruginos*a appears to be microaerophilic as it actively generates a microaerobic environment in response to high aeration by forming a polysaccharide cell capsule and by reducing the oxygen transfer rate to the liquid phase via the production of biosurfactants such as rhamnolipids (Sabra et al. 2002).

Advances in DNA sequencing technologies since 2000 have led to the complete genomes of over 80 clinical and environmental *P. aeruginosa* isolates being published via the Pseudomonas Genome Database (Winsor et al. 2009). Genome sizes vary between 5.5 and 7.5 Mbp. The core genome of *P. aeruginosa* is defined as those genes present in nearly all strains, irrespective of origin (environmental or clinical isolates) and constitutes ~90% of the total genome of PAO1. The core genome is highly conserved relative to those of other bacterial pathogens such as *Escherichia coli* and other *Pseudomonas* species, with interclonal sequence diversity of 0.5–0.7% (Kung et al. 2010; Klockgether et al. 2011; Grosso-Becerra et al. 2014). The core genome includes the vast majority of known virulence factors: approximately 97% of known virulence factors were found to be conserved in a study of 18 strains (Wolfgang et al. 2003). Moreover, it appears that clinically-isolated strains do not constitute a distinct subpopulation of *P. aeruginosa* and that environmental isolates of diverse origins can be pathogenic (Grosso-Becerra et al. 2014). This again underscores the adaptability of this bacterium.

1.1.3 Human disease

Although *P. aeruginosa* has been noted to infect humans since the 19th century, these were considered rare cases and its importance as a major cause of disease was not recognised until the mid-20th century (Botzenhart and Döring 1993). It is still principally considered a saprophyte—growing on dead or decaying matter—though it has come to be regarded as a consummate and common opportunistic pathogen. That is, though it frequently colonises healthy individuals, it typically only causes disease in the immunocompromised. In humans, it can colonise virtually any mucosal surface and invade most tissues. It is carried by a relatively small proportion of the healthy human population (2–10%), but 50–60% of hospitalised patients are colonised (Cholley et al. 2008).

The major forms of *P. aeruginosa* infection are i) bacteraemia in immunocompromised patients, ii) pneumonia in cystic fibrosis (CF) patients, iii) community-acquired ear and pneumonia infections, and iv) hospital outbreaks associated with contaminated reagents or

medical devices (Fujitani et al. 2011). Although *P. aeruginosa* rarely infects healthy tissue, there are few tissues that it cannot infect if host defences are compromised by immune deficiency (immunosuppression, neutropenia), or the breach of a physical barrier to infection (skin, mucous membrane). It is one of the most common healthcare associated infections (HAIs). Using data collected in the USA between 2011 and 2104, the US Centers for Disease Control and Prevention (CDC) found that *P. aeruginosa* was the second most frequently reported pathogen for ventilator-associated pneumonia (16.5%), third for catheter-associated urinary tract infection (10.5%) and sixth across all HAIs (7.3% of all reports) (Weiner et al. 2016). People at particular risk from *P. aeruginosa* infection include those with cystic fibrosis (CF), acquired immune deficiency syndrome (AIDS; 50% mortality attributable to *P. aeruginosa* infection), severe burns (60% attributable mortality), neutropenic cancer patients (30% attributable mortality), and patients with medical implants (38% attributable mortality for ventilator-associated pneumonia in intubated patients) (Mendelson et al. 1994; Laing 1999; Gales et al. 2001). *P. aeruginosa* may account for an increasing disease burden in coming years as vulnerable populations expand: for example aging populations are at greater risk of infection due to higher rates of co-morbidities such as diabetes mellitus and structural lung disease, the presence of invasive medical devices and age-related decline in immune function (Pappas et al. 2009).

The capacity of *P. aeruginosa* to infect diverse organisms and cause such a range of diseases is coupled to its arsenal of virulence factors; these include proteinaceous virulence factors such as elastase, exotoxin A and haemolytic phospholipase C (all secreted *via* type I or II secretion systems), which facilitate *P. aeruginosa* epithelial invasion by breaking down the epithelial glycocalyx (a protective layer of glycoproteins) and plasma membranes, the cytotoxic proteins ExoY, ExoS, ExoT and ExoU, which upon cell contact are injected directly into the host cell cytoplasm via the syringe-like type III secretion system, and small molecule secondary metabolites such as hydrogen cyanide and pyocyanin, which play pleiotropic roles in pathogenesis (e.g. pyocyanin has been reported to depress host immune response and induce apoptosis in neutrophils). In fact, it has been reported that 267 genes (approximately 5% of the genome) encode known or putative virulence factor products (Gallagher and Manoil 2001). Expression of these virulence factors is typically not constitutive, but rather controlled by a complex gene regulatory network and induced in response to environmental cues including iron availability and bacterial cell-density.

1.2 Quorum sensing

1.2.1 Discovery and the archetypal system

Many bacterial species synthesise signalling molecules whose accumulation in the environment is detected by specific cell-associated protein receptors; since the signal-producing cells are themselves signal receivers, these signals have been dubbed "autoinducers". In reference to the concept that these processes are only productive when performed by a sufficiently large number of spatially localised cells, describing such a ``minimal behavioural unit as a quorum of bacteria'', Fuqua et al. introduced the term quorum sensing (QS) to describe the role of autoinducer signalling in cell density-responsive regulation (Fuqua et al. 1994).

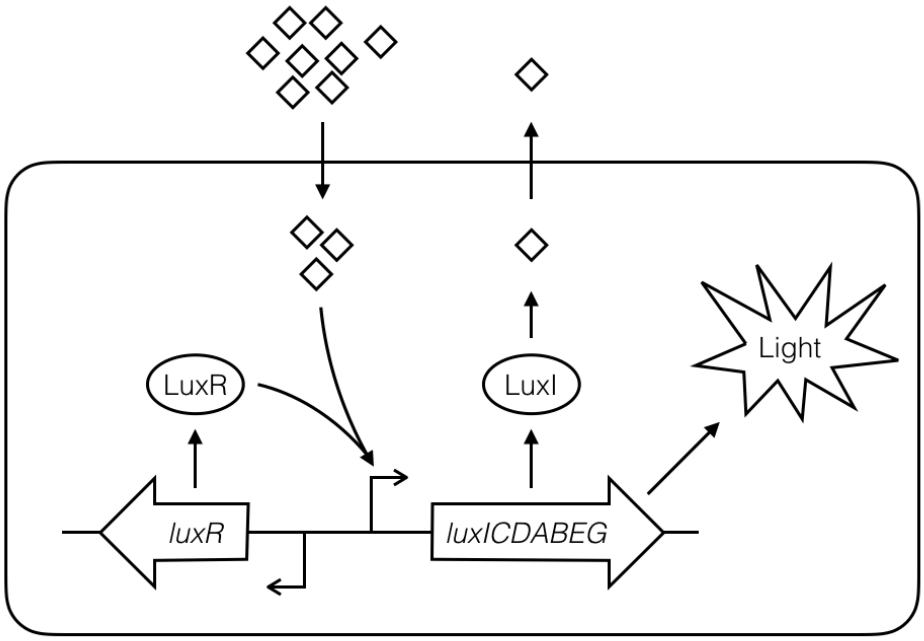

Figure 1.1 The *Vibrio fischeri* LuxI/LuxR QS system.

3OC6-HSL (diamonds) is produced by the enzymatic activity of the LuxI signal synthase. 3OC6-HSL can diffuse across the cell membranes. At high cell densities, binding of 3OC6-HSL to LuxR induces transcription of the *luxICDABEG* operon, forming a positive feedback loop and leading to chemiluminescence.

The first QS system described is the archetypal LuxI/LuxR system of the bioluminescent marine bacterium *Vibrio fischeri* (Nealson et al. 1970; Eberhard 1972). *V. fischeri* exists as a free-living saprophyte, a commensal in the guts of marine mammals and as a mutualistic symbiont in the light organs of squid and fish species; it is in this last niche that the

LuxI/LuxR system performs the archetypal quorum sensing function, linking bioluminescence to bacterial cell density. The best-characterised *V. fischeri* bioluminescent symbiosis is that with the Hawaiian bobtail squid, *Euprymna scolopes*. This provides a captivating illustration of AHL-signalling coordinating the behaviour of bacteria with their eukaryotic host. *E. scolopes* is a small nocturnal predator (weighing up to 2.7 g) that hunts in shallow reef flats. The squid use sophisticated light organ apparatus—including reflective tissue, a lens, yellow filters and an ink-sac shutter mechanism—to direct and manipulate the light produced by *V. fischeri* to match falling moon and starlight, thereby masking their silhouettes from predators below (Montgomery and McFall-Ngai 1998; Jones and Nishiguchi 2004). The bacteria seem to benefit from an advantageous growth environment in the light organ, which provides amino acids and proteins to the bacteria (Graf and Ruby 1998).

Key to this symbiosis is the ability of the bacteria to control their bioluminescence as a function of their population density. Each dawn, the squid vent their light organs of >95% of their *V. fischeri* monocultures (Lee and Ruby 1994); the remaining *V. fischeri* population then recovers to high numbers over the course of the day (approximately 10^7 to 10^8 in an adult's light organ). The constitutively expressed autoinducer synthase LuxI catalyses the formation of *N*-(3-oxohexanoyl)-L-homoserine lactone (3OC6-HSL) from *N*-3-oxohexanoyl-ACP (acyl carrier protein) and *S*-adenosylmethionine (SAM) (Schaefer et al. 1996; Val and Cronan 1998); these AHLs diffuse freely across the cell membranes, so that extra- and intracellular concentrations equilibrate (Kaplan and Greenberg 1985). Hence, as the *V. fischeri* population expands over the course of the day, the increasing *V. fischeri* population density in the squid light organ is mirrored by increasing concentrations of AHL. At dusk, the concentration of AHL exceeds a threshold concentration such that their specific binding to the *V. fischeri* cytoplasmic LuxR receptor protein, induces its binding to a specific palindromic recognition sequence (*lux* box) in the *luxICDABEG* luciferase operon, activating transcription and initiating bioluminescence (Figure 1.1). Since this induced operon includes *luxI*, a positive feedback loop is formed. Such positive feedback synchronises QS activity across bacterial populations and is a hallmark of QS regulatory networks. In addition to population density, the *lux* system responds to multiple additional variables including nutritional cues and the signal mass transfer properties in the light organ. Nonetheless, by linking bioluminescence to AHL concentration, this archetypal QS system enables the bacteria to avoid committing metabolic resources to futile light production during daylight hours.

As in many other bacteria, *V. fischeri* has a second AHL signalling system, comprised of the AI synthase AinS and the receptor protein LuxN. The *ainS/luxN* system is activated at lower cell densities than the *luxIR* system and is required for host colonisation, apparently by regulating phenotypes such as motility as *V. fischeri* reaches deeper into the light organ crypt tissues. In addition to downregulating expression of flagella, AinS/LuxN autoinduction also regulates a number of genes with metabolic functions, such as folate metabolism, histidine metabolism, polysaccharide biosynthesis and iron acquisition, suggesting that these may be important for successful colonisation (Lupp and Ruby 2005). The two signal systems are linked by the transcriptional regulator LitR, which is activated by LuxN:AHL and is required for LuxIR signalling. This network architecture enables the sequential regulation of a number of phenotypes at different stages of colonisation.

Since the discovery of the *lux* system of *V. fischeri*, QS systems using several distinct signals have been identified in a large number of bacteria. For example, while quorum sensing in almost all Gram-negative bacteria is mediated by AHL systems analogous the *V. fischeri* LuxI/LuxR system, Gram-positive bacteria use autoinducer peptides (AIPs) (Waters and Bassler 2005). *P. aeruginosa* produces two AHL signals, *N*-3-oxododecanoyl-L-homoserine lactone (3OC12-HSL, or OdDHL) and *N*-butanoyl-L-homoserine lactone (C4-HSL, or BHL) (Figure 1.2).

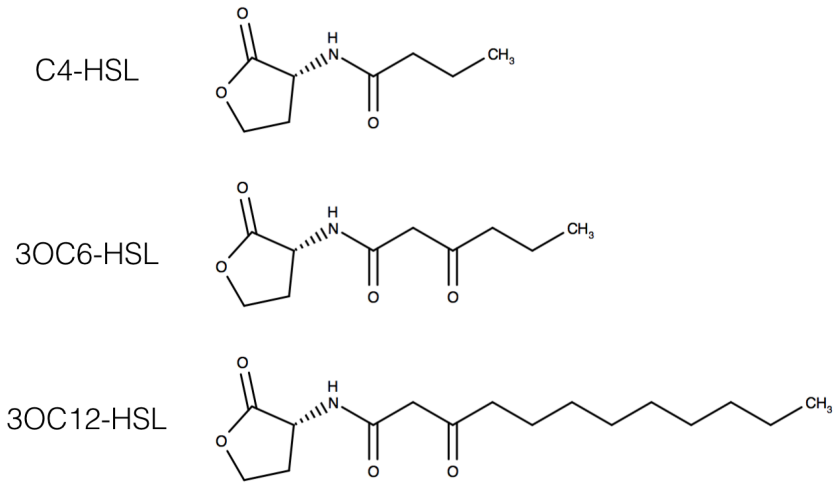

Figure 1.2 AHL quorum sensing signals produced by *Vibrio fischeri* (3OC6-HSL) and *Pseudomonas aeruginosa* (C4-HSL and 3OC12-HSL).

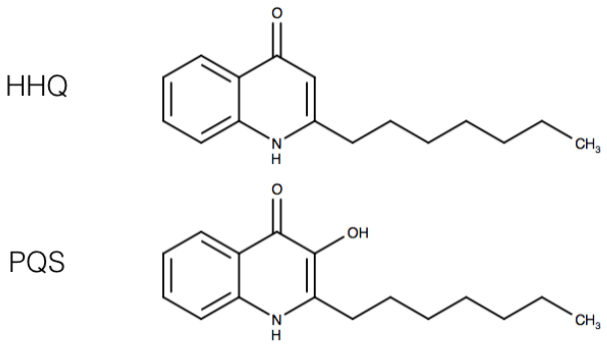

Figure 1.3 Quinolone autoinducers produced by *P. aeruginosa*.

The 2-alkyl-4-quinolone (AQ) signal molecules 2-heptyl-3-hydroxy-4-quinolone (PQS) and 2-heptyl-4-quinolone (HHQ).

1.2.2 Interconnected QS systems in *P. aeruginosa*

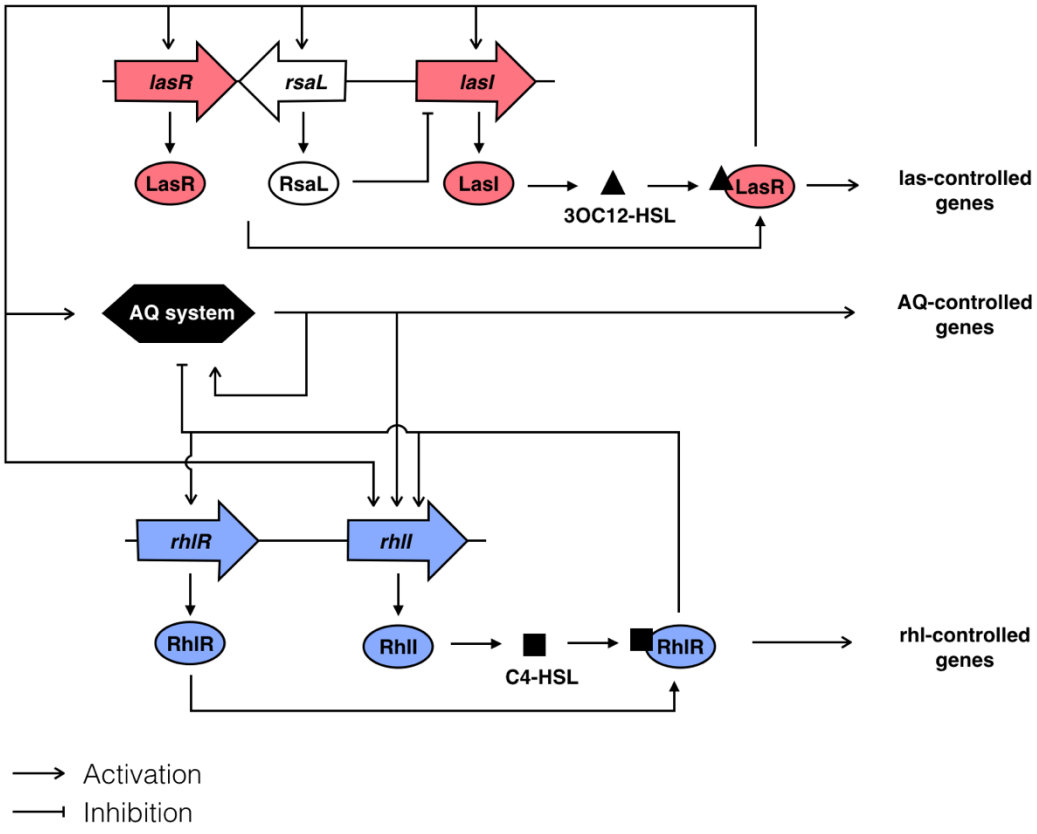

Figure 1.4 *P. aeruginosa* AHL- and AQ-dependent QS regulatory circuits.

The quorum sensing circuitry of *P. aeruginosa* has been subject to intensive study over the past three decades. Two complete classical *N*-acyl-homoserine lactone (AHL) quorum sensing systems have been described, *lasR-lasI* and *rhlI-rhlR*. The *las* system consists of the AHL synthase LasI, which generates *N*-3-oxo-L-dodecanoyl-homoserine lactone (3OC12-

HSL, or OdDHL), and the signal receptor LasR, which binds 3OC12-HSL (Gambello and Iglewski 1991; Passador et al. 1993; Pearson et al. 1994). The *rhl* system consists of the AHL synthase RhlI, which produces *N*-butanoyl-L-homoserine lactone (C4-HSL, or BHL), and the signal receptor RhlR, which binds C4-HSL (Ochsner et al. 1994; Ochsner and Reiser 1995; Pearson et al. 1995). The R-proteins form transcriptional activator complexes upon binding their cognate signal molecules; these activate transcription through the binding of ~20 bp palindromic DNA sequences upstream of target genes known as *las* or *rhl* boxes (Whiteley and Greenberg 2001). Importantly, the R-proteins show high specificity for their cognate ligands: LasR is not activated by C4-HSL and 3OC12-HSL only activates RhlR to low levels (Pearson et al. 1997). In addition to the LasR and RhlR signal receptors, the orphan receptor QscR responds to 3OC12-HSL and regulates its own set of genes in addition to repressing many *las*- and *rhl*-regulated genes (Lee et al. 2006; Lequette et al. 2006).

This picture of AHL-mediated QS in *P. aeruginosa* is further complicated by a third QS system, the PQS system based on 2-alkyl-4-quinolones (AQs) (Diggle et al. 2007). *Pseudomonas aeruginosa* produces over fifty different AQs, though the best studied for their signalling function are the 2-heptyl-3-hydroxy-4-quinolone (*Pseudomonas* quinolone signal, PQS) and 4-hydroxy-2-heptyl-quinoline (HHQ) (Déziel et al. 2004; Lépine et al. 2004) (Figure 1.3). Synthesis of PQS proceeds from anthranilate, which is converted by the *pqsABCD* gene products to 4-hydroxy-2-heptyl-quinoline (HHQ), the immediate precursor of PQS (Déziel et al. 2004). HHQ is exported from the cell and is taken up by adjacent bacterial cells where it is converted to PQS by PqsH. PQS regulates its own production by driving the expression of *pqsABCDE* via PqsR (MvfR) and that of other target genes via PqsE (Déziel et al. 2004; Diggle et al. 2006; Hazan et al. 2010). PqsE also represses expression of the *pqsABCDE* operon, forming a negative feedback loop (Rampioni et al. 2010).

As per the *V. fischeri lux* system, at low cell density autoinducers are synthesized at basal levels and diffuse into the extracellular space; as population cell density increases the autoinducer concentration rises and, above a critical threshold, the formation of R-protein:signal-molecule complexes activates target gene expression. The core QS circuits are modulated by a plethora of additional regulatory factors, for example at low cell densities AHL synthesis is repressed by the QS negative regulators RsmA and QscR. Negative feedback loops balance positive feedback mechanisms at high cell densities, for example the *las* system induces expression of RsaL, which represses its own expression and that of LasI (Rampioni et al. 2007).

The regulatory networks of the three QS systems are highly interconnected: the *las* system sits atop the regulatory hierarchy and regulates both the *rhl* and PQS systems, the *rhl* system regulates the PQS system, and the PQS system in turn can regulate the *rhl* system (Figure 1.4). This leads to a degree of co-dependence, for example expression of RhlR-controlled genes is delayed in a *lasR* mutant, however each system can also be independently activated, for example activation of the *rhl* and PQS systems is delayed rather that fully abrogated in a *lasR* mutant (Dekimpe and Déziel 2009). The presence of three QS systems seems to enable finely tuned gene expression responses to complex environmental cues. This is illustrated by the dense connections between the QS circuitry and a complex global regulatory network involving the sigma factors RpoS and RpoN, the global regulators GacA, DksA, MvaT and Vfr, as well as the LuxR-type regulators QscR and VqsR (Juhas et al. 2005; Schuster and Peter Greenberg 2006). These add context-dependence to the QS regulons, for example growth phase and nutrient availability have important co-regulatory roles and QS signals alone are insufficient for expression of some QS-regulated genes (Diggle et al. 2002; Schuster et al. 2003).

1.2.3 *P. aeruginosa* AHL QS regulons and their global regulatory context

Both the *las* and *rhl* systems were discovered via screens for regulators of secreted virulence factors. LasR was identified in a screen of positive regulators of extracellular elastase activity conferred by expression of LasB, a metalloprotease with broad substrate specificity including elastin, collagen, immunoglobins, transferrin and complement components (Gambello and Iglewski 1991). Similarly, the RhlR gene was identified by genetic complementation of a strain deficient in expression of rhamnolipids, rhamnose-containing glycolipid biosurfactants with roles in motility, biofilm architecture, antimicrobial defence against predators and lysis of eukaryotic immune cells (Ochsner et al. 1994; Cosson et al. 2002; Boles et al. 2005; Soberón-Chávez et al. 2005; Jensen et al. 2007; Alhede et al. 2009). Subsequent research revealed that the *las* system was responsible for upregulating expression of a range of virulence factors in addition to elastase, including LasA protease, alkaline protease and exotoxin A (Toder et al. 1991; Gambello et al. 1993). Similarly, the *rhl* system was found to upregulate an overlapping but distinct set of factors including elastase, alkaline protease, the stationary sigma factor RpoS and secondary metabolites pyocyanin and cyanide (Brint and Ohman 1995; Winson et al. 1995; Latifi et al. 1996).

The development of high-density DNA microarray techniques facilitated more comprehensive analyses of AHL regulation: in 2003, three groups used this approach to assess AHL-dependent gene regulation in a *lasI rhlI* mutant (Hentzer et al. 2003; Schuster et al. 2003; Wagner et al. 2003). Schuster et al., 2003 and Wagner et al., 2003 each found that over 300 genes responded to AHLs, while Hentzer et al. 2003 identified 163 genes, using more stringent criteria and different growth conditions. Only 102, or about 20% of these AHL-regulated genes were modulated in all three studies and comprise what has been called a "general" or "core" AHL QS regulon (Schuster and Peter Greenberg 2006). The most prevalent functional class in this core QS regulon is secreted factors, consistent with earlier studies. However, 80% of the core regulon gene functions were assigned to other classes including a substantial (~20%) fraction with primary metabolic functions, indicating that AHL QS induces broader physiological changes than previously understood. The dependence of the QS regulon on growth conditions is consistent with studies demonstrating that the core QS circuits are embedded within a larger network of regulators that integrates and responds to multiple environmental signals (Schuster and Peter Greenberg 2006; Coggan and Wolfgang 2012; Balasubramanian et al. 2013). Key regulators with direct regulatory links with QS include Vfr, RelA, RpoS and the GacAS/RsmAZ system (Figure 1.5).

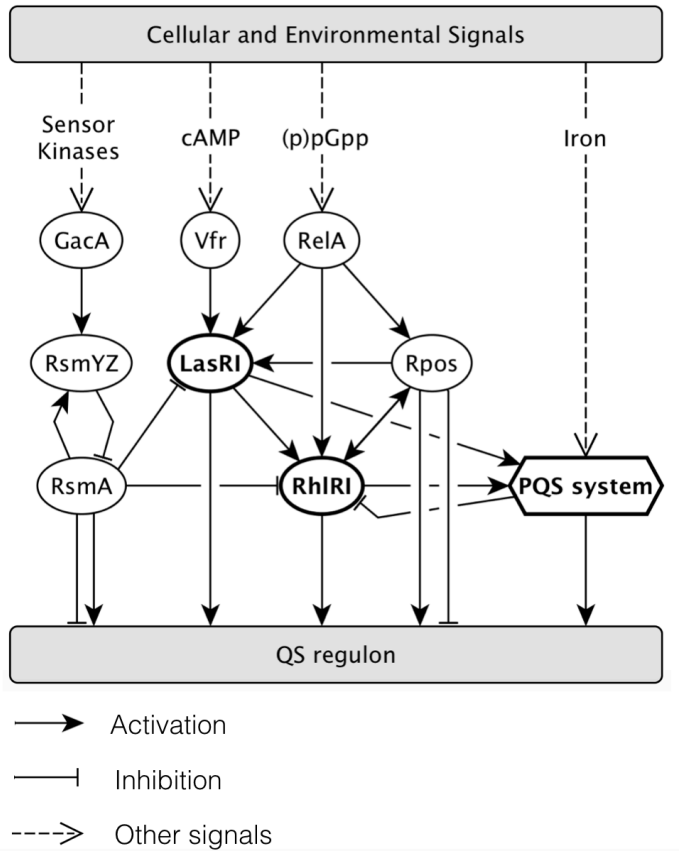

Figure 1.5 Regulatory context of *P. aeruginosa* QS systems—a simplified schematic.

One of the mechanisms by which *P. aeruginosa* senses environmental cues is via so-called two-component systems (TCS). The GacSA proteins comprise one such system that controls a switch between phenotypes associated with acute and chronic infection, including virulence factors, secondary metabolites and biofilm formation (Coggan and Wolfgang 2012). Phosphorylated GacA upregulates the transcription of the small regulatory RNAs RsmY and RsmZ, which bind and sequester the regulatory protein RsmA (Heurlier et al. 2004; Kay et al. 2006; Brencic et al. 2009). RsmA represses AHL QS, while inducing factors such as type III secretion and type IV pili formation (Pessi et al. 2001). RsmA also regulate several QS controlled factors including synthesis of hydrogen cyanide, pyocyanin and rhamnolipids. Several host-associated environmental cues—including host-cell contact, low calcium and chemoattractants such as phosphatidylethanolamine—result in elevated levels of the alarmone cAMP in *P. aeruginosa*, mediated in part by activation of CyaB adenylate cyclase by the Chp chemosensory system. This information is fed into the QS regulon via the CRP (cyclic AMP receptor protein) homologue Vfr (virulence factor regulator), which induces LasR transcription in response to elevated levels of cAMP via a CRP-binding sequence in the *lasR* promoter region (Albus et al. 1997; Wolfgang et al. 2003). Vfr induces cAMP-dependent expression of a number of virulence factors including flagella

(involved in motility and attachment to host cells), and type II and III secretion systems (responsible for delivery of virulence factors to host cells).

Stress response signals feed into the QS regulatory network via the RelA-mediated stringent response and the stationary phase sigma factor and general stress response regulator, RpoS. RelA catalyses the synthesis of the alarmone guanosine 3',5'-bispyrophosphate (ppGpp) in response to amino acid starvation or depletion of energy-sources and induces AHL production as well as expression of LasR, RhlR and RpoS (Van Delden et al. 2001). In *E. coli*, RpoS is important in regulating responses to heat shock, nutrient limitation, osmotic pressure and oxidative stress (Loewen et al. 1998). The role of RpoS in *P. aeruginosa* is less clear but seems to be comparable: disruption of the *P. aeruginosa* PAO1 *rpoS* gene increases stationary phase sensitivity of the bacterium to heat stress, acid stress, osmotic stress, oxidative stress and organic solvents (Jørgensen et al. 1999; Suh et al. 1999). The RpoS regulon in *P. aeruginosa* also includes many genes not obviously involved in stress responses, such as genes involved in chemotaxis (Schuster et al. 2004*b*). The QS and RpoS systems tune each other's activities; RpoS upregulates expression of LasR and RhlR, and the *rhl* system in turn induces expression of RpoS (Latifi et al. 1996; Whiteley et al. 2000; Schuster et al. 2004*b*). This interconnection is illustrated by the observation that the RpoS regulon includes 40% of the AHL QS core regulon, many genes of which appear to be directly regulated by RpoS (Schuster et al. 2004*b*).

The PQS system plays a complex role in this network, serving both as an intercellular signalling system in its own right and also responding directly to iron availability, a major regulator of virulence. AQs, including PQS, regulate multiple virulence factors and genes involved in iron acquisition, including pyoverdine and pyochelin. PQS itself chelates and its activity is modified by Iron(III) (Bredenbruch et al. 2006; Diggle et al. 2007; Hazan et al. 2010).

1.2.4 Metabolic strategies and evolutionary stability

The preponderance of virulence factors amongst *las*- and *rhl*-regulated genes in early studies indicated that these AHL QS systems are global regulators of virulence. This lead to the proposal that regulation of virulence traits by QS could enable communities of *P. aeruginosa* to mount a concerted attack on a host in response to bacterial population density or other environmental or nutritional cues (Passador et al. 1993). The intercellular communication and positive feedback mechanisms of QS would synchronise behaviour, thereby avoiding the premature triggering of a strong host immune response until

conditions favour a coordinated switch to virulence. The importance of AHL QS to *P. aeruginosa* virulence has been demonstrated in a number of animal models, in which QS mutants are attenuated in their virulence (Smith and Iglewski 2003). However, QS systems are frequently inactivated by mutation in *P. aeruginosa* isolates from chronic infections and other environments, demonstrating that QS is an unstable trait in some contexts (Cabrol et al. 2003; Dénervaud et al. 2004; Salunkhe et al. 2005; Heurlier et al. 2006).

Although bacterial population density is a key variable determining the state of QS systems—evoked by the term *quorum*—such signalling occurs in diverse and sometimes complex environments in which other variables, such as mass transfer rates, can play significant or even dominant roles. This was highlighted by (Redfield 2002), who proposed that QS systems may serve to assess the rate at which secreted molecules move away from the producing cell—"Diffusion Sensing" DS—and not necessarily serve any social or cooperative function. In the DS hypothesis, AHL concentrations serve as proxies for the fates of more metabolically expensive exoproducts, such as secreted enzymes, whose concentrations are determined by similar environmental parameters. Both QS and DS models are supported by empirical evidence and different parameters likely dominate in different physical environments (West et al. 2012).

QS controls the production of both "public" goods (i.e. secreted factors that provide benefits to a local neighbourhood of cells) and "private" goods (i.e. "non-shared" cellular factors of benefit only to the producing cell). The benefit of such public goods often increases with cell density and QS allows bacteria to tune gene expression accordingly (Darch et al. 2012; Pai et al. 2012). However, co-operative individuals can be vulnerable to competitive exploitation by non-co-operative 'cheats' that reap the rewards of public goods without contributing to their costs. Thus under conditions requiring quorum sensing induction of extracellular proteases for growth, QS "signal-blind" cheater mutants—typically lacking LasR function—have a competitive advantage over wild-type cells (Sandoz et al. 2007). Nonetheless, correlation between signal concentration and cheater frequency means that QS can stabilise co-operative production of public goods in mixed populations of co-operators and cheats, by allowing individuals to display "general reciprocity", that is to "co-operate when surrounded by co-operators" (Pfeiffer et al. 2005; Allen et al. 2016; Bruger and Waters 2016).

The cost of producing public goods is a function of the specific nutritional context and the AHL QS regulatory network integrates such information when coordinating metabolic strategies. Under growth-rate limiting concentrations of macronutrients, expression of

AHL-controlled extracellular enzymes and secondary metabolites is unrelated to cell density and instead depends on whether the limiting nutrient is a building block of the secreted products, a strategy termed "metabolic prudence" (Xavier et al. 2011; Mellbye and Schuster 2014).

The evolutionary stability of co-operativity is also influenced by QS regulation of private goods. Growth on adenosine requires LasR-dependent expression of the cytoplasmic enzyme nucleoside hydrolase gene (*nuh*) (Heurlier et al. 2005). Mutants in *lasR* are rapidly eliminated from adenosine-enriched medium when co-cultured with wild-type bacteria, i.e. QS regulation of a private good penalizes the appearance of "social cheats" (Dandekar et al. 2012).

There is growing evidence that AHL QS may coordinate a variety of additional metabolic strategies, including stress responses. Working with Burkholderia spp., Goo et al. 2012 showed that QS-dependent production of excreted oxalate counteracts ammonia-mediated alkaline toxicity and is required for stationary phase survival (Goo et al. 2012). One interpretation of these findings is that QS regulation allows the bacterium to "anticipate" stationary phase alkaline toxicity. Similarly, AHL QS acts as a "metabolic brake" in the rice pathogen *Burkholderia glumae*, down-regulating glucose uptake, substrate level and oxidative phosphorylation, and *de novo* nucleotide biosynthesis as the bacterial population density increases (An et al. 2014). It is argued that this QS-regulated slowing may serve to maintain metabolic homeostasis under crowded conditions.

1.3 Metabolomics and analysis of metabolic perturbations

Metabolomics refers to the measurement of the complement of small molecule metabolites (the metabolome) of an organism, tissue, cell or biofluid, in a broad and comprehensive way (Oldiges and Takors 2005). Metabolism is context dependent: data from metabolomics experiments can be used to characterize the impact of changes in a biological system (e.g. a gene mutation in a metabolic pathway) and its environment (e.g. the available carbon source) upon the concentrations and fluxes of metabolites.

1.3.1 Considerations regarding sampling protocols

The protocols used for sampling cell cultures can have a large impact on metabolomic investigations. Two key aspects of the sampling process must be addressed in order to ensure that measured metabolite concentrations are representative of in vivo metabolism: i) metabolic reactions should be arrested—"quenched"—efficiently, ii) metabolites should be extracted efficiently, with minimal bias and leakage from the cell. Quenching/extraction protocols may include addition of solvents, acids, application of high temperatures to denature enzymes, or cold temperatures to slow chemical reactions. Hot and cold quenching can both result in artifacts including cellular leakage, however cold quenching with isotonic saline and a single wash step has been found to result in low contamination from the supernatant and minimal leakage of metabolites from the cell (Bolten et al. 2007). The duration of the sampling protocol is also an important factor: the turnover rate of metabolites inside a cell—approximately equal to the concentration of the metabolite divided by the flux through the pathway of which it is a member—can be less than 1 second, even for metabolites present in mM concentrations; wash steps are often used to reduce the contamination of cellular fractions with extracellular metabolites but come at the cost of additional processing time and so increased risk that metabolite concentrations will depart from in vivo levels through metabolic turnover and cellular leakage. Of the many possible extraction methods, methanol-cholorform extraction is a common choice because it results in i) high recovery of a wide range of metabolites in either the aqueous or organic phases, ii) high efficiency in inactivating enzymes, thereby minimising interconversion of metabolites, iii) low rates of degradation of metabolites (cf extraction methods using high temperature or extremes of pH) (Belle et al. 2002; Maharjan and Ferenci 2003; Canelas et al. 2009).

1.3.2 The extracellular metabolome

Microorganisms secrete a large number of metabolites into their environment: these include products of primary (e.g. uracil and xanthine, alcohols from fermentation) and secondary metabolism (e.g. *P. aeruginosa* secretes phenazine, lipid and amino acid secondary metabolites). These activities are a reflection of (intra-) cellular metabolism. In contrast to intracellular metabolites, secreted metabolites are diluted in the extracellular space, where the concentrations of metabolic enzymes are also much lower: the turnover rates of secreted metabolites are therefore lower and so can be accurately measured without the added complications of quenching metabolism. This approach, by which

samples of culture media are analysed by a metabolomic technique, is termed metabolic footprinting (Kell et al. 2005). Such methods have demonstrated that the extracellular (or exo-) metabolome, in reflecting metabolite uptake from and secretion into the extracellular space, can be used to investigate perturbations to metabolism; this approach has been used to classify single-gene yeast mutants, investigate tryptophan metabolism in *E. coli*, discriminate between the modes of action of antifungal compounds and examine metabolic adaptations of *P. aeruginosa* CF lung isolates (Allen et al. 2003, 2004; Kaderbhai et al. 2003; Behrends et al. 2013). Metabolomic analysis of mammalian biofluids such as urine, and even serum and plasma, might be considered equivalent to metabolic footprinting; such analyses have of course been used widely to infer the metabolic state of the organism in question (e.g. in the case of diabetes) (Atherton et al. 2006).

1.3.3 Metabolomic analysis methods

There are many analytical techniques available for the measurement of metabolites, which vary in their sensitivities to different classes of compounds, their detection limits and their capacity to resolve many compounds within complex mixtures. 1H-nuclear magnetic resonance spectroscopy (^{1}H-NMR) and mass spectroscopy (MS) are the most widely used techniques in metabolomics. Datasets generated by metabolomics experiments contain many variables (often several hundred or more): multivariate statistical methods, such as principal components analysis (PCA), are valuable tools for the interpretation of this data.

^{1}H-NMR is robust, rapid and non-destructive. An ^{1}H-NMR spectrum consists of a series of peaks corresponding to the chemical shifts of protons in differing electronic environments (i.e. in different positions within a compound, or in different compounds). Each compound gives rise to a unique pattern of chemical shifts. The chemical shift patterns of a large number of biological molecules have been reported making metabolite identification relatively straightforward. ^{1}H-NMR spectroscopy has proved to be a valuable tool in metabolomic analysis of biofluids and is used routinely in the Department of Biochemistry for metabolic profiling (Pears et al. 2005; Atherton et al. 2006).

Mass spectrometric analysis techniques can be many times more sensitive compared to ^{1}H-NMR analysis and are often combined with prior chromatographic separation to improved

resolution of metabolites in complex mixtures. [1] The GC-MS instrument used for experiments described in this dissertation (a Thermo Electron TraceGC fitted to a Trace DSQ single quadrupole mass spectrometer, Thermo Scientific, USA) offers an approximately ten-fold increase in sensitivity over ^{1}H-NMR and GC separation facilitates metabolite resolution; over 1000 metabolites have been detected in *Arabidopsis thaliana* extracts by GC-MS (Nikiforova et al. 2005). The DSQ mass spectrometer uses electron impact (EI) ionisation and so metabolite identification can be semi-automated by reference to EI ionisation spectra, such as those available in the National Institute of Standards and Technology (NIST) mass spectral reference library.

One disadvantage of GC-MS is that detection is limited to those metabolites that are sufficiently volatile to enter the GC column, or those that can be chemically derivatised to increase their volatility beyond that threshold. Liquid chromatography (LC)-MS is not limited in this regard and so is capable of detecting a complementary range of metabolites. The QTof-Micro™ LCMS (Waters, USA) instrument used in experiments described in Chapter 6 is capable of metabolite identification by accurate mass and neutral loss fragmentation.

1.3.4 Multivariate data analysis

The number of variables in a metabolomics datasets is often more than an order of magnitude greater than the number of samples. Multivariate statistical methods consider all variables simultaneously and resolve correlated variation, thereby reducing the dimensionality of the dataset and facilitating its interpretation. Principle components analysis (PCA) is an unsupervised method commonly used to summarize variation in multivariate data by representing correlated variation using only a few dimensions (PCA components). PCA components are orthogonal to each other and therefore explain different correlated variation. The first PCA component represents the largest proportion of the total variation in the dataset and each subsequent component explains progressively less.

[1] ^{1}H-NMR has been used with chromatographic separation, but this still has the disadvantage of low sensitivity relative to MS, as well as currently being low throughput, and is therefore little used in metabolomics.

Projection to latent structures through partial least squares (PLS) is a supervised regression extension of PCA, in which PCA components are adjusted (rotated in X variable space) to maximise covariance between dependent (X) and independent "response" (Y) variable matrices. PLS thus refines PCA components to better explain Y variables. PLS Discriminant Analysis (PLS-DA) is an extension of PLS that regresses against class membership (e.g. sample type). In PLS-DA, membership of a class is represented by a Y variable for which 1 = membership, 0 = non-membership.

PCA and PLS models have associated parameters that describe how they relate to the underlying data. In PCA and PLS, R^2X is the fraction of total variation in the X matrix that is explained by a PCA/PLS component, this can be summed over several components for a measure of the variation explained by a model. Q^2 is the fraction of variation in the Y matrix that can be predicted by a PLS component, as calculated by internal cross-validation (ICV). Thus Q^2 is a measure of the predictive ability of a model and is indicative of the probability of an observed trend being reproducible (0 signifies no better than chance, 1 is the theoretical maximum). Values of Q^2 over 0.80 are typically considered to indicate excellent predictability, while less than 0.40 indicates that the model is not robust.

1.3.5 Multiple comparison procedures

In inferential statistics the "null hypothesis" describes the default position that there is no relationship between select variables. The *p*-value is the probability, under the null hypothesis, of obtaining a result equal to or more extreme than that actually observed. Experimenters often choose to reject a null hypothesis if a calculated *p*-value is smaller than a predetermined (though ultimately arbitrary) value α; if a *p*-value is calculated correctly, this guarantees that the probability of incorrectly rejecting a true null hypothesis—a "false discovery", or type I error—is at most α. If a calculated *p*-value is greater than α, the experimenter accepts the null hypothesis: incorrect acceptance of the null hypothesis is a type II error (a "false negative"). The probability of a type II error occuring determines the statistical power of a study: statistical power is the probability that a statistical discovery is identified when the null hypothesis is false.

Metabolomic analyses typically involve testing many null hypotheses simultaneously.

Table 1.1 illustrates how the outcomes of multiple tests can be classified according to the accuracy of each decision to accept or reject the null hypothesis. When m hypotheses are tested, the probability of at least one type I error (V) at a given α is $m \times \alpha$. Multiple comparison procedures (MCPs) have been developed to control the type I error rate. For example the popular Bonferroni correction controls the family wise error rate (FWER), which is the probability of *one or more* type I errors occurring in a family of tests: the Bonferroni correction is performed by rejecting hypotheses for which $p \leq \frac{\alpha}{m}$, thereby controlling the FWER at ≤ α (Dunn 1958, 1961). The Bonferroni correction thereby achieves stringent control over false discoveries, although it results in a corresponding reduction in statistical power ($power = 1 - \frac{T}{m_1}$, where T = number of type II errors).

Table 1.1 Classification of outcomes from multiple hypothesis tests.

If we reject or accept m null hypotheses then the outcomes can be classified into count variables according to the following table. For example V = number of type I errors ("false discoveries"), T = number of type II errors ("false negatives").

	Null hypothesis accepted	Null hypothesis rejected	Total
Null true	U	V	m_0
Alternative true	T	S	m_1
Total	W	R	m

An alternative approach is to control the *proportion* of type I errors amongst *all rejected null hypotheses*, termed the false discovery rate (FDR). By controlling for FDR rather than the FWER, the statistical power of the analysis can be increased. Moreover, controlling the FDR is experimentally adaptable, intuitive and scalable: adaptable because alpha can be varied to make the procedure more or less conservative; intuitive and scalable because the experimenter learns what proportion of all statistical discoveries are likely to be false discoveries and can control the cost of further investigation accordingly. Benjamini and Hochberg (1995) proposed the first means of controlling the FDR, using a step-up p-value method: for null hypotheses $H_1, H_2, \cdots, H_m$, with probabilities $P_1, P_1, \cdots, P_m$, i) find $\hat{k}$, the largest k such that $P_k \leq \frac{k}{m}\alpha$, ii) reject null hypotheses $H_1, H_2, \cdots, H_k$. This controls the FDR when defined as the expected proportion of false discoveries among all rejected hypotheses times the probability of rejecting at least one hypothesis: $\text{FDR} = E\left(\frac{V}{R}\middle| R > 0\right)\Pr(R > 0)$. Importantly, $\Pr(\text{R} > 0)$ is close to 1 for many relevant datasets, including those analysed using this method in this dissertation. The Benjamini-Hochberg step-up procedure controls the FDR when the tests are independent and also under quite general conditions of positive dependency (Benjamini and Yekutieli 2001). However, like the Bonferroni correction, the statistical power of the Benjamini and Hochberg procedure typically decreases as m increases.

A variation on the FDR approach that scales well to large values of m was proposed by (Storey 2002). This approach exploits the fact that for studies with larger values of m we have more information about the distribution of p-values and can use this to estimate the number of true null hypotheses (m_0). If each test is independent, then each p-value comes from the null distribution (i.e. uniform[0,1]) with probability $\pi_0 \equiv \frac{m_0}{m}$ and from the alternative distribution with probability $\pi_1 \equiv 1 - \pi_0$. Larger p-values are more likely to

have come from the null distribution, so we can conservatively estimate π_0 by calculating the ratio of the observed number of *p*-values greater than a threshold λ and the number expected to greater than λ if all *p*-values were from the null distribution, i.e. $\hat{\pi}_0(\lambda) = \frac{\#\{p_i > \lambda\}}{(1-\lambda)m}$. This approach is conservative regardless of the chosen value of λ. However, estimates of π_0 using low values of λ are biased by inclusion of alternative distribution whereas higher values of λ result in greater variance in $\hat{\pi}_0$ due to smaller sample sizes: this variance-bias tradeoff can be addressed by estimating $\pi_0$using a bootstrap approach (Storey et al. 2004). The Storey method controls what has been termed the positive FDR (pFDR), a slightly modified version of the FDR, defined as $\text{pFDR} = E\left(\frac{V}{R}\middle| R > 0\right)$ and also allows calculation of a pFDR analogue of the *p*-value, termed the *q-value*, which is the minimum pFDR at which the test is called significant. This amounts to an intuitive means of controlling the false discovery rate while maintaining statistical power for studies with large numbers of tests.

1.4 Aims of the present work

AHL QS systems can infer and integrate valuable information about a bacterium's physical, social and intracellular environments. Bacteria use this information to coordinate a variety of adaptive growth strategies and there is growing evidence that this may involve close coupling between AHL QS and primary metabolism. Several AHL-dependent perturbations to *P. aeruginosa*'s primary metabolism have been identified including genes in the "core" QS regulon, but it is difficult to draw conclusions without measuring the metabolites involved.

The primary thesis motivating the present work is that the primary metabolism of *P. aeruginosa* is tightly coupled to its AHL QS systems and that a metabolomic analysis will provide insight into a relationship overlooked by other approaches. The approaches taken in investigating these relationships—metabolomic and proteomic—are hypothesis-generating, in that they provide complex multivariate data collected with the expectation that they will stimulate the post-hoc formulation and testing of hypotheses. Nonetheless, some broad hypotheses can be stated at the outset: i) the *las*, *rhl* and PQS systems convey different information about the cellular environment and regulate distinct regulons, they will therefore coordinate distinctive metabolic transformations; ii) the information conveyed by QS systems relates to population density and associated environmental stressors and so the effects of QS on metabolism will include adaptation to such environments, for example adaptations to stationary phase stresses.

Brief descriptions of objectives and approaches taken to investigate these relationships are outlined below:

Chapter 3

- Validate metabolic footprinting for studying QS, including determining whether QS mutants have measurable and distinct effects on primary metabolism.
- Investigate whether the metabolic impact of the antibiotic azithromycin is consistent with inhibition of QS.

Chapter 4

- Analyse the temporal dynamics of AHL QS systems in batch culture, using measurement of AHLs, QS-regulated transcripts and metabolic footprinting.
- Correlate QS system activity with effects on metabolic footprints.
- Perform a targeted analysis of early post-exponential changes to primary metabolism by measurement of cellular small molecule metabolites and the cellular proteome.

Chapter 5

- Focused analysis of the impact of AHL QS on fatty acid metabolism.

Chapter 6

- Focused analysis of the impact of AHL QS on amino acid and polyamine metabolism.

Chapter 2

Methods

2.1 Chemicals, solutions, growth media

Table 2.1 Growth media, solutions.

[a] Individual components were added from sterile components to the final indicated amounts. [b] Solution was prepared fresh and dissolved at below 37 °C in order to minimise the formation of cyanate ions from urea (which react with primary amines, thereby rendering them unavailable for reaction with iTRAQ reagents). [c] Prepared from HPLC-grade reagents.

Medium/Solution	Composition (per litre unless otherwise stated)
Growth media	
Luria Broth (LB)	10 g Tryptone (Duchefa Biochemie)
	5 g NaCl (Riedel-de Haen)
	5 g Yeast extract (Duchefa Biochemie)
Luria Broth agar	LB, 15 g Bacto Agar
AGS [a]	5 g L-alanine (>=98 %, Fluka)
	5 g NaCl (Riedel-de Haen)
	3 g Potassium phosphate dibasic (Sigma)
	1 mL 7.5 mM $ZnCl_2$
	1 mL 100 mM $CaCl_2$
	1 mL 5 mM $FeCl_3$
	10 mL 1 M $MgSO_4$
	10 mL 50 % glycerol
	(adjust to pH 7.0 with HCl or NaOH)
AGSY [a]	5 g L-alanine (>=98 %, Fluka)
	5 g NaCl (Riedel-de Haen)
	3 g Potassium phosphate dibasic (Sigma)
	3 g Yeast extract (Duchefa Biochemie)
	1 mL 7.5 mM $ZnCl_2$
	1 mL 100 mM $CaCl_2$
	1 mL 5 mM $FeCl_3$

Medium/Solution	Composition (per litre unless otherwise stated)
	10 mL 1 M $MgSO_4$
	10 mL 50 % glycerol
	(adjust to pH 7.0 with HCl or NaOH)
Glycerol stocks	700 µl culture
	300 µl 50 % glycerol
PBS	Phosphate Buffered Saline tablets (Oxoid), pH 7.3.
	Final concentration g/l: 8 g sodium chloride, 0.2 g potassium chloride, 1.15 g disodium hydrogen phosphate, 0.2 g potassium dihydrogen phosphate
iTRAQ	
CHAPS lysis buffer	8 M urea hydrochloride, 4 % (w/w) CHAPS, 5 mM magnesium acetate, 10 mM Tris pH 8.0, 2 × Roche Complete Mini protease inhibitor Cocktail tablets (Roche), 1 mM PMSF
iTRAQ labelling buffer[b]	8 M urea, 25 mM triethylammonium bicarbonate (TEAB), 2 % (v/v) Triton X-100, 0.1 % (w/v) SDS, pH 8.5
Trypsin for iTRAQ	200 µg/mL solutions were prepared fresh, by adding 100 µL 50 mM TEAB to one vial of sequencing grade Trypsin (Promega)
SCX buffer A[c]	20 % acetonitrile (ACN) and 10 mM KH_2PO_4-H_3PO_4 (pH 2.7)
SCX buffer B[c]	1 M KCl, 20 % ACN and 10 mM KH_2PO_4-H_3PO_4 (pH 2.7)
RP solvent A[c]	0.1 % (v/v) Formic acid, 5 % ACN
RP solvent B[c]	0.1% (v/v) Formic acid, 95 % ACN

2.2 Bacterial strains and growth conditions.

The bacterial strains, plasmids and bacteriophage used in this study are listed in Table 2.2. Experiments in Chapter 3 were conducted using wild-type PAO1 ($PAO1_{BI}$ in Table 2.2) generously provided by Barbara Iglewski (University of Rochester, New York), PDO100 (a *rhlI*::Tn501-2 derivative of PAO1) and PAO-JP1 (a *lasI*::Tet derivative of PAO1) and MP551 (a *pqsR*::IS*phoA*/hah-Tc derivative of PAO1), a gift from Colin Manoil (University of Washington Center for Genome Sciences, Seattle, USA).

Experiments in 0, Chapter 5 and Chapter 6 were performed using wild-type PAO1 ($PAO1_{JM}$ Table 2.2) and a *lasI rhlI* mutant derived from this strain (PAO1 Δ*lasI*::Gm^R Δ*rhlI*::Tet^R in Table 2.2). This *lasI rhlI* mutant was constructed "fresh" using previously described suicide plasmids (Beatson et al. 2002). This resulted in a *lasI rhlI* mutant strain with insertional inactivations of both the *lasI* and *rhlI* signal synthase genes. QS mutants of *P. aeruginosa* are known to accumulate secondary mutations in other global regulators, e.g., *vfr* or *algR*. To ensure that the double mutant was otherwise isogenic with the wild-type progenitor and to reduce the possibility of unlinked accrued secondary mutations being responsible for the observed metabotype(s), the relevant markers were transduced into a wild-type strain using bacteriophage *φ*PA3 as described by (Monson et al. 2011)).

Bacterial cultures were grown in alanine-glycerol-salts (AGS) (Chapter 3) or alanine-glycerol- salts medium supplemented with yeast extract (AGSY medium, Chapter 4, Chapter 5 and Chapter 6). Specific growth rates were calculated by linear regression in R 3.1 (R Development Core Team 2008) by fitting log-transformed optical density at 600 nm (OD_{600}) data during the exponential portion of growth from 0 h to 3 h. Analysis of covariance (ANCOVA) was used to test for significant differences in growth rates.

Planktonic cell cultures were prepared by washing cells from overnight cultures in fresh medium, resuspending them to an OD_{600} of 0.05 in 50 mL fresh medium, and then incubating them in 500 mL conical flasks at 37°C with vigorous aeration in an orbital shaker (300 rpm).

Complementation assays were performed using synthetic AHLs (kindly provided by Drs James Hodgkinson and David Spring, Department of Chemistry, University of Cambridge, United Kingdom). OdDHL and BHL were dissolved in dimethyl sulphoxide (DMSO) and added to growth media at final concentrations of 15 μM and 10 μM, respectively. An equal volume of DMSO was added to both AHL-complemented and non-complemented cultures.

Table 2.2 Bacterial strains, plasmids and bacteriophage.

Identifier	Relevant genotype or phenotype [a]	Reference or source
P. aeruginosa strains		
$PAO1_{BI}$	Wild-type PAO1 from laboratory of Barbara Iglewski (University of Rochester, New York)	(Holloway 1969)
PAO-JP1	A *lasI*::Tet derivative of PAO1	(Pearson et al. 1997)
PDO100	A *rhlI*::Tn501-2 derivative of PAO1	(Brint and Ohman 1995)
MP551	A *pqsR*::IS*phoA*/hah-Tc derivative of PAO1	(Gallagher et al. 2002)
$PAO1_{JM}$	Wild-type PAO1 from laboratory of John S. Mattick (University of Queensland, Australia)	(Beatson et al. 2002)
PAO1 Δ*lasI::* Gm^R	PAO1 with Gm cartridge inserted into unique *Eco*RI site of *lasI*	This study
PAO1 Δ*rhlI*:: Tet^R	PAO1 with Tc cartridge inserted into unique *Eco*RI site of *rhlI*	This study
PAO1 Δ*lasI*::Gm^R Δ*rhlI*::Tet^R	Double mutant generated by using φPA3 to transduce (first) the Tet^R marker from PAO1 Δ*lasI*::Tet^R, and (second) the Gm^R marker from PAO1 Δ*rhlI*::Gm^R to PA01	This study
E. coli strains		
S17-1	*thi pro hsdR recA* chr::RP4-2	(Farinha and Kropinski 1990)
JM109	F´ *traD36 proA+B+ lacIq* Δ*(lacZ)M15/* Δ*(lac-proAB) glnV44 e14-gyrA96 recA1 relA1 endA1 thi hsdR17*	(Swift et al. 1997)
Plasmids		
pSB219.8A	pRIC380 carrying *lasI*::Gm on *Spe*I fragment from pSB222.7A	(Beatson et al. 2002)
pSB224.12B	pRIC380 carrying *rhlI*::Tc on *Spe*I fragment from pSB224.8A	(Beatson et al. 2002)
pSB536	BHL biosensor	(Swift et al. 1997)

pSB1075	OdDHL biosensor	(Winson et al. 1998)
pQF50	Broad-host-range transcriptional fusion vector; Cb^r *lacZ incP*	(Farinha and Kropinski 1990)
pβ01	pQF50 derivative containing *lasB-lacZ* transcriptional fusion	(Ikeda et al. 2001)
pβ02	pQF50 derivative containing *rhlA-lacZ* transcriptional fusion	(Ikeda et al. 2001)
Bacteriophage		
φPA3	*P. aeruginosa* generalized transducing phage	(Monson et al. 2011)

[a] Antibiotic resistance abbreviations: Tc, tetracycline; Gm, gentamicin

2.3 AHL bioassays

The biosensors were calibrated using standard curves of synthetic AHL standards in fresh growth medium and responded linearly in the ranges 0.03-1 μM for BHL/JM109(pSB536) and 0.1-3 μM for OdDHL/JM109(pSB1075). Synthetic OdDHL and BHL (kindly provided by Drs James Hodgkinson and David Spring, Department of Chemistry, University of Cambridge, United Kingdom) were used to generate standard curves. Neither reporter strain generated detectable signal in response to their noncognate AHL.

Sample preparation: Two mL samples were collected from bacterial cultures using sterile serological pipettes "Stripettes" (Corning Costar, New York, USA). Cells and cell debris were removed by centrifugation (6,000 × g, 20 min, 4°C). A 1.5-mL aliquot of the upper part of the supernatant was filtered (0.2-μm pore size) (Sartorius Minisart Sterile EO filters; Sartorius AG, Göttingen, Germany), and 1 mL of this aliquot was snap frozen in liquid nitrogen and stored at -80°C.

To quantify BHL, *Escherichia coli* JM109(pSB536) was grown overnight at 37°C with shaking in LB broth containing 50 μg/mL carbenicillin. This overnight culture was then subcultured into LB with a 1:10 dilution. Once the subculture had grown to an OD_{600} of 0.5, 100 μl was transferred to a 96-well sterile white opaque microtiter plate (Greiner Bio-One, Germany) containing 100 μl sterile supernatant from the test culture. The microtiter plate was incubated statically at 30°C, and bioluminescence readings were taken after 3 h using a luminometer (Lucy1; Anthos Labtec Instruments, Austria). The same protocol was used to monitor OdDHL with the following modifications: *E. coli* JM109 (pSB1075) was grown overnight at 30°C with 10 μg/mL tetracycline (Winson et al. 1998), the microtiter plate was incubated at 30°C, and bioluminescence readings were taken after 4 h of incubation.

2.4 β-galactosidase assays

Transcriptional activity from the *lasB* and *rhlA* promoters was assayed using promoter-*lacZ* fusions. The plasmids pQF50, pβ01, and pβ02 (Table 2.2) (kindly supplied by Junichi Kato, Graduate School of Advanced Sciences of Matter, Hiroshima University, Japan) were introduced into *P. aeruginosa* by the protocol of Choi et al. (Choi et al. 2006). Cultures were

grown in 50 mL AGSY medium (containing 250 µg/mL carbenicillin) at 37°C with good aeration (shaking at 250 rpm). β-Galactosidase activity was measured by the protocol of Ramsay et al (Ramsay 2013). The fluorogenic substrate 4-methylumbelliferyl-β-D-galactoside (catalogue no. M1095; Melford) was used at a final concentration of 0.25 mg/mL. Fluorescence was measured using a SpectraMax Gemini XPS fluorescence plate reader (Molecular Devices, Sunnyvale, CA) as follows: 360 nm excitation; 450 nm emission; cutoff 435 nm; reading every 30 s for 20 min at 37°C. β-Galactosidase activity was calculated as relative fluorescence units (RFU) per second and normalized to the OD_{600} of the corresponding sample.

2.5 pH measurements

The pH of culture supernatants was measured with a S20 SevenEasy™ pH meter (Mettler-Toledo, Columbus, OH, United States), calibrated at the appropriate temperature with standard solutions (pH 7, 4, and 10) and according to the manufacturer's instructions. Calibration was carried out before and after the experiments, and in no case did the pH of the calibration solutions differ significantly (0.05 U).

2.6 ^{1}H-NMR spectroscopy of extracellular metabolites—"metabolic footprints"

Sample preparation: Two mL samples were collected from bacterial cultures using sterile serological pipettes "Stripettes" (Corning Costar, New York, USA). Cells and cell debris were removed by centrifugation (6,000 × g, 20 min, 4°C). A 1.5-mL aliquot of the upper part of the supernatant was filtered (0.2-µm pore size) (Sartorius Minisart Sterile EO filters; Sartorius AG, Göttingen, Germany) and snap frozen in liquid nitrogen. One mL of this aliquot was dried overnight in a Speed Vac (Savant) and then stored at -80°C.

Dried samples were reconstituted in 600 µl D_2O buffered with sodium phosphate (pH 7.0, 0.24 M) supplemented with 1 mM sodium 3-trimethylsilyl-2,2,3,3- tetradeuteriopropionate (TSP) (Cambridge Isotope Laboratories Inc., Andover, MA) and then transferred to 5-mm-internal-diameter NMR tubes for analysis. Samples were analysed using a Bruker Avance II + spectrometer operating at 500.13 MHz for the ^{1}H frequency (Bruker, Coventry, United

Kingdom) equipped with a 5 mm broad-band inverse probe (Bruker). Spectra were acquired using a conventional solvent suppression pulse sequence based on a one-dimensional (1D) nuclear Overhauser spectroscopy (NOESY) pulse sequence, which was used to saturate the residual water ^{1}H signal (Atherton et al. 2006). The solvent suppression pulse was applied during the relaxation delay (2 s) and mixing time (150 ms). The spin-lattice relaxation time (T_1) was 3 s. A total of 128 transients were collected into 32,768 data points over a spectral width of 16.0 ppm at 300K. Spectra were processed using Advanced Chemistry Development (ACD) SpecManager 1D NMR processor (version 8; ACD Inc., Toronto, Canada). Spectra were multiplied by an exponential window function and then Fourier transformed from the time to frequency domain (line broadening 0.3 Hz). Spectra were phased, baseline corrected, and referenced to the TSP singlet at 0 ppm, and integrated between 0.1 and 4.45 ppm and 4.60 and 9.60 ppm over a series of 0.01 ppm integral regions (thereby excluding the TSP and H_2O resonances). Each spectral region was normalized to the integral of the TSP singlet at 0 ppm. Spectral peaks were assigned to metabolites by comparison with chemical standards and with resonances reported in the literature (1D and 2D spectra), including data available in the Human Metabolome Database (www.hmdb.ca) and Biological Magnetic Resonance Data Bank (www.bmrb.wisc.edu).

2.7 GC-MS analysis

2.7.1 Sample preparation

Cellular metabolites were extracted using a modified version of the methanol-chloroform extraction described by (Atherton et al. 2006). A volume of bacterial culture equivalent to 2.9×10^{10} viable cells was pelleted by centrifugation (5,000 × g, 5 min, 4°C), washed twice with 10 mL of 0.9% NaCl, snap frozen in liquid and stored at -80°C. Cell pellets were then resuspended in 900 µl of a 2:1 (v/v) mixture of methanol and chloroform. The cells were further disrupted by tip sonication (24 × 2.5 s bursts on ice). Chloroform (300 µl) and water (300 µl) were added, and the samples were mixed by vortexing (30 s). Insoluble material was pelleted by centrifugation (6,000 × g, 20 min) before the aliquots of the aqueous (top) or organic (bottom) fractions were removed for analysis.

2.7.2 Instrumentation

GC-MS analysis was performed using a Thermo TraceGC Ultra coupled to a Thermo Trace DSQ single quadrupole mass spectrometer (Thermo Scientific, Waltham, MA). An AS 3000 autosampler (Thermo Scientific), was fitted to facilitate sample handling. Gas chromatography: the injector temperature was 230 °C, the carrier gas was Helium (1.2 mL min^{-1} constant flow). Mass spectroscopy: full scan mode, 3 scans s^{-1} across a range of 50-650 m/z.

2.7.3 Analysis of metabolites in aqueous phase extracts

The aqueous (top) fraction (300 µl) of the samples prepared as in section 2.7.1 was removed by pipetting and dried overnight in a Speed Vac concentrator (Savant). Aliquots of the aqueous phase of chloroform-methanol cell extracts were derivatised first with methoxyamine hydrochloride in pyridine (30 µl, 20 mg mL^{-1} solution, 17 h, 22°C) and then with *N*-methyl-*N*-(trimethylsilyl)trifluoroacetamide (MSTFA) (30 µl, 1 h, 22°C). An aliquot (50 µl volume) of the derivatised sample was added to 50 µl hexane before analysis. GC-MS analysis was performed using a Thermo Trace GC Ultra gas chromatograph coupled to a Thermo Trace DSQ single quadrupole mass spectrometer (Thermo Scientific, Waltham, MA). One microliter of the derivatised sample was injected onto a 5%-phenyl- 95%-dimethylpolysiloxane Zebron column (30 m [length] by 0.25 mm [internal diameter]; 0.25 µm film thickness [d_f]) (Phenomenex, Inc., Torrance, CA). A 35-min chromatography method was used with an initial temperature of 70°C, ramped to 130°C (10°C min^{-1}), then to 230°C (5°C min^{-1}), and finally to 310°C (20°C min^{-1}).

2.7.4 Analysis of fatty acids in organic phase extracts

Aliquots of the organic phase of chloroform-methanol cell extracts were dissolved in chloroform-methanol (1:1; 500 µl volume) and boron trifluoride in methanol (10%; 125 µl volume) and heated to -80°C for 90 min (Morrison and Smith 1964; Atherton et al. 2006). Samples were vortexed with deionized water (200 µl) and hexane (400 µl). The organic (top) layer was removed, dried, and reconstituted in 100 µl hexane prior to analysis. Two microliters of derivatised sample was injected onto a 100% polyethylene glycol Zebron column (30 m by 0.25-mm-internal diameter; 0.25 µm d_f) (Phenomenex, Inc., Torrance, CA).

Analytes were separated using a 38 min chromatography method with an initial temperature of 60°C, ramped to 150°C (10°C min^{-1}), and finally to 230°C (4°C min^{-1}).

2.7.5 GC-MS data processing

All GC-MS data was processed using Qual Browser and Quan Browser of Xcalibur version 2.0 (Thermo Scientific, USA). The peaks were individually integrated and normalized to the total peak area for each spectrum. Metabolites were identified by comparison of retention times and MS fragmentation patterns with in-house reference data and libraries available in the National Institute of Standards and Technology (NIST) Mass Spectral Search Program (version 2.0). Commercially available mixed FAME standards were used to aid assignment of FAMEs (food industry FAME mix; Sigma-Aldrich, United Kingdom).

2.8 LC-MS analysis

2.8.1 Sample preparation and derivatisation

Cellular metabolites were extracted using a modified version of the methanol-chloroform extraction described by (Atherton et al. 2006). For the analyses described in this chapter 300 µL of the aqueous (top) fraction was removed by pipetting and dried overnight in a Speed Vac concentrator in 30 µL aliquots (Savant). The order of samples was randomized before being reconstituted in 100 µL phosphate-buffered saline (PBS) containing homoarginine, methionine-d3, and homophenylalanine as internal standards. The internal standard (HARG, MET-d3 and HPHE) concentrations provided with the EZ:faast kit were too high, saturating the MS detector; this was also the case for the concentrations of some analytes in the bacterial extracts. The internal standards and bacterial extracts were therefore diluted 100-fold to reduce their responses to within the linear range of instrument. Analytes were then separated from matrix components and chloroformate-derivatised using the EZ:faast amino acid analysis (AAA) MS kit (Phenomenex, Torrance, CA, USA). The EZ:faast kit consists of i) a solid phase extraction, in which analytes are first concentrated onto a cation exchange sorbent before wash and elution steps separate analytes from proteins, salts and other matrix components, ii) a liquid phase derivatisation step with *n*-propyl chloroformate and *n*-propanol, using picoline as a catalyst, which converts carboxylic groups to *n*-propyl esters and amine groups to n-propyl carbamate

esters, iii) a liquid/liquid aqueous/organic extraction step, during which the derivatised analytes are extracted into an organic phase. The removed organic phase was dried under N_2. Chemical reference standards for all analytes were supplied by Phenomenex, except agmatine, putrescine, spermidine, spermine and cadaverine, which were supplied by Sigma-Aldrich (USA).

2.8.2 Liquid Chromatography

Liquid chromatography was performed as described by Ubhi et al. (2013). Following extraction and derivatisation using the EZ:faast kit, dried-down analytes were reconstituted in 100 µL of a 1:2 (v/v) mixture containing 10 mM ammonium formate in water and 10 mM ammonium formate in methanol. Analytes were separated using a Waters Acquity UPLC system (Waters, United Kingdom). Sample aliquots of 5 µL were injected onto a Phenomenex EZ:faast AAA-MS column (250 mm × 2.0 mm) held at 25 °C. The eluents were 1 mM ammonium formate (Buffer A) and 10 mM ammonium formate in methanol (Buffer B). The EZ:faast chromatographic method was shortened by reducing both the run time from 21 to 15 min and the equilibration time from 4–7 min to 2 min with no loss of resolution or sensitivity (credit due to Baljit Ubhi). Analytes were eluted using the following gradient: 0–11 min from 68 to 83% Buffer B, 11–11.01 min 83 to 68% Buffer B and 11.01–13.00 68% Buffer B. A system re-equilibration was performed for 2 min prior to each injection. A constant eluent flow of 0.25 mL/min was used throughout the analysis. After each injection, a strong needle wash (83:17 methanol:water) and a weak needle wash (10:90 methanol:water) cycle were used to eliminate carry-over. Amino acid and polyamine standards in a mixture were used to create an 11-point calibration curve and run at the beginning and end of the analysis (with concentrations of target analyte spanning the range 0.5 nM to 50 µM). A quality control (QC) sample was run every ten injections to allow the assessment of system reproducibility. The QC sample consisted of the three internal standards, HARG, MET-d3 and HPHE, diluted 1:100. A pooled QC (pQC) sample was created by combining 10 µL from each sample, then processing this pool as per a standard sample. Pooled QC sample (5 µL) was injected after every block of ten samples. Blank injections were included following every 5 samples in order to monitor for any carryover between samples.

2.8.3 Mass Spectrometry

Mass spectrometric data were collected using a Waters Quattro Premier XE Triple Quadrupole mass spectrometer equipped with an electrospray source used in positive ionisation mode (Waters, Manchester, UK). The source temperature was set to 120°C with a cone gas flow of 50 l/h, a desolvation temperature of 350°C and a desolvation gas flow of 700 l/h. A capillary voltage of 1000 V was applied. The optimal MS tuning conditions (e.g. cone voltage) for each analyte derivative m/z are usually different, requiring individual tuning in positive ionisation mode. The parent mass was detected to two decimal places and fragmented using a collision gas at optimised collision energy. The resulting daughter ions were then observed using a daughter scan experiment. At least one unique daughter ion was selected for quantification of each amino acid and another as a qualifying ion to confirm identification. A multiple reaction monitoring (MRM) method was then created using specific transitions for each analyte and its unique fragment(s) to allow quantification for all of the analytes in one method. A scan time of 5 ms with an inter-scan delay of 5 ms was used for all the analyses. For each amino acid to be considered quantitative at least 15 data points across the peak were required. Analytes detected by MS were compared with authentic standards for confirmation.

Optimisation of the MS method for amino acid and polyamine derivatives resulted in the parent and product ions shown in Table 1. Structural isomers with the same parent mass, such as leucine and isoleucine, were distinguished using different product masses and/or resolved by liquid chromatography.

2.8.4 LC-MS data processing

Raw data were processed using Waters QuanLynx software version 4.1 (Waters, Milford, MA, USA). QuanLynx was employed to quantitate the data using response values of target analytes and homophenylalanine from the calibration curves. QuanLynx output includes the retention time and area under each peak for each detected metabolite (corrected for background noise). From the total ion chromatogram (TIC), extracted ion chromatograms (XICs) were generated for each analyte derivative. Responses were calculated relative to the homophenylalanine internal standard, and concentrations were calculated from mean-averaged calibration curves of each analyte according to the following equations. Alanine concentrations were extremely high, several-fold higher than glutamate. It seems probable

that this corresponds to carryover from the growth medium and so alanine was excluded from further analysis.

HPHE-normalised responses (R_N) for target analytes were calculated as $R_N = \frac{R}{R_{Hph}}$, where R is the baseline-subtracted area of the target analyte peak and R_{HPHE} is the area of the HPHE peak (internal standard). For each target analyte, a curve was fitted by linear least-squares regression to the linear portion of $\log_{10}$-transformed R_N values from calibration curves (as per Figure 6.3): $log_{10}(R_N) = a \times log_{10}(C) + b$. This was then used to estimate measured concentrations of target analytes (C_M) in the cell extracts. Estimated cellular concentrations (C_{Cell}) of target analytes were estimated using $C_{Cell} = C_M \times \frac{V_{Ex}}{V_{Cell} \times N_{Cells}}$, where V_{Ex} is the volume of the cell extract analysed (50 µL), V_{Cell} is the typical volume of a *P. aeruginosa* cell (2.2 fL) (Cohen et al. 2015), N_{Cells} is the number of cells harvested (2.9×10^{10} viable cells). This estimate assumes 100% extraction efficiency into the aqueous phase and constant cell volume.

2.9 Metabolomics data analysis

The order of all samples was randomized prior to data acquisition by ^{1}H-NMR, GCMS and LCMS. Unpaired Student's t tests with no equal-variance assumption ("Welch's unequal variance *t* test") were used to calculate univariate statistical significance (Welch 1947). The Benjamini-Hochberg step-up procedure ($\alpha = 0.1$) was applied to control the false discovery rate for all metabolomics data and was implemented using the "p.adjust" function in R's "stats" package (Benjamini and Hochberg 1995; R Development Core Team 2008).

Principal component analysis (PCA) and partial least squares analysis (PLS) was performed using SIMCA-P 11.5 (Umetrics, Umeå, Sweden). NMR footprinting data was Pareto scaled before PCA analysis: each variable was mean centred and then multiplied by $1/S_k$, where S_k is the standard deviation of the variable. This scaling increases the contributions of variables with low means to the model, without introducing excessive noise. Metabolic perturbations were identified by analysis of the corresponding loadings plots. The robustness of all PCA models was assessed using R^2 values (i.e., the fraction of variance explained by the components). Where glog transformations were applied, this was implemented using the Bioconductor "LMGene" R-package (Rocke et al. 2013).

2.10 iTRAQ proteomics

2.10.1 Sample preparation

Twelve biological samples (2 genotypes × 2 OD_{600} values × n of 3) and 4 pooled standards were differentially labelled and analysed in two MS/MS experiments as follows: Cells were harvested from planktonic bacterial cultures as for the metabolomic analyses, but with the following volumes: 40 mL at OD_{600} 1.5, 13.33 mL at OD_{600} 4.5. Cells were pelleted by centrifugation (3220 × g, 15 min, 4°C), washed in PBS (10 mL, 4°C), pelleted by centrifugation (3220 × g, 15 min, 4 °C), the supernatant carefully removed and the cell pellet snap frozen in liquid N_2.

Pellets were thawed on ice while they were simultaneously resuspended in CHAPS lysis buffer (Table 2.1). Cells were transferred to 2 mL microcentrifuge tubes and lysed by sonication (3 × 10 s, MSE microtip, on ice). Cell debris and insoluble protein was pelleted by two rounds of centrifugation (the supernatant was transferred to clean tubes after each round): 1) 16,060 × g, 10 min, 4°C, 2) 100,000 × g, 1 hr, 4 °C. Proteins were precipitated in acetone: 6 × supernatant volume of acetone at 4°C was added and proteins precipitated overnight at -20°C. Precipitated protein was pelleted by centrifugation (3220 × g, 20 min, 4°C) and the acetone decanted. The clean protein pellets were dissolved in 200 μL freshly prepared iTRAQ labelling (Table 2.1). Sonication was used to improved resuspension of protein (2 × 5 s pulses, on ice) and the protein solution was clarified by centrifugation (16,060 × g, 5 min, 10°C). Protein concentrations were measured in duplicate using the BCA Protein Assay Reagent kit (Pierce) before diluting with labelling buffer to 5 mg/mL. Pooled standard was prepared at this stage by combining equal volumes of all 12 biological samples. The pooled standard was then divided into 4 aliquots that were prepared in parallel to the individual biological samples. Protein (100 μg, 20 μL) from each sample was reduced, alkylated, digested and differentially labelled with 8-plex iTRAQ reagents *per* manufacturer's instructions (Applied Biosystems):

1) Reduction: disulphide bonds were reduced by adding 2 μL tris-(2-carboxyethyl)phosphine (TCEP), vortex mixing, then incubating on a shaker at room temperature for 1 hr.
2) Alkylation: cysteine sulphydryls were blocked by adding 1 μL methyl methanethiosulphonate (MMTS), vortex mixing, then incubating on a shaker at room temperature for 10 min.

3) Digestion: samples were diluted to below 1 M urea (to prevent inhibition of trypsin) by diluting samples 1:10 with 50 mM TEAB (i.e. added 180 μL 50 mM TEAB), added 12.5 μL 200 μg/mL Trypsin in 50 mM TEAB, vortex mixed, and incubated for 1 hr at 37°C. The trypsin digestion was repeated (adding a further 12.5 μL 200 μg/mL Trypsin in 50 mM TEAB, incubated 1 hr at 37°C), then again overnight (12.5 μL 200 μg/mL Trypsin in 50 mM TEAB, incubated 16 hr at 37°C).
4) Labelling: insoluble parts were removed by centrifugation (16,000 × g, 5 min), the supernatant from which was dried in an evacuated centrifuge (Eppendorf) then resuspended in 25 μL 1 M TEAB and 60 μL isopropanol, vortex mixed for 1 min, transferred to the appropriate labelling vial (Table 2.3), vortex mixed for 2 min, incubated for 2 hr shaking at room temperature. Residual iTRAQ reagents were hydrolysed by adding 100 μL H_2O and incubating at room temperature on a shaker for 2 hr. Samples were then pooled, vortex mixed, and dried using an evacuated centrifuge.

Table 2.3 Experimental design for iTRAQ labelling.

[a] Pooled Standard, consisting of equal parts of each of the 12 biological samples (OD_{600} label does not apply to pooled standards).

OD_{600}	MS/MS reporter ion							
	113	114	115	116	117	118	119	121
1.5	Δ*lasI* Δ*rhlI*	PAO1	Δ*lasI* Δ*rhlI*	PS[a]	PAO1	Δ*lasI* Δ*rhlI*	PS[a]	PAO1
4.5	Δ*lasI* Δ*rhlI*	PAO1	Δ*lasI* Δ*rhlI*	PS[a]	PAO1	Δ*lasI* Δ*rhlI*	PS[a]	PAO1

Strong cation-exchange chromatography of iTRAQ-labelled peptides

iTRAQ-labelled peptides were fractionated by cation-exchange chromatography (SCX) on a PolySULFOETHYL A™ (poly[2-sulphoethyl aspartamide]-silica) column (PolyLC, Columbia, MD; 2.1 × 200 mm, 5 μm, 300 Å) using BioLC HPLC system (Dionex). Immediately before sample application, BSA digest (40 μl of 10 mg/mL BSA in iTRAQ labelling buffer added to 280 μl of 10 % ACN, 50 mM TEAB and digested with 2.5 μg trypsin overnight) was run to test the separating conditions of the column before each run. The iTRAQ-labelled peptides samples were resuspended in 5 mL of SCX buffer A and pH of the samples adjusted to 2.7 using phosphoric acid (to increase protonation of peptides for thus their binding to the column). Samples were loaded onto the column and washed with SCX buffer A at 200 μl/min

for 1 hr, to remove detergents and free iTRAQ reagents. Peptides were eluted using a 70 min linear gradient of SCX buffer B at 200 µL/min. Sixty fractions were collected at 2 min intervals and lyophilized using an evacuated centrifuge.

Desalting SCX fractions

Lyophilised SCX fractions were desalted prior to MS analysis using UltraMicro Spin Columns (The Nest Group, MA, USA). The columns were conditioned by spinning them twice with 100 µl 100 % ACN (1500 × g, 1 min) and twice with 100 µl of 0.1 % formic acid (1500 × g, 1 min). SCX fractions were resuspended in 0.1 % formic acid then loaded onto a column, washed twice with 100 µl 0.1 % formic acid (1500 × g, 1 min, to remove salt). Finally, iTRAQ-labelled peptides were eluted in 100 µl 80 % methanol , 0.1 % formic acid (1500 × g, 1 min).

LC-MS/MS analysis of SCX fractions

Cleaned and desalted SCX fractions were separated on an Ultimate nano-LC system (Dionex) coupled to a QSTAR XL QTOF mass spectrometer (Applied Biosystems). Prior to sample application, a phosphorylase b standard test was performed according to the manufacturer's protocol in order to verify chromatographic conditions. The fractions were resuspended in HPLC-grade water with 0.1 % (v/v) formic acid loaded onto an Acclaim PA C16 trap column (5 mm x 300 µm ID, Dionex) at 20 µl/min using a FAMOS autosampler (Dionex). The trap was washed for 25 min with RP solvent A and then peptides were eluted onto a PepMap C18 analytical column (15 cm × 75 µm ID, Dionex) at 150 nL/min with 265 min gradient of 0–95 % RP solvent B and ionized via 2,000 V applied to a distal coated PicoTip electrospray needle (10 µm tip ID, New Objective). The QSTAR XL was operated in Information-Dependent Acquisition (IDA) mode whereby a 1 s survey scan (m/z 400 to 1600) was used to select 2 precursor ions (highest counts per second with charge states of +2 or +3 in range 100-1580 m/z). A ten minute dynamic exclusion of precursor ions with the repetitive m/z value was applied.

2.10.2 iTRAQ data processing

Peptide identification

QSTAR XL raw data files (.wiff files) resulting from all LC-MSMS analyses of the iTRAQ-labelled cation exchange fractions were converted using wiff2dta v. 1.0.97 software (http://sourceforge.net/projects/protms/) into two types of text files (.txt files): centroided and uncentroided peak lists. Centroided peak lists contained the m/z value and ion counts corresponding to the centre of every ion peak which was present in each product ion spectrum. Uncentroided peak lists contained the m/z values and ion counts for the entire peaks. Next, the Mascot v. 2.0.01 software (Matrix Science) was used to assign peptide sequences to product ion spectra by searching the centroided peak lists against the MIPS (Munich Information Center for Protein Sequences) *Pseudomonas aeruginosa* database. The following parameters of Mascot searches were used: trypsin specificity, one missed cleavage, fixed iTRAQ-8plex (K), fixed iTRAQ-8plex (N-term), fixed MMTS (C), variable oxidation (M), variable iTRAQ-8plex (Y), ESI-QUAD-TOF fragmentation, 2.0 Da window for precursor ion mass and 0.8 Da for fragment ions. Each centroided peak list was searched again using the Mascot algorithm with the same parameters as above but against a nonsense version of the relevant sequence database, which was created by reversing the order of the amino-acid sequences for each protein so that the C termini became the N termini. Database reversal was achieved by using the fasta_flip.pl Perl script (Matrix Science). For every proteomics experiment, a separate MySQL database (MySQL v. 4.0; MySQL AB; http://www.mysql.org) was created. Ultimately, the peptide identification and scoring information from Mascot output files (.dat files) were transferred to the relevant MySQL databases using the xGAPP.pl Perl script (Shadforth et al. 2006).

Peptide quantitation

Based on the uncentroided peak lists generated, the xITRACKER.pl Perl script (Shadforth et al. 2005) was used to calculate the areas under the reporter ion peaks in every product ion spectrum and to transfer this quantitation information into the appropriate MySQL database. The areas under the peaks were calculated using trapezoid approximation, corrected for isotope impurities (based on the purity correction factors supplied with every iTRAQ kit by its manufacturer) and normalized to one by dividing the value of area by the sum of all reporter ion areas in a MS/MS spectrum.

Grouping peptides into proteins

Data was processed according to (Sadowski et al. 2006). SQL scripts were used to communicate with the relevant MySQL database (4.5.1) in order to determine a Mascot score threshold application and limit the number of false positive identifications in the final results table to a maximum of 1%. This was performed by creating the tables in each MySQL database containing the highest scoring version of every peptide identified in the forward and reversed sequence database searches. Peptides were next grouped into proteins and the numbers of proteins identified from the forward and reversed database searches using different peptide Mascot score values were determined (this was performed separately for proteins identified by single and multiple peptides). The false protein identification rate was then calculated by dividing the number of protein identifications from the reversed database search by the number of identifications from the normal database search and multiplying it by 100. The Mascot score threshold was calculated as the first ratio value below 1%. Next, an SQL script was used to: (i) apply thresholds for peptide identification and peptide quantitation; (ii) link the identification information with the quantitation information about each single peptide; (iii) to group peptides into proteins; (iv) quantitate these proteins. Grouping peptides into proteins was performed as follows: in cases where more than one peptide was assigned to a single MSMS spectrum, the highest scoring assignment was chosen; in cases where more than one MS/MS spectrum was assigned to a single peptide, only the highest scoring assignment was processed and for the calculation of Mascot score in the final results table. For peptide identification, the threshold that was applied was equal to the Mascot score threshold calculated above. This threshold was applied separately to proteins identified by single and multiple peptides. Additionally, the requirement of at least one unique peptide sequence to be identified per protein (unique peptides threshold) was applied as well as the requirement of at least two distinct peptide sequences (distinct peptides threshold) based on the general agreement in the field that to claim the presence of a protein in a sample, the detection of at least two distinct peptides is needed.

For protein quantitation, following rules were applied:

1. Intensity threshold: only MS/MS spectra of iTRAQ reporter ions with intensity values above 15 ion counts were used for quantitation;
2. Missing value threshold: among the MS/MS spectra selected for quantitation, the maximum intensity of only one iTRAQ reporter ion was permitted to fall below the previously mentioned iTRAQ reporter ion intensity threshold;

3. Mascot score threshold: only MS/MS spectra assigned to a protein sequence with Mascot score 20 were used for protein quantitation; these included redundant sequences assigned to proteins more than once;
4. Non-unique peptide threshold: which meant that all the homologous peptides assigned to more than one protein were discarded from the quantitation if more than one such protein was listed in the final results table.

For quantitation of proteins, the arithmetic average and percentage standard deviation was calculated from the area under the curve of normalized iTRAQ reporter ions in all spectra assigned to a single protein. The final lists of proteins were generated as Apro, Bpro and ABpro MySQL tables which were exported into text files for differential statistical analysis in R. Data was pre-filtered for proteins with data for at least 2 peptides. The number of proteins detected with these constraints were 931 in total, 870 at OD1.5 and 700 at OD4.5.

Multiple comparison procedure

Unpaired Student's *t* tests with no equal-variance assumption ("Welch's unequal variance *t* test") were used to calculate univariate statistical significance (Welch 1947). The false discovery rate was controlled using the Bioconductor "q-value" R-package to estimate Storey's *q*-values; π_0 was estimated using the automatic "bootstrap" method and validated by manual inspection of plots of λ versus $\hat{\pi}_0(\lambda)$ and p-value density histograms (Storey 2002; Storey et al. 2004, 2015).

Chapter 3

Pilot study: Use of metabolic footprinting to assess the effects of Quorum Sensing and azithromycin

3.1 Introductory comments

Studying the dynamics of *P. aeruginosa* QS and metabolism in batch culture requires the analysis of bacterial cultures throughout the growth curve. Metabolic footprinting by ^{1}H-NMR has the potential to facilitate such analysis, since the technique requires small sample volumes and minimal sample preparation. This chapter describes efforts to evaluate the feasibility of such an approach. I investigate the range of exometabolites that can be monitored by ^{1}H-NMR analysis and whether these metabolites are modulated in strains with inactivating transposon insertions in the QS genes *lasI*, *rhlI* and *pqsR*.

This study is extended with an analysis of the impact of sub-MIC concentrations of the macrolide antibiotic azithromycin (AZN) on the *P. aeruginosa* exometabolome. The symptoms of CF and diffuse panbronchiolitis (DPB) include chronic airflow limitation and airway inflammation, rendering patients highly susceptible to chronic endobronchial infection by *P. aeruginosa*. *P. aeruginosa* infection is associated with progressive deterioration in lung function, and in a high proportion of cases eventually leads to respiratory failure (Boucher 2004). Aggressive antibiotic therapy fails to eradicate *P. aeruginosa* infections from CF and DPB patients and so strategies to reduce tissue damage and slow disease progression are wanted. AZN is thought to inhibit bacterial growth by blocking the peptide exit channel of 23S rRNA in the 50S ribosomal subunit and several clinical studies have found that treatment with AZN improves clinical parameters of DPB and CF lung diseases (Hansen et al. 2005; Marvig et al. 2012). This is in apparent contradiction with AZN acting via its established mechanism of inhibition of protein synthesis via the 50S ribosomal subunit, since minimum inhibitory concentrations (MIC) of AZN for clinical *P. aeruginosa* isolates are typically an order of magnitude higher than clinically achieved sputum concentrations: Howe and Spencer (Howe and Spencer 1997) report MICs in the range 128 to 512 μg/mL; Baumann et al. (Baumann et al. 2004) report

typical sputum concentrations of 0.6 to 79.3 μg/mL. Sub-MIC concentrations of AZN have been reported to inhibit virulence factor expression, motility and biofilm formation in *P. aeruginosa* (Molinari et al. 1993; Favre-Bonté et al. 2003; Gillis and Iglewski 2004; Hoffmann et al. 2007; Tsai et al. 2009). The association of these phenotypes with QS—especially expression of secreted virulence factors—spurred the hypothesis that sub-MIC AZN may act by inhibiting QS (Tateda et al. 2001; Nalca et al. 2006; Kai et al. 2009). Indeed, sub-MIC AZN inhibits synthesis of AHLs and transcription of the AHL synthases *lasI* and *rhlI* (Tateda et al. 2001; Kai et al. 2009). A study combining transcriptomic and proteomic analyses found that 2 μg/mL AZN affect the expression of 8 out of 77 genes (10.4%) of the "general quorum sensing regulon" (genes that have been identified as QS-regulated in three recent microarray studies of *P. aeruginosa* quorum sensing), as well as a number of genes involved in protein synthesis (e.g. ribosomal subunits, initiation and elongation factors) (Arevalo-Ferro et al. 2003; Schuster et al. 2003; Wagner et al. 2003; Nalca et al. 2006). These authors (Nalca et al.) interpreted their data as being in support of the hypothesis that AZN interferes with QS. I investigate whether the metabolic footprints of AZN-treated *P. aeruginosa* support this hypothesis.

Aims and objectives: First, to validate metabolic footprinting for studying QS, including determining whether QS mutants have measurable and distinct effects on primary metabolism. Second, to investigate whether the metabolic impact of the antibiotic azithromycin is consistent with inhibition of QS. The power of statistical analyses to detect significant features can be heavily influenced by the choice of pre-processing operations and their parameters; In the course of these experiments I also identify parameters and metrics for reliable multivariate analysis of ^{1}H-NMR metabolic footprinting data.

Part of this work has been published in an original research article in PLOS One (Swatton et al. 2016).

3.2 Results

3.2.1 Experimental design

Seven culture conditions were used, each with four biological replicates, as outlined in Table 3.1. Planktonic cultures of the bacteria were grown in AGS to stationary phase (18 h, OD_{600} 7.5), samples of the extracellular liquid medium were prepared by centrifugation and filtration, then analysed by ^{1}H-NMR spectroscopy. The NMR spectra contained over 100 peaks, from which 19 metabolites spanning central carbon, amino acid and nucleotide metabolism were identified (Figure 3.1) by comparison to spectra of reference compounds and Statistical Total Correlation Spectroscopy (STOCSY).

Table 3.1 Experimental design for ^{1}H-NMR footprinting.

N = number of biological replicates. †Two replicates of PAO1Δ*lasI* were lost during sample preparation.

Strain	Genotype	AZN (μg/mL)	N
$PAO1_{BI}$	PAO1	0	4
PAO-JP1	PAO1Δ*lasI*	0	4†
PDO100	PAO1Δ*rhlI*	0	4
MP551	PAO1Δ*pqsR*	0	4
$PAO1_{BI}$	PAO1	2	4
$PAO1_{BI}$	PAO1	8	4
$PAO1_{BI}$	PAO1	32	4

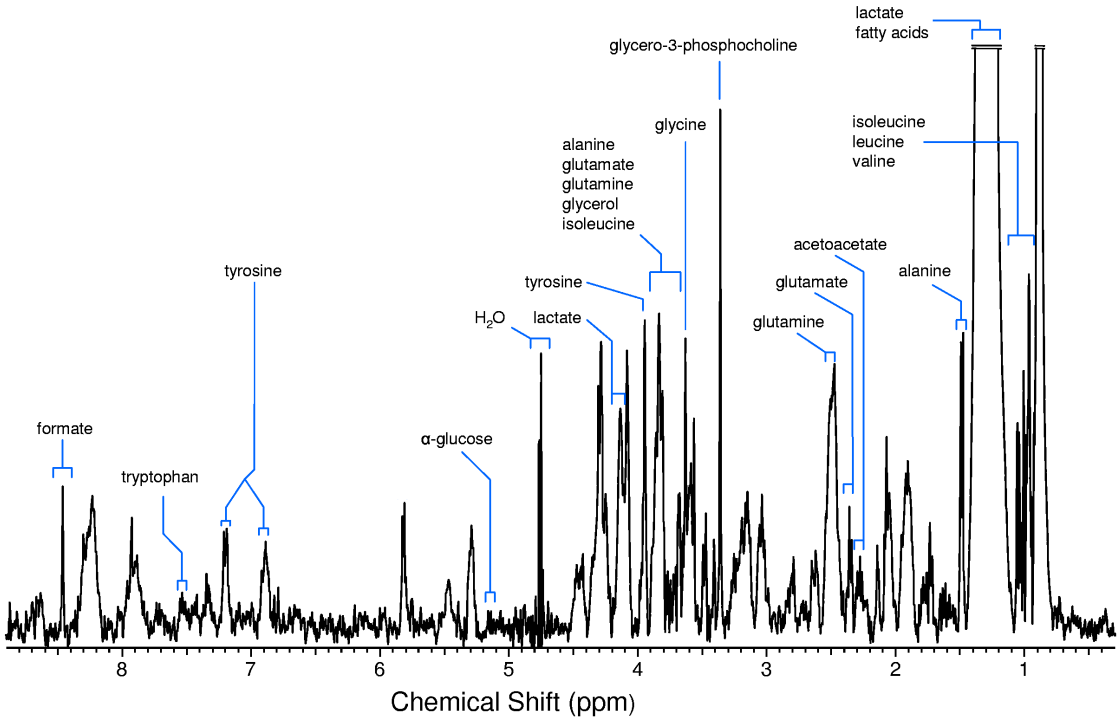

Figure 3.1 Representative ^{1}H-NMR spectrum of PAO1 supernatant: a metabolic ``footprint''

Table 3.2 Effect of data pre-processing on class discrimination by PCA.

Cohen's d was used as a measure of class discrimination (effect size; mean difference divided by standard deviation) and was calculated between wild-type and the "mean QS mutant" in PCA component space. This is represented in the table relative to the initial pre-processing method used: 0.04 ppm simple-buckets, mean-centred.

		Simple-buckets		Overlap-buckets	
Scaling	Noise filter	0.04 ppm	0.01 ppm	0.04 ppm	0.01 ppm
Mean-centred	0	1	1	1	1
Pareto	0	0.93	0.94	0.93	0.94
Autoscaled	0	0.55	0.59	0.54	0.59
Glog	0	0.66	0.66	0.64	0.66
Mean-centred	1	1	1	1	1.01
Pareto	1	0.96	0.97	0.95	0.95
Autoscaled	1	1.02	1.02	0.67	0.62
Glog	1	0.79	0.8	0.73	0.74

Table 3.3 Univariate effect size: number of features called significant by Student's t-test.

Significance is based on t-test comparing each mutant to wild-type, p<=0.05, corrected for multiple testing using the Benjamini and Hochberg step-up procedure. The number of features called significant was then averaged across the three wild-type to mutant comparisons.

		Simple-buckets		Overlap-buckets	
Scaling	Noise filter	0.04 ppm	0.01 ppm	0.04 ppm	0.01 ppm
Mean-centred	0	35	124	73.7	250.7
Mean-centred	1	41.7	156	52	149
Glog	0	33	117.7	68.7	243.3
Glog	1	47.7	158	51.3	144.7

3.2.2 Comparison of data-processing methods

Several methods were investigated for i) definition of x variables, ii) scaling, and iii) filtering variables. The preprocessing methods were evaluated according to the sensitivity with which multivariate and univariate statistical tests could distinguish wild-type from QS mutant metabolic footprints. Principal component analysis (PCA) was used for multivariate analysis (MVA) and the metric for sensitivity was Cohen's *d* effect size (mean difference divided by standard deviation) between wild-type and QS mutants in principle component space (Table 3.2). The effect of the data processing methods on downstream univariate statistical analyses (UVA) was evaluated by examining the number of features called significant by Student's t-test (Table 2.3).

Definition of x variables

"Simple-bucketing" was chosen as a starting point for its simplicity (ease of implementation) and its established use in metabolomics studies. This method defines dependent variables as the sum of spectral intensity within fixed-width intervals. A bucket size of 0.04 ppm is typical, although this can be several times broader than some metabolite peaks and so has the potential to confound data-interpretation.

Reduction of bucket width from 0.04 ppm to 0.01 ppm had very little effect on multivariate effect size (Table 3.2). However, inspection of UVA results revealed that 0.01 ppm enabled identification of significantly modulated peaks that were missed with a 0.04 ppm bucket width: these were typically narrow peaks, whose modulation was masked by adjacent peaks or background noise when 0.04 ppm buckets were used.

A concern with the use of "simple-bucketing" is that information (signal:noise ratio) could be lost where peaks are arbitrarily split across buckets. An alternative "overlap-bucketing" approach was tested whereby two sets of buckets were defined, the second set offset from the 1st by half a bucket width. This should increase the probability of a bucket symmetrically straddling the maximum of any given spectral peak. The overlap-bucketing method resulted in similar MVA effect sizes as simple-bucketing for unfiltered datasets; this was expected since for every bucket with increased signal:noise ratio, buckets may also be created with lower signal:noise ratios. However, UVA showed that even after correcting for multiple testing the overlap-bucketing method resulted in a greater number of features called significant: this increase was proportionally greater with a 0.04 ppm bucket width (55 to 75) than for 0.01 ppm (203 to 240), consistent with reduced bucket width and overlap-bucketing reducing loss of information from the same sources.

Scaling

Mean and variance of dependent variables tend to be highly correlated in metabolomics datasets. Higher concentration metabolites can therefore dominate multivariate analyses, obscuring valuable information regarding lower concentration metabolites. Variance-stabilising transformations can be used to counter this, for example autoscaling (division by the standard deviation) results in equal variance for all dependent variables, with the penalty that this also amplifies noise. Noise is a particular concern in bucketed Fourier-transformed NMR (FT-NMR) spectral data, which has a background of high frequency, low amplitude noise. Pareto scaling (division by the square root of the standard deviation) is often used in FT-NMR preprocessing as a compromise between stabilising variance and dampening noise. Other scaling methods have been developed based on log-transformation such as the generalised logarithm "glog" transformation. Whereas the log transformation stabilises the variance for variables with high but not those with low or zero means, the glog transformation results in constant variance and approximately symmetric errors in data for both low and high means. The glog transformation was originally developed to normalise variance in microarray expression data for which error can be modelled as $y = \alpha + \mu e^{\eta} +$

ε, where y is the measured expression, μ is the true expression and η and ε are normally distributed error terms with mean 0 and variance ${\sigma_\eta}^2$ and ${\sigma_\varepsilon}^2$, respectively. Based on this two-component error model Durbin et al., (2002); Huber et al., (2002) and Munson (2001) independently developed the glog transformation to stabilise the variance in such data: $\text{glog}(y, \alpha, c) = \ln\left[(y-\alpha) + \sqrt{(y-\alpha)^2 + c}\right]$, where $c = {\hat{\sigma}_\eta}^2 / {\hat{\sigma}_\varepsilon}^2$ (Geller et al. 2003). The following scaling methods were selected for assessment: mean-centred (no-scaling), Pareto, autoscaling and glog.

Mean-centering resulted in the highest multivariate effect size, followed by Pareto, glog and autoscaling (Table 3.2). The Student's t-statistic is scale-invariant and so is unaffected by UV and Pareto scaling, hence only mean-centred and glog transformed data were compared: no large or consistent difference was observed between the performance of mean-centering or glog transformation for UVA (Table 2.3).

Noise filtering

Filtering variables based on their noise component was investigated as a complementary approach to scaling. Excluding noisy variables was also expected to reduce the loss of power of univariate analyses to multiple testing. The filtering method entailed: 1) Calculating the mean and standard deviation of background noise (these parameters were constant across the NMR spectrum); 2) Defining the limit of detection "LOD" as the mean of the noise plus 3 standard deviations; 3) Excluding all variables for which fewer than 4 samples (the number of biological repeats) had a magnitude greater than the LOD. Noise filtering resulted in increased multivariate effect sizes, with the greatest increase seen for autoscaled data (1.84 fold for 0.01 ppm buckets). This is illustrated in the plots of PCA scores in Figure 3.2. Overlap bucketing and noise filtering interacted with unexpectedly consequences: the improvement on effect size due to noise filtering was largely abrogated by overlap-bucketing. With regard to univariate analysis, noise filtering increased the number of features called significant in simple-bucketed data, while the opposite was true for overlap-bucketed data.

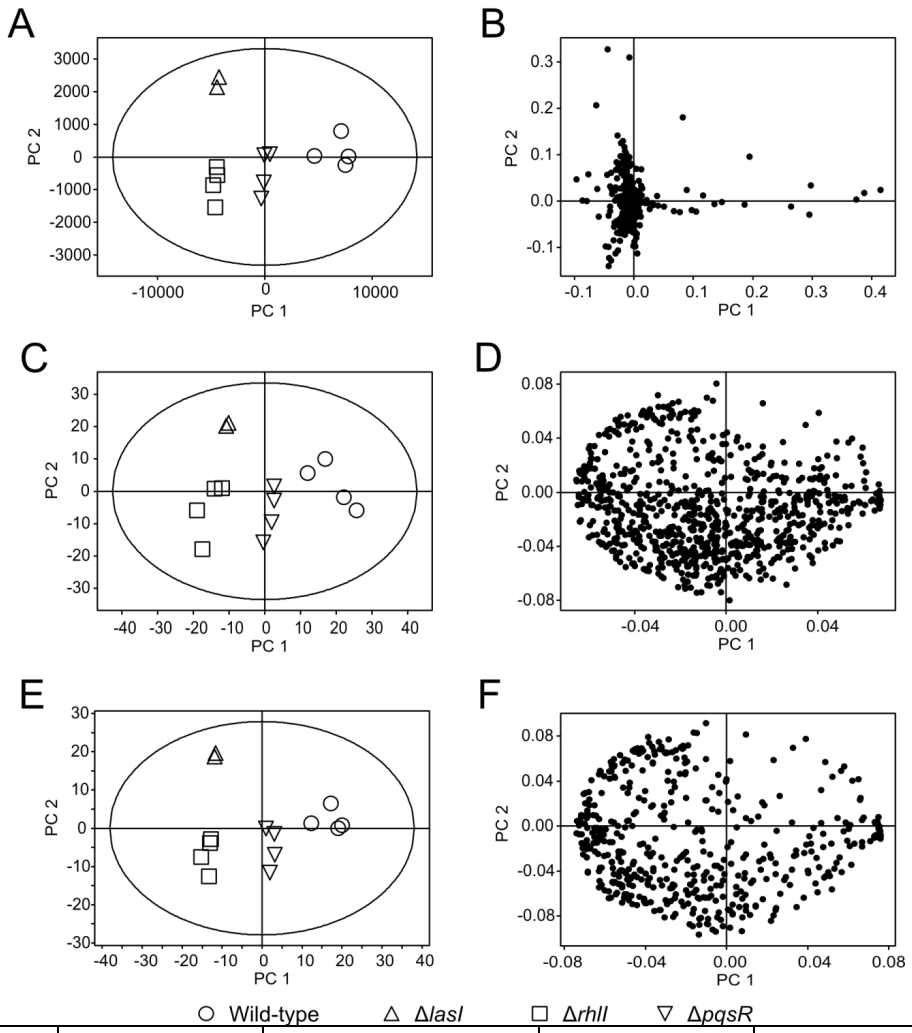

Plot label	Bucket width	Bucketing method	Noise filtering	Scaling
A, B	0.01 ppm	Simple	0	Mean-centred
C, D	0.01 ppm	Simple	0	Autoscaling
E, F	0.01 ppm	Simple	1	Autoscaling

Figure 3.2 Effect of noise-filtering on Principle Components Analysis of metabolic footprints.

Subplots represent PCA scores (A, C, E) and loadings (B, D, F) illustrating the effect of noise-filtering. All data was mean-centred and processed using a simple bucket method with a bucket width of 0.01 ppm. Autoscaling (to unit variance) was applied to data in C-F. A noise filtering method (described in the body text) was applied to data in E-F.

Conclusions

The choice of data pre-processing steps had a large effect on the sensitivity of both multivariate and univariate analysis. Bucket widths of 0.01 ppm were preferable to 0.04 ppm. Noise-filtering improved sensitivity of both multivariate and univariate analysis and facilitated interpretation of PCA loadings plots. Use of an overlap-bucketing method revealed significantly modulated features that would otherwise have been masked, but mitigated the benefits of noise-filtering. Since no single combination of preprocessing steps outperformed all others in both multivariate and univariate analysis, the choice of preprocessing method depends on the relative importance of multivariate analysis and univariate analysis.

In the following study of *P. aeruginosa* QS mutants, multivariate analysis was used to investigate global patterns in metabolic metabolism, while univariate analysis was used to investigate the underlying features of such patterns. By equalising variance, autoscaling enables a more "global" assessment of patterns amongst variables (as illustrated by the loading plots in Figure 3.2). Since noise-filtering mitigated the loss of sensitivity (effect size) due to amplification of noise, the following pre-processing procedure was chosen as a compromise: i) 0.01 ppm simple-bucketing, ii) noise-filtering, iii) autoscaling.

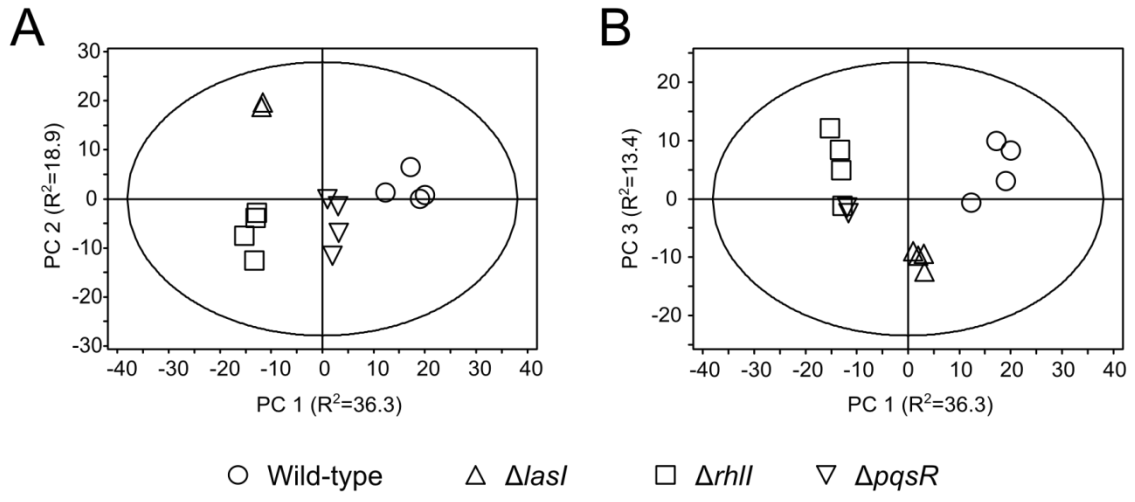

Figure 3.3 Principal Components Analysis of QS mutant metabolic footprints.

Table 3.4 Extracellular metabolites differentially regulated in ^{1}H-NMR metabolic footprints of *lasI*, *rhlI* and *pqsR* mutants.

The *lasI*, *rhlI* and *pqsR* mutants show similar perturbations in their metabolic footprints, with similar changes to their amino acid and fatty acids profiles relative to wild-type *P. aeruginosa*. Direction of modulation indicated in the table is relative to wild-type PAO1 (Student's t-test, $p < 0.05$).

	Metabolites	
Strain	Up	Down
Δ*lasI*	glycero-3-phosphocholine, glycine, isoleucine, sarcosine (*N*-methylglycine), tryptophan, tyrosine	fatty acids, glutamine
Δ*rhlI*	formate, glycero-3-phosphocholine, glycine, isoleucine, sarcosine (*N*-methylglycine), trimethylamine, tryptophan, tyrosine	fatty acids, glutamine
Δ*pqsR*	formate, glycine, isoleucine, sarcosine (*N*-methylglycine), tyrosine	fatty acids, glutamine

3.2.3 The effects of *las*, *rhl* and PQS intercellular signalling can be distinguished by ^{1}H-NMR metabolic footprinting

Comparison of ^{1}H-NMR spectra by PCA indicated that the metabolic footprints of the three signalling mutants deviated from the wild-type in a similar manner: each mutant could be distinguished from the wild-type in the same direction in the first principal component, which accounted for 36% of the variation in the dataset (Figure 3.3). The *lasI* and *rhlI* mutants were clearly distinguished from each other and the *pqsR* mutant by the second (R^2 = 19%) and third (R^2 = 13%) principal components, indicating that the *las* and *rhl* systems have pronounced and distinct impacts on *P. aeruginosa* metabolism. At this global level of analysis, the *pqsR* mutant could be distinguished from the other strains in degree rather than quality of metabolic effect. The effect sizes of the *lasI* and *rhlI* mutants were approximately twice that of the *pqsR* mutants (Figure 3.3). This is consistent with models of QS networks in which the PQS system sits under the AHL systems, though it is important to consider that these metabolic footprints represent only a portion of the complete extracellular metabolome at a single point in batch culture.

Student t-tests were used to determine which ^{1}H-NMR spectral regions, and hence which metabolites, distinguished the mutants from the wild-type. After correction for multiple testing, this analysis identified 60 spectral regions as being modulated in one or other of the signalling mutants relative to the wild-type (Student's t-test, $p<0.05$); of these, 35 spectral regions were assigned to 10 metabolites and a broad fatty acid CH_2 peak. The majority of the 60 modulated spectral regions were affected similarly in all three QS mutants compared to wild-type: glycine, isoleucine, sarcosine (*N*-methylglycine) and tyrosine were at higher concentrations in the QS mutants, whereas the signal intensities of glutamine and the broad fatty acid peak were lower (Table 3.4). This suggests that the various QS systems share control of a core set of metabolic functions.

A smaller number of metabolites were modulated in only a subset of the QS mutants: i) trimethylamine concentrations were elevated in the *rhlI* mutant footprints and to a lesser degree in the *las* mutant, but no effect was detectable in *pqsR* mutant cultures, ii) there was a higher concentration of formate in the *rhlI* and *pqsR* mutants but not in the *las* mutant, iii) glycero-3-phosphocholine concentrations were higher in the *las* and *rhl* mutants, but not in the *pqsR* mutant. These modulations remained specific to the above subsets even when the threshold for significance was decreased from $p<=0.05$ to $p<=0.3$.

In addition to an overall decrease in the concentration of fatty acids in the QS mutants, there was a shift in the profile of the fatty acid peak towards lower chemical shift (Figure 3.5).

Wild-type spectra had a peak centred at 1.30 ppm, whereas *lasI* and *rhlI* mutants had peaks centred at 1.24 ppm. The *pqsR* mutant had an intermediate phenotype, showing similarly sized peaks centred at both chemical shifts. These metabolic changes indicate the *las*, *rhl* and PQS systems have marked effects on the metabolic function of *P. aeruginosa*, encompassing fatty acid and amino acid metabolism.

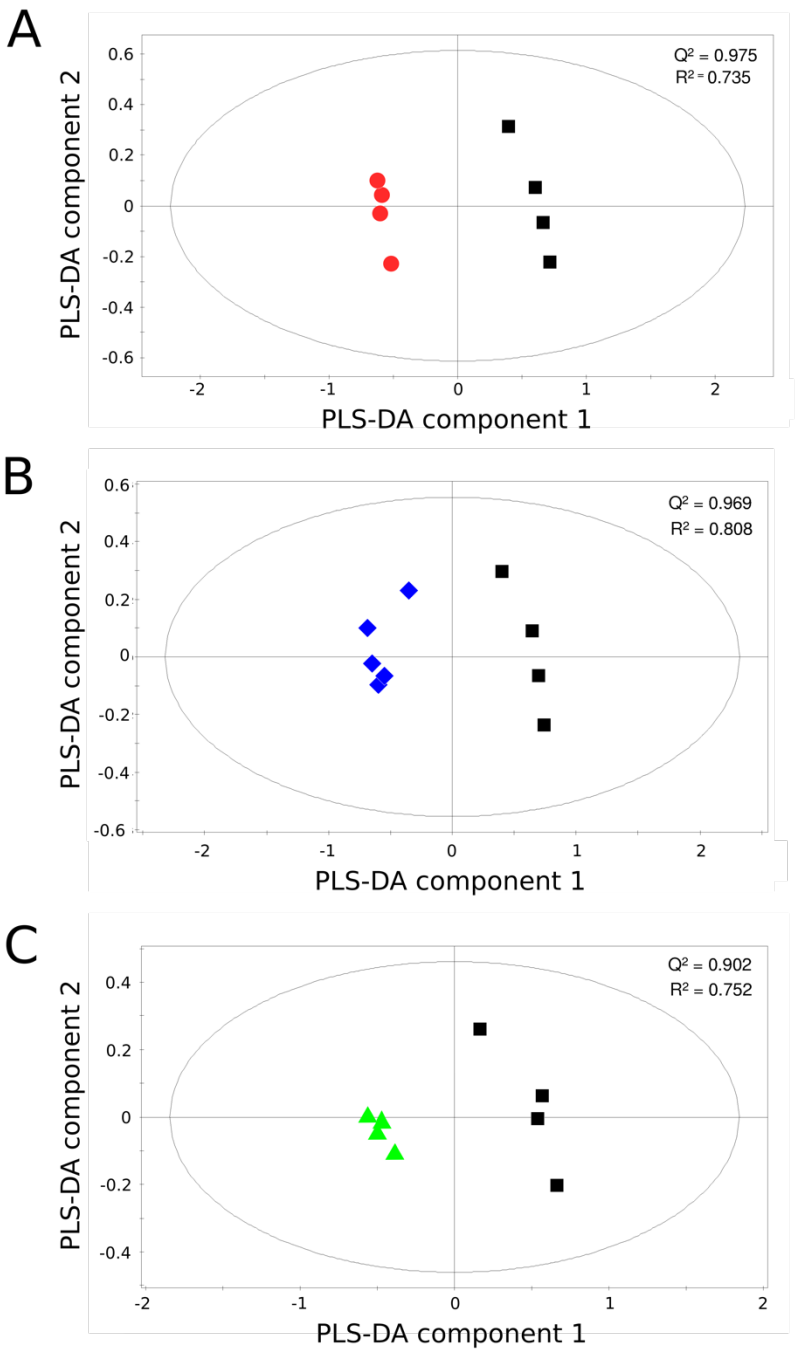

Figure 3.4 Distinct clustering of signal mutants by PLS-DA.

PLS-DA generated robust models separating wild-type PAO1 from *lasI*, *rhlI* and *pqsR* signalling mutants. PAO1: black squares, Δ*lasI*: red dots, Δ*rhlI*: blue diamonds, Δ*pqsR*: green triangles. Separation of each mutant from wild-type in Principal Component 1 of each model was found to be significant in each case (Student's t-test): *lasI* ($p=3.12^{-06}$), *rhlI* ($p=2.20^{-16}$), *pqsR* ($p=2.20^{-16}$).

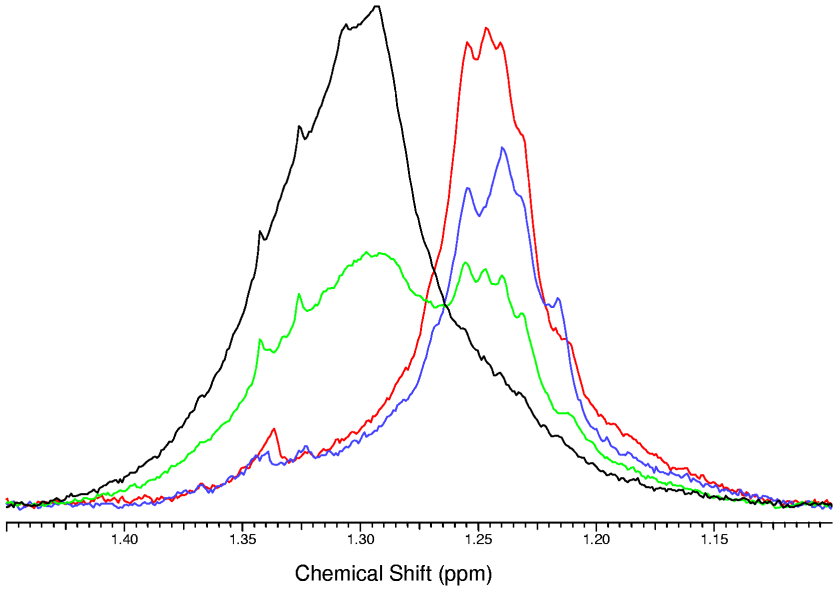

Figure 3.5 ^{1}H-NMR footprinting indicates QS-modulated fatty acid metabolism.

The broad resonance due to saturated $(CH_2)_n$ groups is centred at lower chemical shift in the *lasI, rhlI* and *pqsR* signalling mutants, indicating a shift in length and/or saturation in their fatty acids profiles. PAO1: black, Δ*lasI*: red, Δ*rhlI*: blue, Δ*pqsR*: green.

3.2.4 Metabolic footprinting indicates that sub-inhibitory azithromycin has a QS-independent mode of action

Wild-type *P. aeruginosa* was grown in AGS media supplemented with 2, 8 or 32 μg/mL AZN. Under these conditions AZN has no discernible effect on the growth of *P. aeruginosa*, though the upper concentration was chosen selected to be within a factor of two of inhibitory concentrations (64 μg/mL AZN results in a slight growth defect in AGS). The full dataset, consisting of all seven conditions (Table 3.1), was re-processed in order to filter-out peaks due to AZN: ^{1}H-NMR spectral peaks due to azithromycin were first identified with reference to spectra of pure azithromycin and were removed prior to processing as above. A PCA model was built to compare wild-type *P. aeruginosa*, AZN-treatment and QS mutants (Figure 3.6A). The first principal component, accounting for 40% of variation in the dataset, separated wild-type samples from the QS mutants, but AZN-treated co-clustered with wild-type in this dimension. Both the QS mutants and the AZN-treated samples showed a small deviation away from the wild-type in the second principal component (R^2=23%). The majority of the QS effect was therefore unrelated to that of azithromycin treatment. On the other hand, the largest discernible AZN effect in this model was correlated with QS (detected in the second principal component): AZN does appear to affect a small portion of QS-regulated metabolites.

As a complementary approach to addressing this relationship, a PLS model was built using only wild-type samples, treating AZN concentration as an independent ("Y") variable. The advantage of this PLS model over the previous PCA is that the PLS model focuses on AZN effects, whereas these may be obscured in the PCA by the much larger QS effects. Plotting the AZN concentration of each sample against AZN concentrations predicted by the PLS model resulted in a linear dose-response curve with good fit (Figure 3.7, $R^2 = 0.81$). Model validation by bootstrapping confirmed that this was a robust model of a dose-dependent effect of AZN-treatment. This reflects that higher concentrations of AZN result in a greater degree of modulation of the same metabolites as lower AZN doses, consistent with AZN acting via the same mechanism(s) at all concentrations tested.

The AZN PLS model was then used to predict pseudo-concentrations of AZN of the QS mutants, a measure of the strength of AZN-like effects in these samples. In this analysis, the QS mutant profiles were equivalent to intermediate AZN concentrations (7-19 μg/mL AZN, Figure 3.7), confirming that the metabolic impact of AZN-treatment correlates with aspects of QS-inhibition. PLS coefficients were analysed to determine the proton resonances driving the dose-dependent effect of AZN. Although more than 40 spectral regions contributed significantly (Student's t-test, $p < 0.05$) to the separation of sample types, only a small number could be confidently assigned to specific metabolites: these corresponded to tyrosine (increased in AZN samples), fatty acids (decreased in AZN samples) and glutamine (decreased in AZN samples).

Finally, Student's t-tests were used to compare the metabolic profiles of the wild-type to each of the QS mutants and AZN treatments in turn. These results were consistent with the multivariate analyses, showing similar changes to concentrations of tyrosine, fatty acid and glutamate. Notably, the 8 and 32 μg/mL AZN-treated samples also showed similar changes in the fatty acid peak profile as the QS mutants (Figure 3.8). Concentrations of other QS-modulated metabolites, such as tryptophan, sarcosine and formate, were not affected by AZN treatment (Figure 3.5). Several spectral peaks were specifically modulated in AZN-treated samples (that is, not modulated in QS mutants), though none of these could be confidently assigned to specific metabolites.

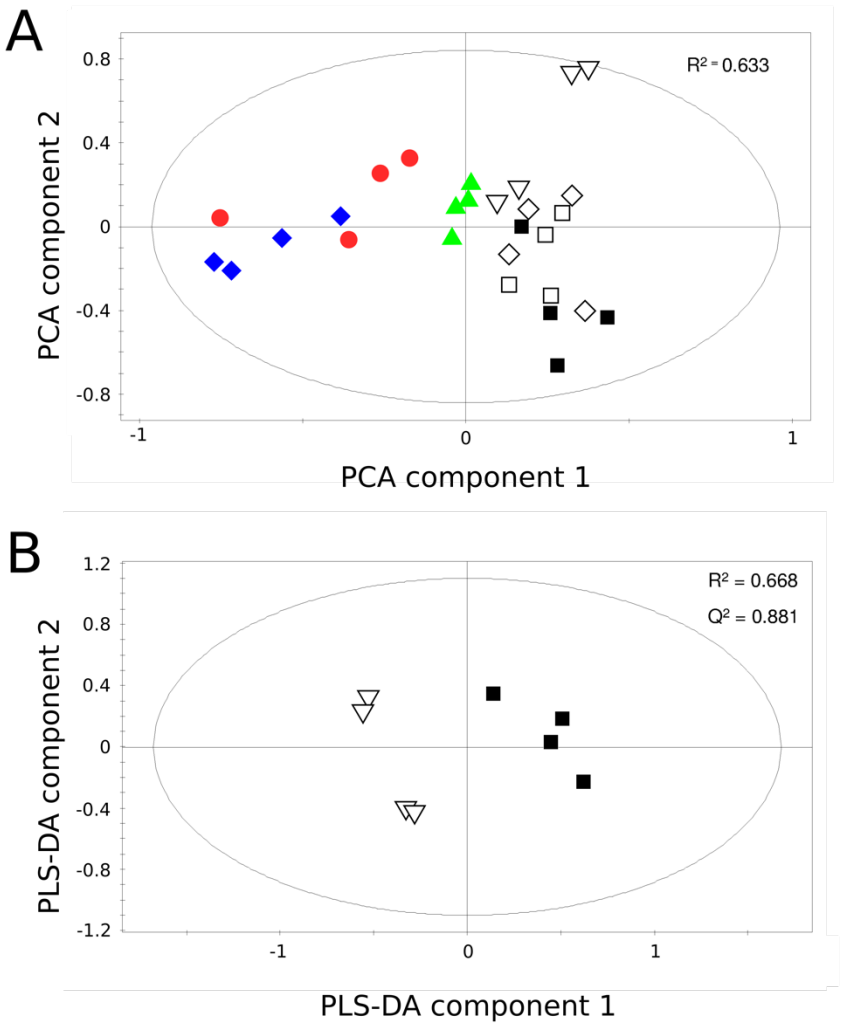

Figure 3.6 Effects of sub-MIC azithromycin apparent in ^{1}H-NMR metabolic footprints.

A) PCA plot showing separation of signalling mutants from untreated and AZN-treated PAO1 samples along component 1. B) PLS-DA plot showing separation of untreated PAO1 from 32 μg/mL AZN-treated PAO1 samples. PAO1: black squares, Δ*lasI*: red dots, Δ*rhlI*: blue diamonds, Δ*pqsR*: green triangles, 2 μg/mL AZN-treated PAO1: open squares, 8 μg/mL AZN-treated PAO1: open diamonds, 32 μg/mL AZN-treated PAO1: open inverted triangles.

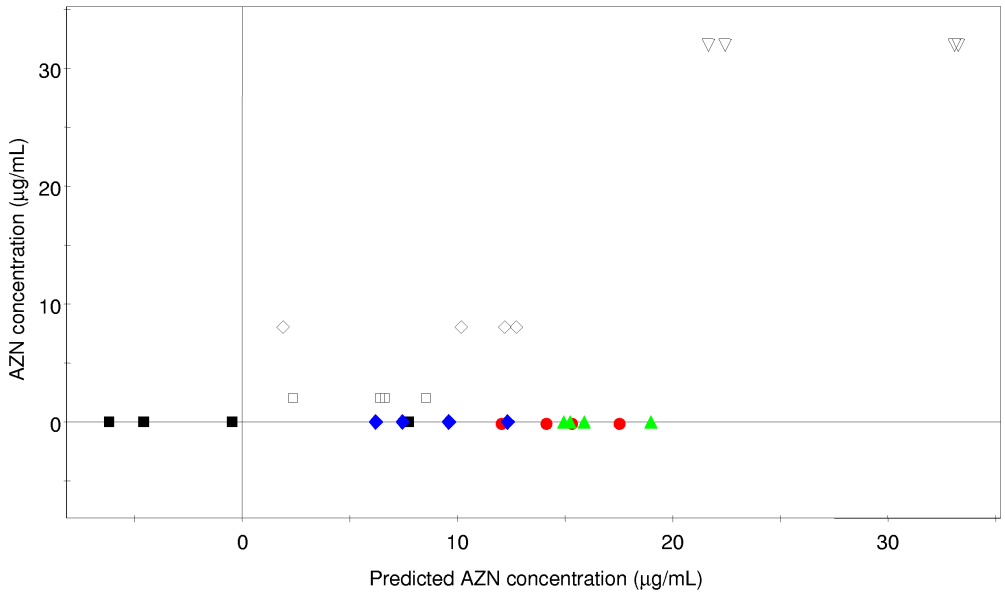

Figure 3.7 Effect of azithromycin on *P. aeruginosa* metabolic footprint is orthogonal to quorum sensing mutants.

A PLS model was built using wild-type PAO1 and AZN-treated samples, with AZN concentration as the Y variable. The model was then used to predict AZN concentrations of the signalling mutants (coloured symbols). PAO1: black squares, Δ*lasI*: red dots, Δ*rhlI*: blue diamonds, Δ*pqsR*: green triangles, 2 µg/mL AZN-treated PAO1: open squares, 8 µg/mL AZN-treated PAO1: open diamonds, 32 µg/mL AZN-treated PAO1: open inverted triangles.

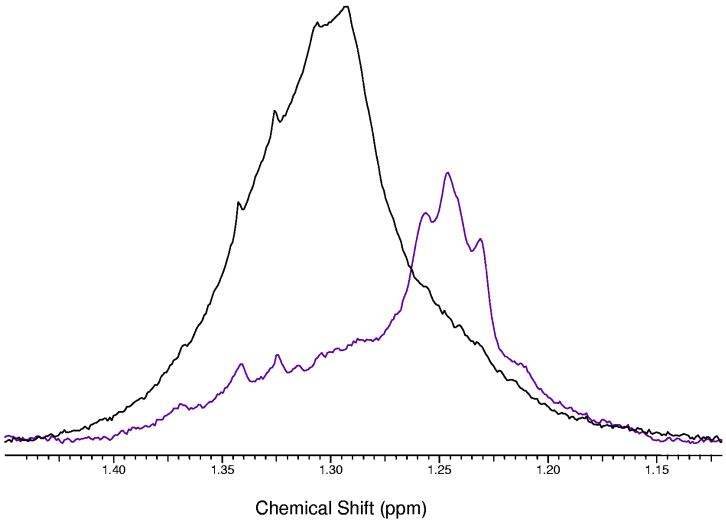

Figure 3.8 Exposure to azithromycin modulates the ^{1}H-NMR fatty acid $(CH_2)_n$ peak to lower chemical shift.

The ^{1}H-NMR resonance of saturated $(CH_2)_n$ groups is centred at lower chemical shift in AZN-treated PAO1, in a manner similar to that seen for the QS deficient *lasI*, *rhlI* and *pqsR* mutants (see Figure 3.5). PAO1: black, 32 μg/mL AZN-treated PAO1: purple.

Table 3.5 Extracellular metabolites differentially regulated in QS mutants and AZN-treated *P. aeruginosa*.

Exposure of *P. aeruginosa* to sub-MIC concentrations of azithromycin perturbs extracellular concentrations of amino acids —notably aromatic amino acids—and fatty acids. Direction of change is relative to untreated wild-type PAO1 (Student's t-test, $p < 0.05$).

		Metabolites	
Strain	AZN (μg/mL)	Up	Down
PAO1	32	tyrosine	fatty acids, glutamine
PAO1	8	tyrosine	fatty acids, glutamine
Δ*lasI*	0	tyrosine, tryptophan	fatty acids, glutamine
Δ*rhlI*	0	sarcosine, tyrosine, tryptophan	fatty acids, glutamine
Δ*pqsR*	0	formate, tyrosine	fatty acids, glutamine

3.3 Discussion

The present study found that mutants in the *las*, *rhl* and PQS systems each had a significant and distinct impact on metabolism, including changes to amino acids and fatty acids. These findings also validated ^{1}H-NMR footprinting as a tool for monitoring metabolic effects of QS: the low sample volume required and relative ease of data-processing would make it a convenient choice for experiments involving profiling large numbers of conditions, e.g. for example monitoring and comparing changes throughout the growth curve.

Biosynthesis of AHL and PQS signalling molecules branches from primary metabolism at different points. The homoserine lactone ring of AHLs originates from SAM and the acyl side chains are derived from fatty acids loaded onto acyl carrier protein (ACP). PQS is derived from anthranilate (Heurlier et al. 2006). The major metabolic effects of the *lasI*, *rhlI* and *pqsR* mutations were similar, suggesting that these perturbations were due to co-regulation of common functions by these QS systems, rather than synthesis of signalling molecules. Moreover, PQS signalling is typically activated by the *las* system and repressed by the *rhl* system; the similarity in the metabolic footprints of the *lasI*, *rhlI* and *pqsR* mutant is consistent with the *las* system dominating the regulatory hierarchy under the conditions tested. However, such interpretations come with the caveats that: i) only a portion of metabolic processes are represented in the footprint; ii) samples from only a single point in the growth curve were analysed, but the expression of AHL- and AQ-regulated genes varies significantly between different growth conditions and optical densities (Schuster et al. 2003; Déziel et al. 2004); iii) the AHL mutants used are "signal-null" whereas the *pqsR* mutant is a form of "signal-blind" mutation, in which AQ signalling is expected to be repressed but may not have been abolished.

The small number of metabolites identified in the metabolic footprints limits interpretation of specific metabolic phenotypes. However, the data does suggest several lines for further investigation. The broad fatty acid peaks observed in all samples were smaller (total area under the curve) in all three QS mutants. More strikingly, the QS mutants showed a shift in distribution of intensity between higher (1.30 ppm) to lower (1.24 ppm) chemical shift. This could reflect a variety of QS-related activities including impacts on AHL synthesis (the alkyl chains of AHLs are synthesised from the fatty acid pool), energy metabolism, membrane function and lipid metabolites such as rhamnolipids (biosurfactants proposed to be involved in motility, virulence and biofilms). The higher levels of glycero-3-phosphocholine observed in the *lasI* and *rhlI* mutant samples further suggests alterations to membrane metabolism.

Changes in glutamine concentration could reflect changes in amino acid synthesis or of its use in amino group transfer, for example as donor in the synthesis of nitrogen containing small molecule secondary metabolites such as the phenazines (e.g. aminotransfer from glutamine to chorismate in the synthesis of the phenazine precursor 2-amino-4-deoxyisochorismate). Several amino acids were modulated in the QS mutants, this may reflect changes in the rate or type of QS-regulated protein and secondary metabolite synthesis.

In a second line of investigation, the metabolic effects of sub-inhibitory concentrations of AZN were compared to those of the three QS mutants. The major metabolic impact of AZN was closely related to QS, however the reverse was not true: the major portion of QS effects were unrelated to those of AZN. These observations contradict the proposed role of AZN as a specific modulator of QS at low concentrations. The partial overlap of the metabolic profiles of AZN-treatment and QS metabolic profiles may simply reflect the association of QS with stress-responses. In this light, it would be interesting to explore the shift in fatty acid profile: is this part of a general stress response?

The present study was primarily intended as a proof-of-principle investigation for studying QS by ^{1}H-NMR footprinting. The results suggest that several areas of metabolism are perturbed in the signal mutants; these changes could be probed further by more focused metabolic profiling. Given the large perturbations observed and the small sample sizes required for analysis, these footprinting methods could be useful for tracking metabolic profiles through the growth curve, thereby facilitating the study of temporal relationships between QS and metabolism.

Chapter 4

Metabolic footprinting and open profiling of QS mutants

4.1 Introductory comments

The *rhlI* and *lasI* mutants studied in Chapter 3 had highly correlated metabolic footprints, in keeping with our understanding of their regulatory interactions and overlapping regulons. Given this regulatory integration, I chose to investigate their metabolic influence using a *lasI rhlI* double mutant. Using this design, the metabolic roles of the *las* and *rhl* systems can be revealed by comparison with the wild-type and by chemical complementation with BHL and OdDHL.

Aims and objectives: To characterise QS activity and the associated metabolic activity of wild-type PAO1 and a *lasI rhlI* mutant in batch culture. QS activity will be assessed by measurement of i) BHL and OdDHL using cellular biosensor assays, ii) the transcriptional activity of canonical QS-regulated promoters, using *lacZ* transcriptional fusion assays. The global metabolic status of the bacteria will be assessed using i) ^{1}H-NMR metabolic footprinting at hourly intervals, ii) MSTFA-GCMS analysis of aqueous cell extracts, iii) LCMS-based analysis of the cellular proteome.

Part of this work has been published as an original research article in the Journal of Bacteriology (Davenport et al. 2015). Proteomic analysis was performed at the Cambridge Centre for Proteomics (CCP, UK) with advice and assistance from Prof. Kathryn Lilley: LC-MS analysis and peptide identification was performed by Svenja Hester; all other steps including sample preparation, iTRAQ labelling and data analysis was performed by Peter Davenport.

4.2 Results

4.2.1 Generation and verification of a *lasI rhlI* double mutant

Beatson et al. (2002) reported that mutations in *lasI* and *rhlI* select for secondary mutations in *vfr* and *algR* respectively, resulting in pleiotropic phenotypes including deficiency in twitching motility (Beatson et al. 2002). This illustrates the importance of minimising the opportunity for selection of secondary mutations. In order to ensure that the *lasI rhlI* mutant was otherwise isogenic with its wild-type progenitor a 'fresh' mutant was constructed using suicide plasmids. This was achieved first by generating *lasI* and *rhlI* mutants by marker exchange as described in (Beatson et al. 2002), then transducing these mutations (separately) into a wild-type strain to generate a *lasI rhlI* mutant with insertional inactivations of both the *lasI* and *rhlI* signal synthase genes.

4.2.2 Planktonic growth of a *lasI rhlI* mutant

Cultures of the (phage-transduced) *lasI rhlI* mutant and its wild-type progenitor were grown aerobically in AGSY growth medium. This growth medium has previously been used to characterise planktonic, colony and biofilm growth of *P. aeruginosa,* providing useful reference data for the physiological state of the bacterium under these conditions (Mikkelsen et al. 2007).

The growth profile of the wild-type in AGSY exhibited no obvious lag phase and grew exponentially (growth rate [μ] = 1.12 h^{-1}) between 0 and 3 hours before decelerating between 3 and 5 hours (idiophase) to approximately linear growth, which continued from 5 hours until the end of observation at 10 hours (Figure 4.1). Notably, the wild-type cultures turned bright green between 3 and 5 hours, indicative of accumulation of the QS-regulated exoproduct pyocyanin, whereas the mutant cultures showed no such colour change and remained grey-brown throughout.

The growth of the *lasI rhlI* mutant matched that of the wild-type during the exponential phase (0-3 h) and the linear phase (5-10 h), but was faster during the intervening 2-hour deceleration phase (3-5 h). Consequently, after 5 hours' growth the mutant had reached an

18% higher optical density, which it maintained (+/- 5%) for the remainder of observations (Figure 4.2).[2]

Viable cell counts were performed at 3 and 6 hours' growth to account for the possibility that the observed differences in optical density were due to differences in cell morphology or other optical effects distinct from growth rate *per se* (for example accumulation of cell debris or cell exoproducts) (Figure 4.3). At 3 h, no difference was observed, whereas at 6 h cell counts for the mutant were 15% higher than for the wild-type ($P \leq 0.05$, Student's t test), consistent with the mutant growing faster than the wild-type at the end of the exponential growth phase.

The growth advantage of the *lasI rhlI* mutant is limited to a short period during the transition from exponential to stationary phase growth. Previous studies in rich media have found that most genes in the *las* and *rhl* regulons are upregulated during this period (Schuster et al. 2004*a*).

[2] The *lasI rhlI* mutant had a higher optical density than the wild-type at each time point from 5 to 10 h ($P \leq 0.05$ Student's t test).

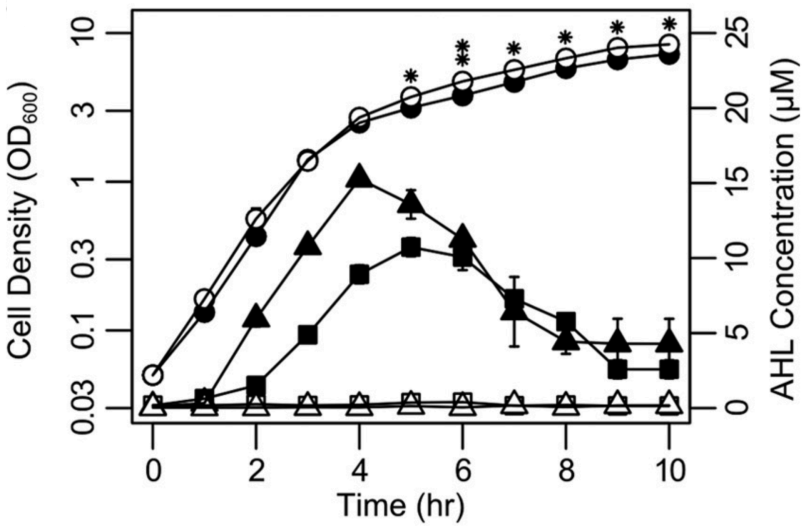

Figure 4.1 *P. aeruginosa* and *lasI rhlI* mutant growth curves and AHL profiles.

Growth characteristics of wild-type PAO1 and a *lasI rhlI* mutant strain of *P. aeruginosa.* Growth of the wild-type (filled symbols) and mutant (open symbols) was monitored in AGSY medium. Samples were removed at the indicated times and assayed for OD_{600} (circles), OdDHL (triangles) and BHL (squares). No significant differences in optical density were found during exponential phase growth (1-3 hours, p<=0.05, Student's t-test or ANCOVA). A small but significant difference growth between the wild-type and *lasI rhlI* mutant is apparent following a deceleration in growth between 3 and 4 hours: this was assessed by Student's *t* tests (indicated by asterisks in (a), * *p*<=0.05, ** *P*<=0.01) and by ANCOVA (p<=0.001, Tukey's HSD, considering data between 5 and 10 hours). Error bars represent standard deviations of means.

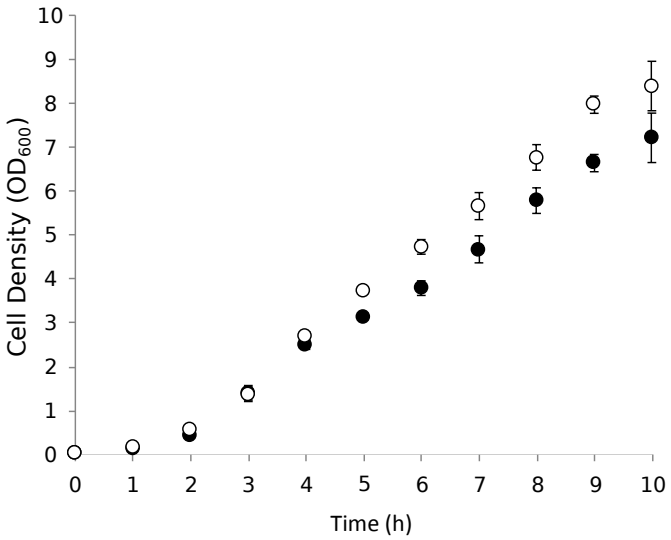

Figure 4.2 *P. aeruginosa* growth curves plotted to a linear scale.

Growth of wild-type (filled symbols) and *lasI rhlI* mutant (open symbols) plotted on a linear optical density scale. The growth rate of the wild-type decreases relative to that of the mutant between 4 and 5 hours.

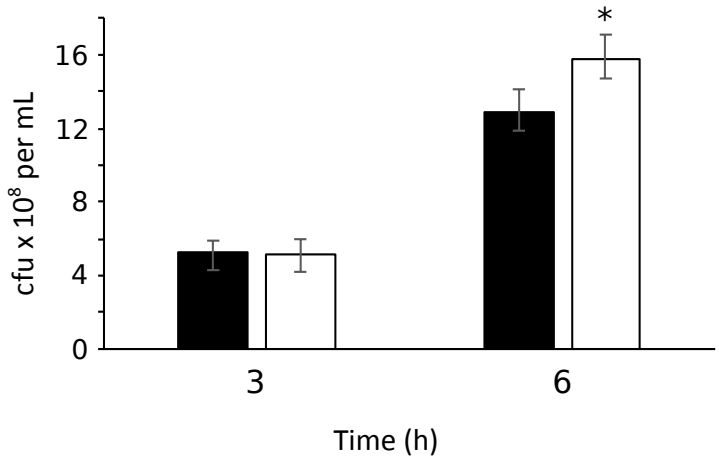

Figure 4.3 Viable cell counts of wild-type PAO1 (black bars) and *lasI rhlI* mutant (white bars) sampled at three and six hours' growth.

Cultures of the *lasI rhlI* mutants grew to higher densities of viable cells, consistent with optical density measurements (see Figure 4.1 and Figure 4.2).

4.2.4 AHL concentrations during planktonic growth

Canonical QS-regulatory functions were characterised by measuring the concentrations of AHL signal molecules and the promoter activities of the QS-regulated genes *lasB* and *rhlA*. This data provides benchmarks for the timing of AHL signalling activity under the present growth conditions.

The concentrations of BHL and OdDHL were measured using *E. coli* biosensors assays. The BHL biosensor strain *E. coli* JM109(pSB536), contains the *Aeromonas hydrophila ahyR* gene and the cognate *ahyI* gene promoter fused to the *luxCDABE* luminescence operon (Swift et al. 1997). The resulting biosensor luminesces in response to addition of exogenous BHL. The OdDHL biosensor strain JM109(pSB1075) contains the *lasRI'* regulatory region of *P. aeruginosa* fused to *luxCDABE* so that the biosensor expresses the luminescence operon in response to OdDHL (Winson et al. 1998). To provide quantitative analyses of AHL concentrations in culture supernatant these biosensor assays were first calibrated using standard curves of synthetic AHL standards in fresh growth medium.

As expected, OdDHL and BHL were only detected in wild-type culture supernatants and not in those of the *lasI rhlI* mutant. In wild-type culture supernatants OdDHL peaked after 4 h growth at 15 μM, then steadily declined to below 0.1 μM over the following 4 h (Figure 4.1). Similarly, the concentration of BHL peaked after 5 h growth at 11 μM, then decreased to below 0.1 μM. Such drops in AHL concentrations following exponential growth in batch culture have been linked to alkalization of the growth medium and consequent lactonolysis (Yates et al. 2002). Under our growth conditions the pH of both wild-type and *lasI rhlI* mutant culture supernatants increased from pH 7.0 at 0 h to pH 8.4 at 10 h, sufficiently alkaline to induce lactonolysis. These results indicate that AHL profiles in AGSY during batch culture are qualitatively similar to those in other rich media, including LB.

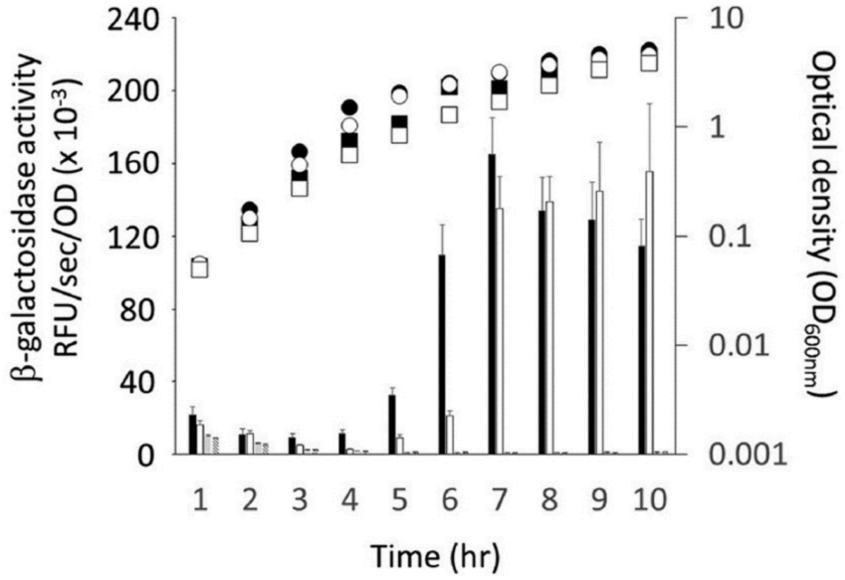

Figure 4.4 Timing of AHL QS-regulated *lasB* and *rhlA* promoter activity.

Promoter activity was measured as β-galactosidase activity encoded by pβ01 (the P_{lasB} reporter) and pβ02 (the P_{rhlA} reporter). β-Galactosidase activity symbols: black bars, *P. aeruginosa* PAO1 carrying pβ01; white bars, PAO1(pβ02); stippled bars, *lasI rhlI* mutant carrying pβ01; hatched bars, *lasI rhlI* mutant(pβ02). Growth curve symbols: filled circles, PAO1(pβ01); filled squares, PAO1(pβ02); open circles, *lasI rhlI* mutant(pβ01); open squares, *lasI rhlI* mutant(pβ02).

4.2.5 Activities of QS-responsive promoters

Quorum sensing is a transcriptional regulatory mechanism. To examine the dynamics of the canonical quorum sensing transcriptional regulon, I measured the promoter activity of *lasB* and *rhlA*, genes whose expression is primarily dependent on OdDHL and BHL, respectively. I used pQF50-based *lacZ* reporter constructs: pβ01 to measure P_{lasB} promoter activity and pβ02 to measure P_{rhlA} activity (Farinha and Kropinski 1990; Ikeda et al. 2001). These reporter plasmids were transformed into the wild-type and *lasI rhlI* mutant and grown with antibiotic selection for plasmid maintenance.

In the wild-type, P_{lasB} activity increased rapidly between 4 and 6 h growth and P_{rhlA} activity increased rapidly between 5 and 7 h of growth (Figure 4.4), consistent with the accumulation of OdDHL and BHL, respectively. In contrast P_{lasB} and P_{rhlA} promoter activities were negligible in the *lasI rhlI* mutant. Again, these results are qualitatively similar to observations in other rich media batch growth conditions.

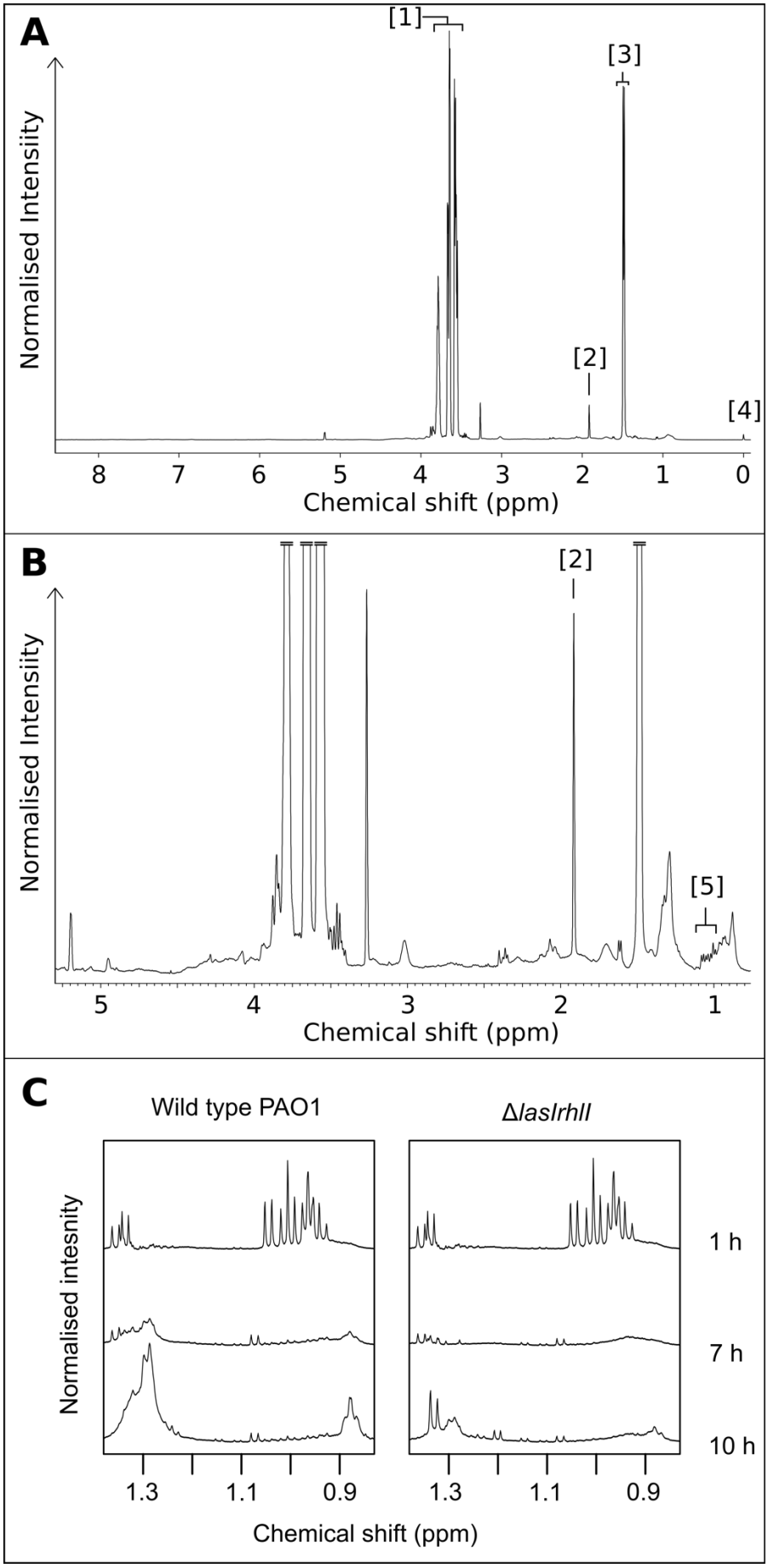
A
[1]
[3]
[2]
[4]
Normalised Intensiity
8
7
6
5
4
3
2
1
0
Chemical shift (ppm)
B
[2]
[5]
Normalised Intensiity
5
4
3
2
1
Chemical shift (ppm)
C
Wild type PAO1
ΔlasIrhII
Normalised intesnity
1 h
7 h
10 h
1.3
1.1
0.9
1.3
1.1
0.9
Chemical shift (ppm)

Figure 4.5 Uptake of nutrients and secretion of secondary metabolites is observable in ^{1}H-NMR spectra of bacterial supernatants.

A representative ^{1}H-NMR spectrum of *lasI rhlI* mutant culture supernatant sampled after 7 hours growth is displayed at two scales: the full spectrum (0–8.5 ppm) in panel A, and an enlarged portion of the same in panel B ([1] = glycerol, [2] = acetate, [3] = alanine, [4] = TSP, [5] = valine). Panel C presents sections of the ^{1}H-NMR spectra (0.8-1.4 ppm) of spectra of wild-type *P. aeruginosa* and the *lasI rhlI* mutant, illustrating differerential utilisation and excretion of metabolites between the two strains.

4.2.6 NMR Footprinting: nutrient uptake and acetate overflow

Experiments described in Chapter 2 indicated that perturbation of QS can have widespread effects on central metabolism. To understand how these metabolic effects relate to the timing of canonical QS functions, the exometabolomes of the wild-type and *lasI rhlI* mutant were compared at hourly intervals throughout growth: Cell-free supernatants from each strain were collected from 0-10 h and analysed by ^{1}H-NMR spectrometry.

As per data presented in Chapter 3, the ^{1}H-NMR-visible metabolic profiles of the two strains were similar early in growth, then diverged as the cultures aged. Example spectra taken at 1, 7 and 10 hr growth are shown in **Error! Reference source not found.**. To identify latent patterns in these data, I used Principal Components Analysis (PCA) (Kell et al. 2005). This revealed that the "metabolic footprints" of the wild-type and QS mutant were essentially indistinguishable until 5 h of growth (Figure 4.6), corresponding to peak AHL concentrations in wild-type cultures. The metabolic footprints of the two strains diverged from this point onwards, this is particularly evident in principal components 2 and 3 as shown in Figure 4.6b and c.

Inspection of the PCA loadings, which underlie the PCA scores shown in Figure 5, revealed that this divergence between hours 5 to 7 is due to the mutant showing i) higher uptake of nutrients including alanine, glycerol and valine, and ii) increased production of extracellular acetate (Figure 4.7). Considering that the mutant simultaneously achieved a higher growth rate than wild-type during this period, this suggests that the QS mutant assimilated carbon more efficiently. The *las* and *rhl* systems are known to upregulate the expression of many secreted factors in early stationary phase (Nouwens et al. 2003). Lower efficiency of carbon assimilation by the wild type could be explained by QS-dependent diversion of cellular resources towards secreted factors. However, this would account for differences in outputs (re growth yield and acetogenesis) and would not prima facie explain differences in inputs

(re uptake of nutrients). This suggests that AHL QS induces a considerable rewiring of central metabolism during the transition to stationary phase growth.

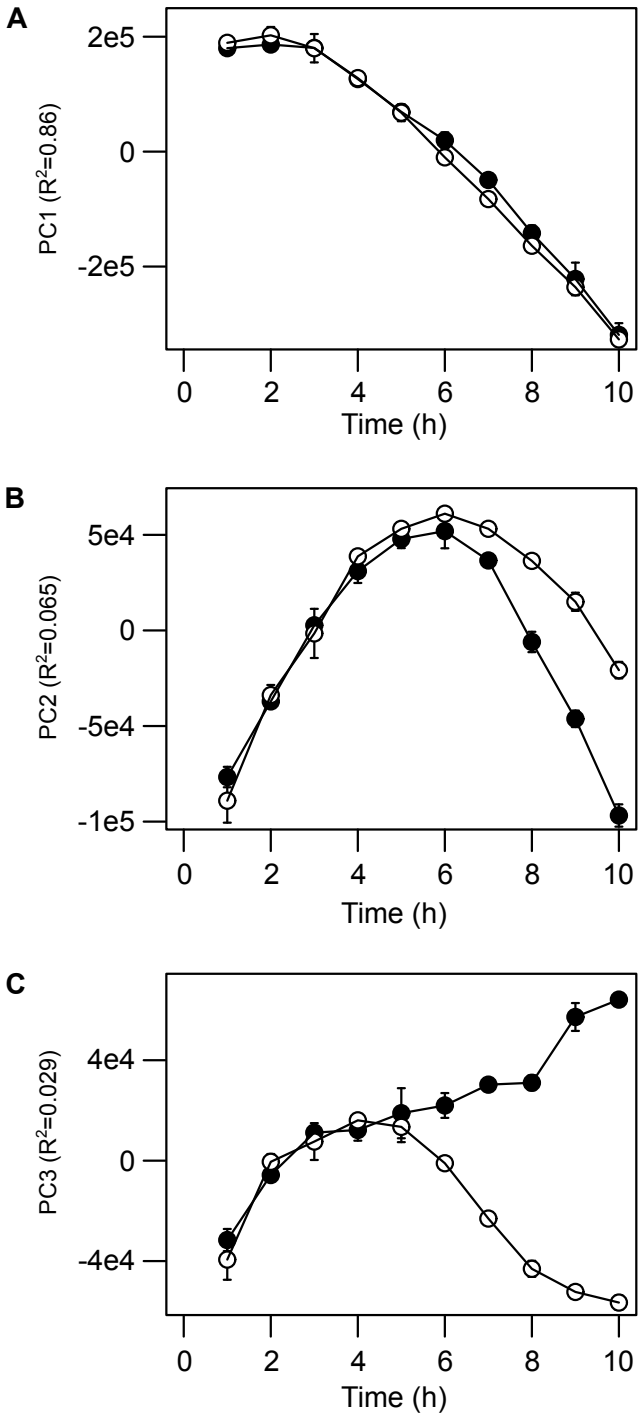

Figure 4.6 ^{1}H-NMR footprints of *lasI rhlI* mutant diverge from wild-type after 5 h growth.

^{1}H-NMR data were analysed using Principal Components Analysis. Wild-type (filled symbols) and *lasI rhlI* mutant (open symbols).

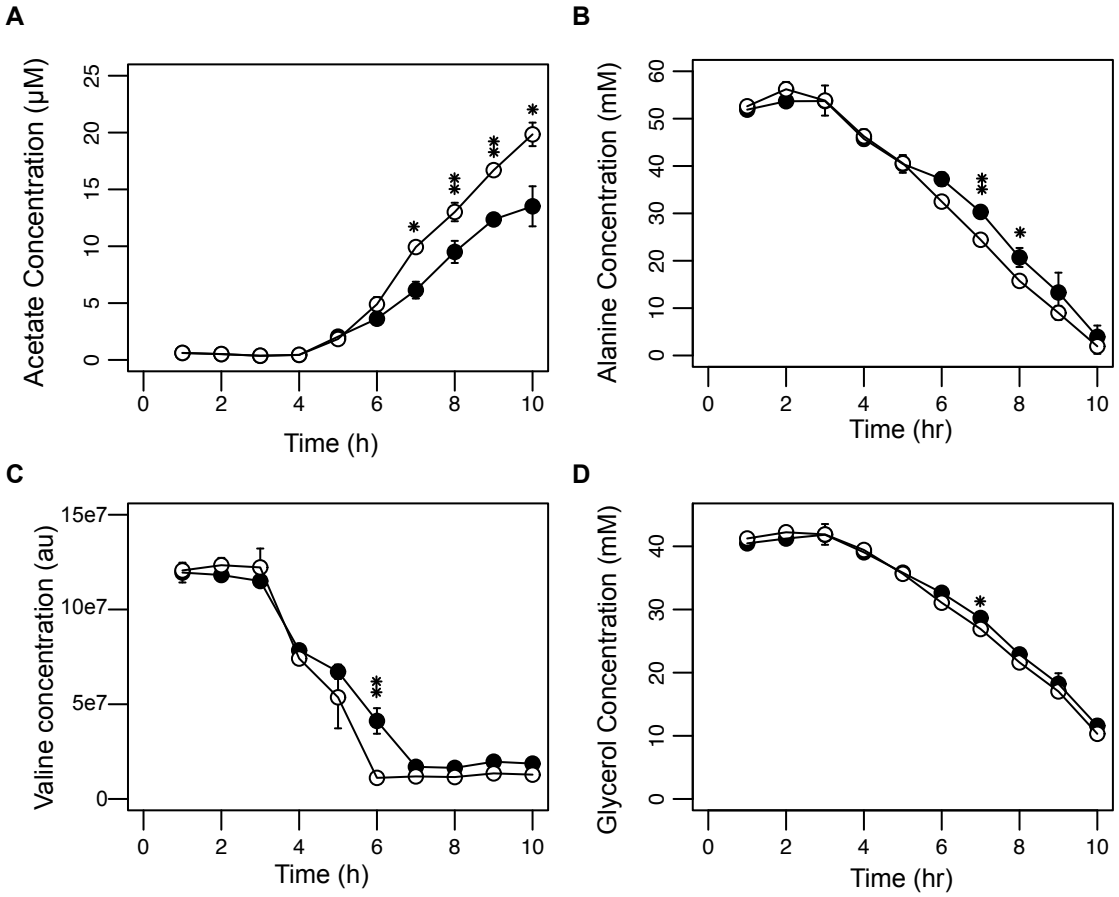

Figure 4.7 Differential accumulation and depletion of metabolites monitored by ^{1}H-NMR.

Wild-type (filled symbols) and *lasI rhlI* mutant (open symbols).

4.2.7 Cellular metabolite profiling: perturbations to central metabolism

To explore the cellular basis of the divergence in metabolic footprints, aqueous fractions of methanol-chloroform cell extracts were analysed by GC-MS. Metabolites in cell extracts were derivatised using MSFTA prior to separation and analysis by GC-MS. Bacterial cultures were grown as previously and samples were taken at ODs of 1.5, 2.5, 4.5, and 6.5, corresponding to 3h, 3h50, 5h30 and 7h40 for the wild-type and 3h, 4h, 6h30 and 8h50 for the *lasI rhlI* mutant. The sampling points were based on optical density measurements (rather than time) to account for differences in growth rates between the bacterial strains and were chosen to bracket the initial point of divergence in the metabolic footprints, which occurred at an OD of ~3.

Consistent with the footprinting data, the cellular metabolic profile of the mutant was essentially identical to that of the wild-type at early sampling points (OD 1.5 and 2.5), whereas by OD 4.5 the concentrations of one third of the 90 metabolite peaks were

perturbed (Table 4.2). Metabolites from all major domains of metabolism were modulated: central carbon, amino acid, nucleic acid, fatty acid and membrane metabolism. Of the metabolic changes identified, the following themes were particularly notable.

Many sugars or sugar-phosphates were perturbed in the *lasI rhlI* mutant. Notably, citrate and malate concentrations were both higher in the *lasI rhlI* mutant at OD 4.5 and by OD 6.5 other tricarboxylic acid (TCA) cycle intermediates, such as succinate and fumarate, were also elevated in the mutant. The TCA cycle is a central hub of metabolism, oxidizing carbon sources and providing anabolic precursors for biosynthesis. Depletion of TCA intermediates in the wild-type may be due to allocation of cellular resources to AHL-induced secreted factors and also help explain the temporary growth deficit relative to the mutant. Levels of sn-glycerol-3-phosphate were 27-fold higher in the mutant at OD 4.5 and 3-fold higher at OD6.5. Differences between the strains in rates of uptake of nutrients such as alanine and glycerol are not sufficient to account the differences in sn-glycerol-3-phosphate, suggesting there is a bottleneck in glycerol assimilation in the *lasI rhlI* mutant, especially during early stationary phase.

The GC-MS measurements also indicated that amino acid and polyamine metabolism is affected in the mutant; nine of twenty-two amino acid metabolites detected were perturbed at OD 4.5. The concentrations of the aromatic amino acids phenylalanine and tyrosine were higher in the mutant at both OD 4.5 and 6.5. These aromatic amino acids share precursors from the shikimic acid pathway with QS-regulated factors including phenazines and quinolones. There were several indicators of perturbed polyamine metabolism: concentrations of putrescine (four-fold by OD4.5), arginine (two-fold by OD6.5) and ornithine (four-fold by OD6.5) were elvated in the mutant.

The concentrations of several metabolites involved in AHL metabolism were perturbed: methionine, adenine, ribose and fatty acids are all linked to AHL synthesis or degradation (Heurlier et al. 2006). Levels of adenine and methionine in the mutant were 60-70% of wild-type at OD4.5, whereas ribose concentrations were almost double wild-type levels. Methionine, adenine and ribose are involved in the synthesis and salvage of S-adenosyl-methionine (SAM), the precursor of the homoserine lactone ring of BHL and OdDHL.

The concentrations of six out of the seven fatty acids detected by GC-MS analysis were perturbed in the *lasI rhlI* mutant relative to the wild type at OD 4.5 and/or OD 6.5: levels of 2-hydroxypentanedioic were up to 5-fold higher in the mutant, whereas levels of 3-hydroxydecanoic acid, hexadecanoic acid, octadecanoic acid, nonanoic acid were reduced by at least 50%. The concentration of a monounsaturated fatty acid that was not

unambiguously identified was also lowered in the mutant. These data indicate that fatty acid metabolism is markedly altered in the *lasI rhlI* mutant during stationary phase growth.

4.2.8 Cellular proteomics

Coverage of PAO1 proteome

Differences in protein abundance in the wild-type and *lasI rhlI* mutant were measured using a mass-spectrometric iTRAQ approach. Bacterial cultures were sampled at OD1.5 and OD4.5 in order to straddle the divergence in cellular metabolism identified by profiling small molecules. In total 931 proteins were identified accounting for 17% of PseudoCAP CDS annotations (Winsor et al. 2009). This is comparable in coverage to previous proteomic studies of *P. aeruginosa*, for example that of Arevalo-Ferro et al., who detected 986 protein spots in an "intracellular" fraction analysed by PAGE (Arevalo-Ferro et al. 2003)[3]. The coverage of the proteome showed bias according to protein localisation. Cytoplasmic and periplasmic proteins are overrepresented whereas membrane-associated proteins are underrepresented (Figure 4.8). More highly expressed proteins such as ribosomal subunits were better represented compared with proteins with typically lower or condition-specific expression profiles (Figure 4.9).

Principal Components Analysis and Principal Least Squares analysis were performed to gauge the co-clustering of samples and to identify major trends in the data (Figure 4.10). The major trends correlate with growth phase (Principal Component 1) and the genotypic effect is evident as the second largest trend (Principal Component 2). This was supported by Principal Least Squares analysis using genotype and optical density as independent ("Y") variables. Univariate analysis of proteins expression levels yielded similar patterns to the mulativariate analyses: This indicated that even at OD 1.5, 28% of proteins were significantly modulated in the mutant relative to the wild-type and that this increased to 52% at OD 4.5 (Table 4.1). At a false discovery threshold of 10%, 6 proteins were modulated in the mutant at OD 1.5 and 96 proteins at OD 4.5.

[3] The number of gel-spots is an overestimate of the number of primary protein sequences detected, due to the influence of post-translational modifications on protein mobility.

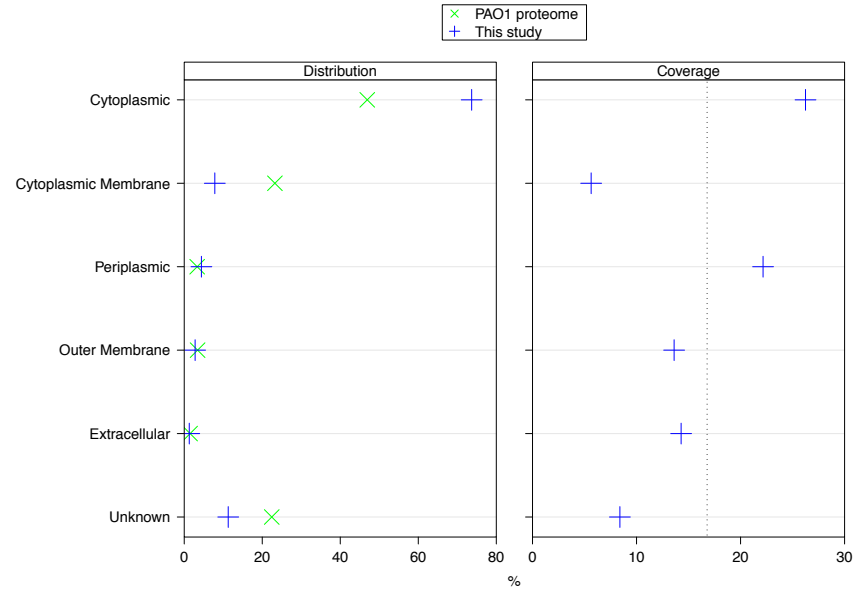

Figure 4.8 Cellular distribution of proteins detected by tandem mass spectrometry.

The left panel illustrates the subcellular localisation of proteins. The right panel illustrates coverage of proteins in each subcellular local by this study. The dotted line in the right-hand panel indicates the global coverage by this study of the PAO1 proteome (17%).

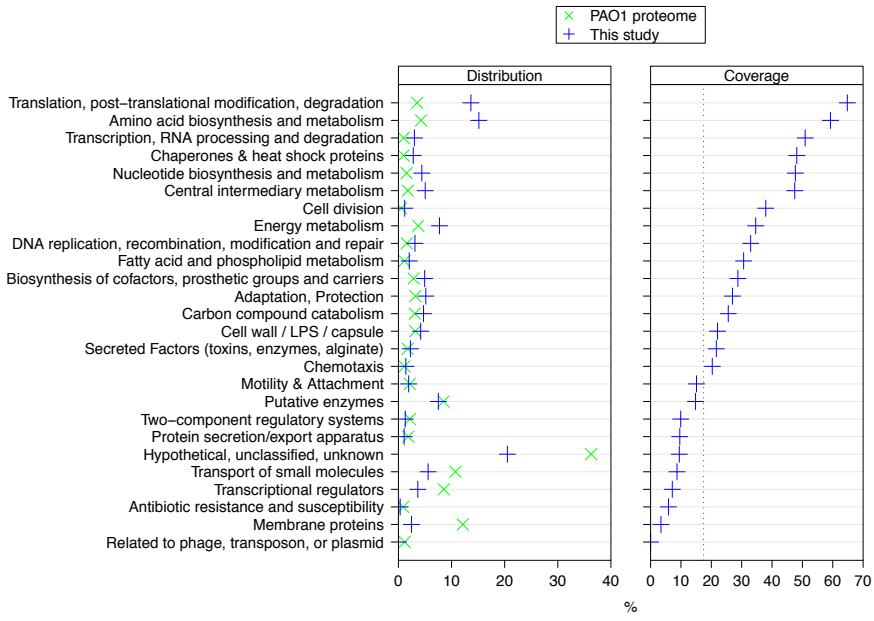

Figure 4.9 Functional distribution of proteins detected by tandem mass spectrometry.

The dotted line in the right-hand panel indicates the global coverage by this study of the PAO1 proteome (17%).

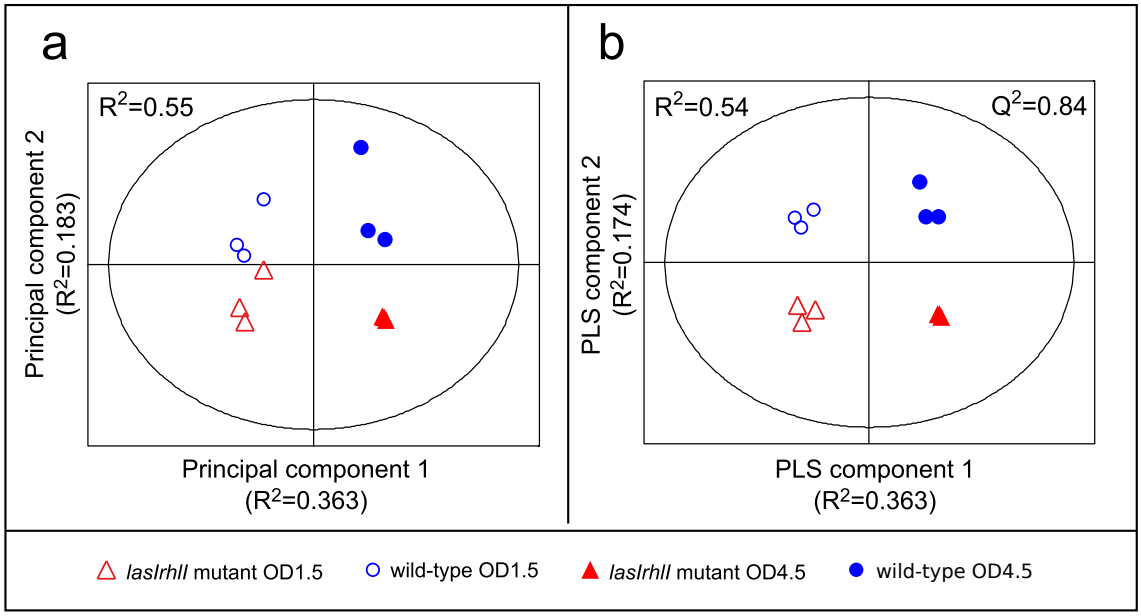

Figure 4.10 Multivariate analyses of iTRAQ proteomic data.

Principal Components Analysis (a) and Partial Least Squares Discriminant Analysis (b) illustrate that all four sample types cluster with no outliers and that growth phase is the largest trend in the data, followed by genotype.

Table 4.1 Total numbers of proteins significantly modulated in the *lasI rhlI* mutant relative to wild-type PAO1.

Bracketed figures indicate the number of proteins downregulated in the mutant. Student's t-tests were performed to calculate *p*-values. These were used to calculate *q*-values using Storey's method so as to control the overall False Discovery Rate. $1-\hat{\pi}_0$ is Storey's estimate of the portion of significantly modulated proteins (true alternative hypotheses) (Storey et al. 2004).

	Growth phase effect	
Significance test	OD 1.5	OD 4.5
p <= 0.01	26 (11)	60 (18)
q <= 0.05	4 (1)	59 (17)
q <= 0.1	6 (3)	96 (36)
$1-\hat{\pi}_0$	0.28	0.52

Slowed growth, adaptations to oxygen limitation and oxidative stress

The most striking difference between the two strains during early stationary phase (OD 4.5) relates to mechanisms of protein synthesis and degradation (Table 4.3). Of the 60 proteins upregulated in the mutant during early stationary phase, 26 were linked to these functions, including ribosomal proteins, elongation factors, initiation factors and ribosomal RNA processing enzymes. Levels of both the core RNA polymerase beta' subunit and of the exponential phase sigma factor RpoD were over 40% higher in the mutant. Enzymes involved in biosynthesis of purines (PurK) and pyrimidines (CTP synthase PyrG) were downregulated in the wild-type. These changes to protein expression are all consistent with the slower growth rate of the wild-type.

The *lasI rhlI* mutant also showed lower expression of arginine deiminase (ArcA), catalase (KatA), nitrite reductase (NirS, cytochrome cd1) and azurin (a nitrite reductase redox partner). These are all regulated by the redox regulator Anr and are induced in response to oxygen depletion (Trunk et al. 2010). Arginine deiminase is essential for arginine fermentation, which provides energy during the transition to anaerobiosis and also contributes to longer term anaerobic survival (Schreiber et al. 2006; Trunk et al. 2010). Carbamoyl phosphate synthetase (CarB) and argininosuccinate lyase (ArgH) (which catalyse the first and final reactions in arginine biosynthesis from glutamine, respectively) were also both downregulated in the wild-type, suggesting a coordinated downregulation of arginine biosynthesis alongside induction of arginine fermentation. Nitrite reductase catalyses the reduction of nitrite to nitric oxide (NO) during the denitrification pathway and is also important in protecting against nitrite-dependent oxidative damage (Scoffield and Wu 2016). Nitrite reductase expression is induced under microaerobic conditions, prior to other enzymes involved in denitrification and this early expression may be important in preparing cells for full expression of denitrification pathways upon exposure to nitrate, nitrite or NO (Alvarez-Ortega and Harwood 2007; Kuroki et al. 2014). In addition to its role in detoxification of hydrogen peroxide generated during aerobic respiration, catalase is induced under anaerobic conditions and is important in protecting the cell from the toxic effects of NO during anaerobic respiration (Su et al. 2014). These patterns in protein expression are consistent with a QS-dependent advance in growth arrest and activation of adaptations to growth in oxygen-depleted environments.

Notably, the two most highly upregulated proteins in the wild-type are involved in the biosynthesis of the siderophores pyochelin and pyoverdine (pyochelin biosynthesis protein PchD and pyoverdine biosynthesis protein PvdA). Pyoverdine has previously been shown

to be induced by AHL QS (Brint and Ohman 1995; Winson et al. 1995; Hentzer et al. 2003). Production of siderophores is regulated in response to as oxidative stress as well as iron availability (Cornelis et al. 2011). Low availability of iron can limit the function of iron-containing proteins, some of which are provide protective functions against oxidative stress (e.g. catalase). Furthermore, ROS can damage such iron sulphur centres. On the other hand, higher concentrations of unbound iron can increase oxidative damage by generating ROS via the Fenton reaction. Increased siderophore biosynthesis in the wild-type again points towards protection against oxidative stress.

Regulation of the TCA cycle and glyoxylate shunt

Several enzymes involved in central carbon metabolism were also differentially regulated in the *lasI rhlI* mutant. The TCA cycle enzymes citrate synthase (GltA), succinate dehydrogenase (SdhA) and isocitrate dehydrogenase (Idh) are upregulated in the mutant. This is consistent with higher levels of TCA metabolites (citrate, succinate, fumarate, malate) observed by GC-MS and a greater flux through the TCA cycle. In contrast isocitrate lyase (AceA), which catalyses the first step in the glyoxylate shunt is downregulated. Relative flux through the glyoxylate shunt and the oxidative CO_2-evolving portion of the TCA cycle is controlled by competition between Idh and AceA for their common substrate isocitrate. The ratio of AceA to Idh levels is 3-fold higher in the wild-type, it therefore seems that while the TCA cycle as a whole is repressed in the wild-type, the glyoxylate shunt is activated. The glyoxylate shunt is an anaplerotic pathway that bypasses the NADH/NADPH and CO_2 producing steps of the TCA cycle; it is the first step leading to gluconeogenesis as well as being used for assimilation of acetyl-CoA, derived for example from acetate re-uptake or fatty acid degradation (Cozzone 1998; Martínez-Gómez et al. 2012). Induction of the glyoxylate shunt has been shown to be important under conditions of oxidative stress, antibiotic stress, and host infection (Dunn et al. 2009; Ahn et al. 2016). The only TCA cycle enzyme to be downregulated in the mutant was fumarate hydratase (FumC1; to 25% of wild-type levels). FumC1 encodes a superoxide resistant fumarase that also participates in mixed acid fermentation and anaerobic respiration. It belongs to the same operon as superoxide dismutase SodA and its expression is induced in response to low iron or oxidative stress (Polack et al. 1996; Vinckx et al. 2011). Interestingly, FumC1 was one of the few proteins to be differentially regulated during exponential growth, suggesting it may be part of an early metabolic response to AHL QS. Levels of AceF, a subunit of the pyruvate dehydrogenase complex, were 30% lower in the mutant. The significance of this is unclear

but is likely linked to restructured fermentative processes and acetate metabolism, since the mutant generates higher levels of extreted acetate.

Interestingly the sigma factor RpoN is downregulated by over 90% in the wild-type. Early work identified its functions in regulating nitrogen assimilation, motility and cell adhesion, however RpoN has subsequently been found to negatively regulate genes involved in siderophore biosynthesis, the glyoxylate shunt (*aceA*), resistance to antibiotics and quorum sensing (Heurlier et al. 2003; Viducic et al. 2007; Hagins et al. 2010; Damron et al. 2012). Although the transcriptional regulatory mechanisms of RpoN are not well understood, they seem to depend on the stringent response via ppGpp concentrations, suggesting it is involved in navigating transitions to less favourable environmental conditions (Szalewska-Palasz et al. 2007). The present data suggests that RpoN downregulation plays a role in the metabolic response to QS during slowed growth.

4.3 Discussion

For *P. aeruginosa* grown in AGSY medium, deceleration from exponential growth occurred between 3 and 5 h, and was followed by consistent linear growth from 5 h to 10 h. The onset of linear growth (between 4 and 5 h) coincided with accumulation of acetate in the culture supernatant; given that high concentrations of alanine and glycerol remained in the growth medium at this time (>35 mM), this is consistent with acetogenesis induced by oxygen limitation (Wolfe 2005). Acetogenesis occurs when the influx of reduced carbon exceeds the catabolic capacity of the TCA cycle and that of other central metabolic pathways; this can occur when oxygen is limited or with high concentrations of highly assimilable carbon. Conversion of acetyl-CoA to acetate by phosphate acetyltransferase (PTA) and acetate kinase (AK) yields ATP and recycles coenzyme A (CoASH), thereby relieving CoASH bottlenecks (e.g. at 2-ketoglutarate dehydrogenase) and supporting faster growth rates (El-Mansi 2004). Acetogenesis can also occur via the pyruvate oxidase (PoxB), which catalyses the oxidative carboxylation of pyruvate directly to acetate, reducing flavin adenine dinucleotide and producing CO_2. Like the PTA-AK pathway, PoxB activity seems to be important under oxygen limiting conditions and may be particularly important under microaerophilic conditions (Wolfe 2005). Under the present growth conditions, it seems that oxygen supply became limiting once the bacterial population reached an optical density of ~2 (3 h), resulting in reduced growth rate and induction of acetogenic overflow.

Metabolic footprinting indicated that the metabolism of the *lasI rhlI* mutant diverged from the wild-type as the growth rates of both strains slowed. Moreover, the growth of the wild-type slowed faster than that of the *lasI rhlI* mutant and this coincided with increased activity of the *las* and *rhl* QS systems in the wild-type strain, as measured by concentrations of OdDHL and BHL and by transcription from *lasB* and *rhlA* promoters. Consistent with its reduced growth rate, levels of factors involved transcription, translation and nucleotide biosynthesis were depressed in the wild-type.

How might QS slow growth? One explanation for the reduced growth rate of the wild-type is QS-directed allocation of biomass and energy towards biosynthesis of secreted factors That QS-regulated products are metabolically costly and are likely to impose an energetic burden on the producer was illustrated by Sandoz et al., who cocultured wild-type *P. aeruginosa* and a *lasR* mutant under conditions in which QS-dependent extracellular proteases are required for growth (Sandoz et al. 2007); the *lasR* mutant (which could exploit the secreted proteases—"public goods" made by the wild type) grew approximately 60% faster than its wild-type counterpart. The redirection of metabolic resources away from central metabolism and toward QS-dependent biosynthesis may, in part, explain why the wild type was more depleted of TCA cycle intermediates compared with the *lasI rhlI* mutant.

However, the wild-type displayed patterns of metabolite and protein levels associated with not just slowed growth, but adaptation to microaerobiosis, suggesting that effects of QS on primary metabolism beyond simple diversion of biomass towards synthesis of secreted products: in addition to TCA cycle intermediates and enzymes being downregulated in the wild-type, enzymes responsible for the glyoxylate shunt and arginine fermentation were elevated. Elevated levels of catalase and the siderophores pyoverdine and pyochelin are also linked to protection from oxidative stress. These changes are typical of growth under oxygen limiting conditions and imply that wild-type QS directs precocious adaptation to microaerobiosis.

An additional consideration is that QS-mediated changes to primary metabolism may be induced via manipulation of the cellular environment: the *las* and *rhl* systems positively regulate a number of factors that can influence cellular redox state and oxidative stress including rhamnolipid surfactants, phenazine redox shuttles, siderophores and catalase. For example work by Sabra et al. and Kim et al. demonstrated that *P. aeruginosa* can manipulate the oxygen transfer rate of cultures and that this is enhanced by iron deficiency (Sabra et al. 2002; Kim et al. 2003). Conversely quorum sensing is strongly affected by both oxygen and iron concentrations (Bollinger et al. 2001; Kim et al. 2005). It therefore seems

that quorum sensing both responds to and in turn influences oxidative potential within the cell, which could help explain many of the observed changes to primary metabolism including to the TCA cycle, glyoxylate shunt and arginine fermentation.

In summary, analysis of cellular metabolic profiles demonstrated that the mutant differs from the wild-type in most major domains of metabolism; the timing and diversity of metabolites affected suggests that the *las* and *rhl* systems are involved in a global rewiring of metabolism during the transition from exponential to stationary phase growth.

Table 4.2 Cellular metabolic profiles recorded by MSFTA-GCMS.

Bacterial cultures were sampled at OD_{600} 1.5, 2.5, 4.5 and 6.5. A methanol-chloroform extraction was used to isolate metabolites prior to being derivatised with MSTFA and analysed by GCMS. Data is ordered by p-value at OD_{600} 4.5. Asterisks indicate significant differences (*P<=0.05, ** P<=0.01, two-tailed Student's t test). Multiple MSFTA derivatives of the same metabolite are indicated by Arabic numerals in brackets. ND = not detected.

Metabolite	Fold change (*lasI rhlI* mutant / wild-type)			
	OD_{600} = 1.5	OD_{600} = 2.5	OD_{600} = 4.5	OD_{600} = 6.5
Glycerophosphoric acid	1.3	2.1	27**	3**
2-Hydroxypentanedioic acid	1.2	1.9	5.4**	3.1**
3-Pyridinecarboxamide (Nicotinamide)	1.1	1.2	2.2**	2.8**
Pentose-phosphate	1.2	1.1	16.5**	10.1**
Phenylalanine (2)	0.8	0.6	0.5**	2.3
3-Hydroxydecanoic acid	0.9	1.1	0.3**	0.1**
Trehalose	1.3	1.1	4.3**	ND
Hypoxanthine (6-Hydroxypurine)	1.2	1.7	2.4**	2.5
Glutaric acid	1.2	0.7	0.4**	1.2
Monosaccharide	1.1	1.1	1.8**	1.9**
Aromatic	0.9	1.1	2.8**	4.4*
Citric acid	0.9	1.6	2**	2.7**
Fructose 6-phosphate	1.1	1.8	2.8**	2.9*
5-Aminopentanoic acid	1.1	1	3.5**	6.5
Inositol	1	1.1	1.6**	1.6**
Citramalic acid	0.8	0.8	1.8**	3.8**
Ribose	1.2	1.7	1.9**	2.5**
Methionine	1.2	0.7	0.7**	0.5**
Ribofuranose	1.2	1.1	0.6**	0.7*
Malic acid	0.8	1.1	1.6**	1.3
Hexose-phosphate	0.8	1.8	3.1**	2.4*
Aspartic acid	1.2	0.8	0.6**	0.8
Tyrosine (1)	1.3	0.9	0.6*	0.8
Adenine	1.1	0.8	0.6*	0.7*
Hexose-phosphate	0.9	1.8	2.7*	2*
Glutamic acid	0.7	0.7	2*	2.5
Pyrimidine	1.5	1.2	1.7*	1.9

Alkane	1.2	0.7	0.6*	0.5**
Putrescine (2)	0.8	1.2	4.3*	5.9*
Phenylalanine (1)	1	0.9	0.5*	1.9
Glucose or galactose	1.8	1.1	0.7*	0.5
Amino acid	1	0.7	1.4*	1.2
Alkane	1	0.8	0.5*	0.5*
Long chain alcohol	1.4	0.8	0.5*	0.6**
Hexadecanoic acid	1.2	0.7	0.5*	0.5**
N-acetylglutamic acid (1)	0.9	1.2	1.9*	1.9
Mono-unsaturated fatty acid (1)	1	1	0.5*	0.5*
Hexose-phosphate	1.2	3.2	2.9*	4.3**
Tyrosine (2)	1	0.7	0.5*	1.9
Alkane	1	0.7	0.6	0.4*
Alkane	1.4	0.6	0.5	ND
Aromatic	0.8	1	0.7	0.7
Octadecanol	1.3	0.5	0.5	0.6
Nonanoic acid	1.2	0.8	0.5	0.7*
d-altro-2-Heptulose, 7-(dihydrogen phosphate)	1.2	3.8	3	5.2**
Octadecanoic acid	1.3	0.7	0.5	0.4**
Spermidine	1	1.2	1.7	3.5
Polyamine	1	1.3	2.7	4.8
5'-Adenylic acid (AMP)	1.5	0.8	0.3	0.1*
Putrescine (1)	0.6	1.3	6	5.3
Lysine	0.9	0.6	1.6	3.3
1-Monopalmitoylglycerol	1.4	1.1	0.6	0.7*
Cysteine	0.6	0.5	0.7	0.6
Aromatic	1.5	0.7	0.5	0.3**
Succinate	1.1	1	1.2	1.4*
Octacosane	1.3	0.7	0.5	0.5*
Glycerol	1	0.9	1.2	1.2
Arginine	1	0.8	1.4	2.3**
Alkane	1	0.6	0.5	0.5**
Long chain alcohol	1.3	1	1.5	1.1
Fumaric acid	1.2	1.1	1.2	1.4**
Adenosine	1	0.9	0.7	0.1
Threonine (2)	1.1	1	0.2	1.1

N-acetyl glucosamine	1.1	1	1.2	1
Alkane	1.4	0.6	0.6	0.5
Pyroglutamic acid	1.1	1.1	1.2	0.9
5'-Uridylic acid (UMP)	1.9	1.4	1.8	3.2
Glucose or Galactose	1.1	1.2	0.9	1.4*
Pantothenic acid	0.9	1.1	1.3	1.5*
Valine	1.1	1.1	1.2	2.3
Threonine (1)	1.3*	1	0.2	0.8
Glucose or Galactose	1.2	1.3	0.9	2**
Glycine	0.9	1.1	1.2	1
Proline	1.1	0.8	1.1	0.9
Beta-alanine	1	1.1	1.2	0.4*
Alkane	1.3	0.6	0.7	ND
Ornithine	0.8	0.5	0.6	4*
Monosaccharide	0.9	0.9	0.9	ND
Tetradecanoic acid	1	0.7	0.8	1
Glucose or Galactose	2.2	1.4	0.9	1.4*
4-Aminobutyric acid	1.1	1	0.9	0.5
Ribofuranose	1.7	1.3	1.3	0.6
Uracil	1.3	1.2	1	1.1
S-Methyl-5-thioadenosine	1.5	1.5	0.9	2.1
N-acetyl glutamic acid (2)	1.1	1.1	0.9	0.7
Ethanol, 2-amino-	0.7	0.5	0.9	4.1
2-Glycerophosphoric acid	1	1	1	1.1
Xanthine	1	1.3	0.9	6.9
Ethanethioic acid S-(3-methylbutyl) ester	1	0.8	1	1.3
2-Methylbenzoic acid (o-Toluic acid)	0.8	0.9	1	1.8

Table 4.3 Proteins differentially regulated in the *lasI rhlI* mutant.

Protein levels were measured by iTRAQ MS. Fold-change was calculated as wild-type/mutant. P values were calculated by Welch t-tests and adjusted to Storey's q-values to control the false discovery rate. Proteins are listed where q<=0.1.

PA No.	Gene name	Protein description	Fold-change	p value	q value
Proteins up-regulated in the wild-type compared to the lasI rhlI mutant at OD 1.5					
PA1904	*phzF2*	probable phenazine biosynthesis protein	14.12	4.07E-04	0.044
PA0588		conserved hypothetical protein	3.98	5.92E-05	0.014
PA4470	*fumC1*	fumarate hydratase	3.54	6.30E-04	0.058
Proteins down-regulated in the wild-type compared to the lasI rhlI mutant at OD 1.5					
PA5316	*rpmB*	50S ribosomal protein L28	0.07	1.77E-06	0.001
PA4268	*rpsL*	30S ribosomal protein S12	0.24	1.23E-04	0.014
PA5555	*atpG*	ATP synthase gamma chain	0.4	9.54E-05	0.014
Proteins up-regulated in the wild-type compared to the lasI rhlI mutant at OD 4.5					
PA4228	*pchD*	pyochelin biosynthesis protein PchD	9.34	6.30E-03	0.039
PA2386	*pvdA*	L-ornithine N5-oxygenase	6.27	1.45E-03	0.032
PA0660		hypothetical protein	4.77	1.83E-03	0.032
PA4470	*fumC1*	fumarate hydratase	4.09	4.30E-03	0.035
PA0519	*nirS*	nitrite reductase precursor	3.83	2.28E-04	0.01

...Cont.

PA No.	Gene name	Protein description	Fold-change	p value	q value
PA2003	*bdhA*	3-hydroxybutyrate dehydrogenase	3.32	3.70E-02	0.099
PA0283	*sbp*	sulphate-binding protein precursor	3.26	2.38E-02	0.086
PA3450	*lsfA*	1-Cys peroxiredoxin LsfA	2.63	1.02E-02	0.051
PA4922	*azu*	azurin precursor	2.55	2.99E-04	0.011
PA0744		probable enoyl-CoA hydratase/isomerase	2.49	3.86E-02	0.099
PA4226	*pchE*	dihydroaeruginoic acid synthetase	2.45	1.61E-02	0.067
PA1456	*cheY*	two-component response regulator CheY	2.34	1.43E-02	0.063
PA4495		hypothetical protein	2.28	2.44E-02	0.087
PA2204		probable binding protein component of ABC transporter	2.15	2.29E-02	0.086
PA0139	*ahpC*	alkyl hydroperoxide reductase subunit C	2.08	2.18E-02	0.084
PA1094	*fliD*	flagellar capping protein FliD	2.04	8.55E-03	0.046
PA5171	*arcA*	arginine deiminase	1.98	9.09E-03	0.048
PA0459		probable ClpA/B protease ATP binding subunit	1.96	1.82E-03	0.032
PA3712		hypothetical protein	1.94	4.96E-03	0.036
PA4461	*lptB*	Lipopolysaccharide export system ATP-binding protein LptB	1.82	9.92E-03	0.05
PA4236	*katA*	catalase	1.78	1.42E-02	0.063
PA2634	*aceA*	isocitrate lyase AceA	1.75	2.85E-02	0.096
PA1337	*ansB*	glutaminase-asparaginase	1.73	1.58E-02	0.067
PA3440		conserved hypothetical protein	1.67	1.53E-02	0.066
PA4370	*icmP*	Insulin-cleaving metalloproteinase outer membrane protein precursor	1.63	1.81E-02	0.074

...Cont.

PA No.	Gene name	Protein description	Fold-change	p value	q value
PA3988	*lptE*	LPS-assembly lipoprotein LptE	1.62	3.68E-03	0.035
PA3171	*ubiG*	3-demethylubiquinone-9 3-methyltransferase	1.6	8.20E-03	0.045
PA5373	*betB*	betaine aldehyde dehydrogenase	1.46	1.10E-02	0.054
PA2823		conserved hypothetical protein	1.45	6.16E-03	0.039
PA5016	*aceF*	dihydrolipoamide acetyltransferase	1.41	5.39E-03	0.036
PA0423	*pasP*	PasP	1.39	1.83E-02	0.074
PA1292		probable 3-mercaptopyruvate sulphurtransferase	1.38	7.72E-03	0.044
PA0546	*metK*	methionine adenosyltransferase	1.3	1.40E-02	0.063
PA5134	*ctpA*	carboxyl-terminal processing protease, CtpA	1.3	1.34E-02	0.063
PA4079		probable dehydrogenase	1.26	1.86E-03	0.032
PA4971	*aspP*	adenosine diphosphate sugar pyrophosphatase	1.23	3.49E-03	0.035
Proteins down-regulated in the wild-type compared to the lasI rhlI mutant at OD 4.5					
PA5425	*purK*	phosphoribosylaminoimidazole carboxylase	0.04	3.28E-03	0.035
PA4566	*obg*	GTP-binding protein Obg	0.06	1.89E-04	0.01
PA4462	*rpoN*	RNA polymerase sigma-54 factor	0.08	1.82E-03	0.033
PA4433	*rplM*	50S ribosomal protein L13	0.16	7.15E-05	0.007
PA0025	*aroE*	shikimate dehydrogenase	0.21	2.10E-03	0.032
PA0140	*ahpF*	alkyl hydroperoxide reductase subunit F	0.24	1.40E-02	0.063
PA4042	*xseB*	exodeoxyribonuclease VII small subunit	0.26	3.09E-02	0.094

...Cont.

PA No.	Gene name	Protein description	Fold-change	p value	q value
PA0865	*hpd*	4-hydroxyphenylpyruvate dioxygenase	0.28	4.15E-03	0.035
PA4268	*rpsL*	30S ribosomal protein S12	0.29	4.62E-03	0.035
PA5036	*gltB*	glutamate synthase large chain precursor	0.31	2.34E-02	0.086
PA4241	*rpsM*	30S ribosomal protein S13	0.32	2.99E-03	0.035
PA4563	*rpsT*	30S ribosomal protein S20	0.32	6.23E-04	0.021
PA1580	*gltA*	citrate synthase	0.37	5.05E-03	0.036
PA4253	*rplN*	50S ribosomal protein L14	0.37	6.07E-03	0.039
PA4274	*rplK*	50S ribosomal protein L11	0.38	1.89E-03	0.032
PA4244	*rplO*	50S ribosomal protein L15	0.39	5.29E-03	0.036
PA0782	*putA*	proline dehydrogenase PutA	0.4	5.48E-03	0.036
PA3645	*fabZ*	(3R)-hydroxymyristoyl-[acyl carrier protein] dehydratase	0.41	3.83E-03	0.035
PA4240	*rpsK*	30S ribosomal protein S11	0.41	2.76E-03	0.035
PA4246	*rpsE*	30S ribosomal protein S5	0.41	1.06E-03	0.027
PA4262	*rplD*	50S ribosomal protein L4	0.43	1.81E-02	0.074
PA4249	*rpsH*	30S ribosomal protein S8	0.49	1.58E-04	0.01
PA4465		conserved hypothetical protein	0.49	7.90E-03	0.045
PA5054	*hslU*	heat shock protein HslU	0.5	7.60E-04	0.023
PA4247	*rplR*	50S ribosomal protein L18	0.51	3.37E-05	0.007
PA1583	*sdhA*	succinate dehydrogenase (A subunit)	0.55	4.65E-03	0.035
PA0579	*rpsU*	30S ribosomal protein S21	0.56	2.70E-03	0.035

...Cont.

PA No.	Gene name	Protein description	Fold-change	p value	q value
PA2967	*fabG*	3-oxoacyl-[acyl-carrier-protein] reductase	0.56	2.03E-02	0.079
PA3068	*gdhB*	NAD-dependent glutamate dehydrogenase	0.56	4.98E-03	0.036
PA4756	*carB*	carbamoylphosphate synthetase large subunit	0.56	2.11E-03	0.032
PA3742	*rplS*	50S ribosomal protein L19	0.57	4.43E-03	0.035
PA2624	*idh*	isocitrate dehydrogenase	0.58	3.15E-03	0.035
PA5263	*argH*	argininosuccinate lyase	0.58	1.13E-02	0.055
PA4744	*infB*	translation initiation factor IF-2	0.59	4.54E-03	0.035
PA5552	*glmU*	glucosamine-1-phosphate acetyltransferase/N-acetylglucosamine-1-phosphate uridyltransferase	0.59	6.08E-05	0.007
PA2619	*infA*	initiation factor	0.6	3.50E-03	0.035
PA2976	*rne*	ribonuclease E	0.6	8.34E-03	0.045
PA4252	*rplX*	50S ribosomal protein L24	0.6	2.40E-03	0.033
PA4258	*rplV*	50S ribosomal protein L22	0.6	2.07E-04	0.01
PA4269	*rpoC*	DNA-directed RNA polymerase beta chain	0.6	1.47E-03	0.032
PA2740	*pheS*	phenylalanyl-tRNA synthetase, alpha-subunit	0.61	9.39E-04	0.026
PA4996	*rfaE*	LPS biosynthesis protein RfaE	0.64	6.38E-03	0.039
PA4568	*rplU*	50S ribosomal protein L21	0.65	3.21E-03	0.035
PA4257	*rpsC*	30S ribosomal protein S3	0.66	4.13E-03	0.035
PA4266	*fusA1*	elongation factor G	0.66	2.35E-03	0.033
PA0008	*glyS*	glycyl-tRNA synthetase beta chain	0.68	2.84E-02	0.096

...Cont.

PA No.	Gene name	Protein description	Fold-change	p value	q value
PA0576	*rpoD*	sigma factor RpoD	0.69	1.34E-02	0.063
PA2742	*rpmI*	50S ribosomal protein L35	0.69	3.86E-02	0.099
PA3655	*tsf*	elongation factor Ts	0.69	3.25E-03	0.035
PA5117	*typA*	regulatory protein TypA	0.69	7.52E-03	0.044
PA4481	*mreB*	rod shape-determining protein MreB	0.71	9.65E-03	0.05
PA4686		hypothetical protein	0.72	2.72E-02	0.094
PA4760	*dnaJ*	DnaJ protein	0.74	6.51E-03	0.039
PA4670	*prs*	ribose-phosphate pyrophosphokinase	0.75	2.48E-02	0.087
PA4263	*rplC*	50S ribosomal protein L3	0.76	1.61E-02	0.067
PA3637	*pyrG*	CTP synthase	0.77	4.34E-03	0.035
PA1794	*glnS*	glutaminyl-tRNA synthetase	0.78	1.91E-02	0.076
PA0555	*fda*	fructose-1,6-bisphosphate aldolase	0.79	2.48E-02	0.087
PA1544	*anr*	transcriptional regulator Anr	0.8	2.34E-02	0.086
PA3001		probable glyceraldehyde-3-phosphate dehydrogenase	0.85	2.36E-02	0.086

Chapter 5

Focused metabolic profiling of fatty acids

5.1 Introduction

Experiments described in Chapter 4 indicate that fatty acid metabolism is perturbed in a *lasI rhlI* double mutant during early post-exponential growth: a) several fatty acid metabolites were differentially modulated in aqueous cellular extracts, b) although only a few fatty acid genes were identified by mass spectrometric proteomic analysis, two (FabG and FabZ) were downregulated in the *lasI rhlI* mutant. Previously reported transcriptomic data acquired across a number of growth conditions shows that transcripts involved fatty acid/phospholipid metabolism are highly represented in the "core" QS regulon, though it is not obvious what impact these changes to gene expression might have on membrane FA composition (Schuster and Peter Greenberg 2006). Prompted by these observations, the present chapter describes experiments designed to provide a targeted, more comprehensive analysis of the effects of AHL QS on fatty acid metabolism.

Aims and objectives: To characterise the impact of *las* and *rhl* QS on fatty acid metabolism in batch culture by comparing the FA profiles of wild-type PAO1 and a *lasI rhlI* mutant. FA profiles were assessed using fatty acid methyl ester (FAME) GC-MS to analyse the total fatty acid content of organic-phase cell extracts. This approach will enable measurement of the total fatty acid pool including both free fatty acids and fatty acid residues from lipids. The roles of the *las* and *rhl* systems were compared by complementing the signal-null *lasI rhlI* mutant with exogenous AHLs.

Data presented here has been published in the Journal of Bacteriology (Davenport et al. 2015).

5.2 Results

5.2.1 AHL-complementation of the *lasI rhlI* mutant growth advantage

Planktonic cultures of *P. aeruginosa* were grown in AGSY medium. The growth characteristics of the wild-type PAO1 strain and the *las rhlI* mutant were similar to those reported in Chapter 3, with the mutant beginning to achieve higher optical density as the bacterial growth rate decelerated around 4 hours. The *lasI rhlI* mutant was also grown with exogenously supplemented AHLs: either BHL (10 μM), OdDHL (15μM) or both. The AHL-complemented cultures had growth phenotypes intermediate to the wild-type and the *lasI rhlI* mutant, indicating that the activities of both the *rhl* and *las* systems influences the growth rate of *P. aeruginosa* (Figure 5.1).

Complementation of the *lasI rhlI* mutant with BHL, OdDHL or both resulted in a decrease in optical density relative to the mutant alone ($P<=0.01$ in each case). For ANCOVA analyses, the optical density of cultures between 5 and 10 hours were treated as the dependent variable, time as a covariate and the growth conditions (strain and AHL complementation) as the independent variable; Tukey's "Honest Significant Difference" method was used to calculate p values. Data represent four biological replicates.

5.2.2 Evaluation of FAME-GCMS analysis of *P. aeruginosa* cell extracts

In order to assess fatty acid profiles, dried aliquots of the organic phase of chloroform-methanol cell extracts were incubated with boron trifluoride in methanol. This results in esterification of the free fatty acids to fatty acid methyl esters (FAMEs) by methylation of the carboxyl group, thereby enabling chromatographic separation and analysis by GCMS. Fatty acid lipid esters of acyl-lipids are also converted to FAME by direct transesterification (alcoholysis) during this incubation (Eder 1995). Thirteen fatty acids were identified by analysis of organic phase extracts of wild-type PAO1. These included saturated (SFA), unsaturated (UFA) and cyclopropane (CPFA) fatty acids. Although the full complement of expected phospholipid-linked fatty acids was observed, no hydroxyl fatty acids were detected. This consisted with previous observations that the boron trifluoride derivatisation method is inefficient at releasing hydroxy fatty acids from lipid A.

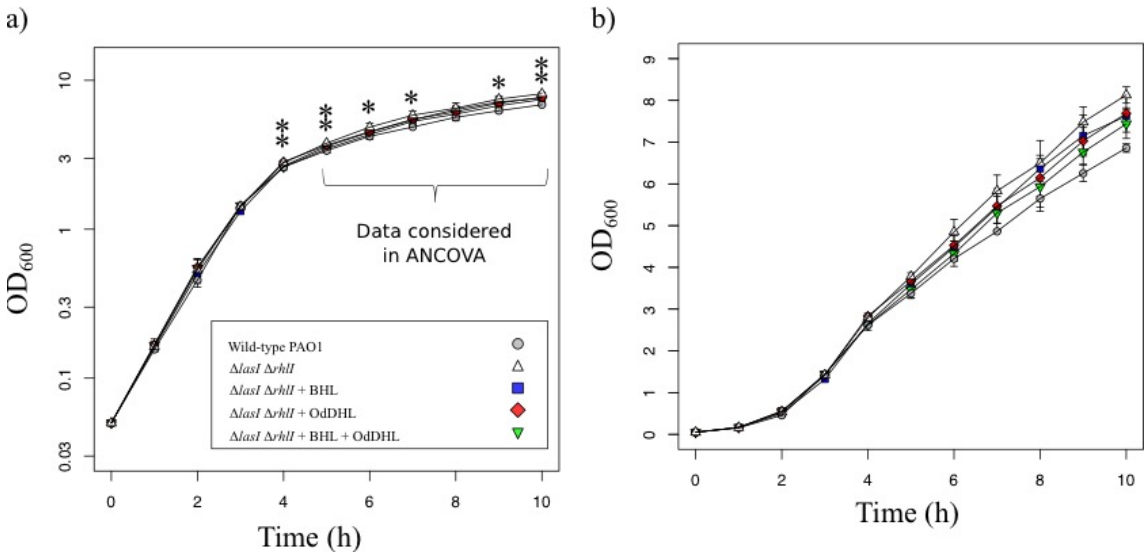

Figure 5.1 Cell growth of *lasI rhlI* and AHL-complemented cultures.

Growth phenotypes of wild-type PAO1, the *lasI rhlI* mutant and the mutant complemented with exogenous BHL (10 μM), OdDHL (15 μM) or both, plotted with optical density on $\log_{10}$ (a) or linear (b) scales. All cultures were grown in AGSY medium. No significant differences in optical density were found during exponential phase growth (1-3 hours, p<=0.05, Student's t-test or ANCOVA). As per chapter 2, small but significant differences growth between the wild-type and *lasI rhlI* mutant were evident following a deceleration in growth between 3 and 4 hours: this was evident when assessed by Student's *t* tests (indicated by asterisks in (a), * *p*<=0.05, ** *P*<=0.01) and by ANCOVA (p<=0.001, Tukey's HSD, considering data between 5 and 10 hours).

Table 5.1 Fatty acid profiles of bacterial cells as determined by FAME GCMS analysis.

Fatty acid profiles of bacterial cells as determined by FAME GCMS analysis. Percent complementation was calculated as the percentage return towards the wild-type phenotype (values are shown only where *P*<=0.05). Student's t-tests were calculated relative to the wild-type (WT, for mean percentages) or to the *lasI rhlI* mutant (LIRI, for percent complementation). Asterisks indicate significant differences (*P<=0.05, ** P<=0.01, two-tailed Student's t test). Upwards (↑) and downwards (↓) arrows indicate an increase or decrease in response to chemical complementation, respectively (relative to the *lasI rhlI* mutant). Abbreviations: SFA = saturated fatty acid, CUFA = *cis*-unsaturated fatty acid, CPFA = cyclopropane fatty acid, ACCL = average carbon chain length. Individual fatty acids are indicated according to the carboxyl-reference system, for example "9*Z*-16:1" indicates a fatty acid with a 16 carbon acyl chain containing a *cis* C=C double bond at the ninth position from the carboxyl carbon (hexadec-9-enoic acid, or palmitoleic acid). "–" = not significant.

		Mean (%)								% Complementation					
		OD_{600} = 1.5		OD_{600} = 2.5		OD_{600} = 4.5		OD_{600} = 6.5		OD_{600} = 1.5			OD_{600} = 4.5		
	Fatty acids	PAO1	LIRI	PAO1	LIRI	PAO1	LIRI	PAO1	LIRI	BHL	OdDHL	BHL+OdDHL	BHL	OdDHL	BHL+OdDHL
% of Total	12:0	0	0	0	0.1	0.1	0	0.4	0.2**	-	-	-	97**(↓)	35**(↓)	109**(↓)
	15:0	1.5	1.7**	1.5	1.8**	1.2	2.2**	2.3	3.5**	-	-	128*(↓)	76**(↓)	43**(↓)	102**(↓)
	7Z-14:1	0.1	0.1	0	0	0	0	0.1	0.1**	-	-	-	84**(↓)	53**(↓)	92*(↓)
	9Z-14:1	0.2	0.1	0.2	0.2	0.2	0.1	0.6	0.5	-	-	-	-	-	-
	15:0	0.2	0.3	0.3	0.3	0.2	0.2	0.2	0.2	-	-	-287*(↑)	-	86*(↑)	203*(↑)
	16:0	39	39	39	38.8	40.2	41.6**	38.3	41.7**	-	-	-	-	-	135*(↓)
	9Z-16:1	18	18.7**	18	19**	14.4	18.4**	10.1	15.7**	-	-	-	69**(↓)	28**(↓)	82**(↓)
	17:0	0.1	0.1	0.1	0.1**	0.1	0.1**	0.3	0.3	-	-	19353*(↑)	46**(↑)	29**(↑)	126*(↑)
	9cyc-17:0	0.3	0.3	0.3	0.3	1.6	1**	3.5	2.1**	46**(↑)	-	116*(↑)	64**(↑)	24**(↑)	44**(↑)
	18:0	5.2	5.1	5.6	5.2	4.9	4**	14	10.7**	-	-	132**(↑)	57**(↑)	-	73*(↑)
	11Z-18:1	35.2	34.5**	34.6	34	35.6	31.9**	26.7	24.1**	-	-	172*(↑)	62**(↑)	34**(↑)	111**(↑)
	11cyc-19:0	0.1	0.1**	0.1	0.1	1.2	0.4**	3.5	0.7**	2**(↑)	-	112*(↑)	54**(↑)	16**(↑)	52**(↑)
	13Z-22:1	0.1	0.1	0.1	0.1	0.1	0**	0.2	0.2	-	-	-	-	-	-
	Sum SFA	46	46.2	46.6	46.3	46.8	48.1**	55.5	56.6	67*(↓)	-	245*(↓)	43**(↓)	36**(↓)	128**(↓)
	Sum CUFA	53.5	53.4	53	53.3	50.4	50.5	37.6	40.5**	-	-	-	-	-	314*(↑)
	Sum CPFA	0.5	0.3**	0.4	0.4	2.9	1.4**	7	2.8**	27**(↑)	-	115*(↑)	59**(↑)	20**(↑)	48**(↑)
	ACCL	16.8	16.8**	16.8	16.7	16.8	16.7**	16.8	16.6**	-	-	166*(↑)	62**(↑)	32**(↑)	101**(↑)
C18/C16 ratio	All	0.7	0.7**	0.7	0.7	0.7	0.6**	0.9	0.6**	-	-	173**(↑)	57**(↑)	28**(↑)	102**(↑)
	SFA	0.1	0.1	0.1	0.1	0.1	0.1**	0.4	0.3**	-	-	148**(↑)	52**(↑)	-	80*(↑)
	CUFA	2	1.8**	1.9	1.8**	2.5	1.7**	2.7	1.5**	-	-	144*(↑)	60**(↑)	26**(↑)	90**(↑)
	CPFA	0.4	0.3**	0.4	0.3	0.8	0.4**	1	0.4**	-	-	-	56**(↑)	16**(↑)	80**(↑)
	CUFA+CPFA	1.9	1.8**	1.9	1.8**	2.3	1.7**	2.2	1.4**	-	-	145*(↑)	61**(↑)	27**(↑)	95**(↑)

5.2.3 Wild-type fatty acid profiles show increased saturation and cyclopropanation during transition to stationary phase growth

Wild-type fatty acid profiles were similar to those measured in other studies of *P. aeruginosa* (Hancock and Meadow 1969; Baysse et al. 2005; Zhu et al. 2006). Hexadecanoic acid (39%), (Z)-11-octadecenoic acid (35%) and (Z)-9-hexadecanoic acid (18%) were the predominant species, together accounting for 92% of measured fatty acids (Table 5.1). The wild-type saturated fatty acid (SFA) content increased from 46% to 55% during the transition to stationary phase growth, paralleled by a decrease in cis-unsaturated fatty acids from 53.5% to 37.6% (Figure 5.2 and Figure 5.3). This change in degree of saturation was driven by an increase in 18:0 octadecanoic acid (5% to 14%), a decrease in 9Z-16:1 (18% to 10%) and a decrease in 11Z-18:1 (35.2% to 26.7%). *P. aeruginosa* can synthesise CUFAs via both FASII and aerobic desaturases, but 11Z-18:1 is understood to be produced exclusively via FASII (Zhu et al. 2006). The overall 0.85-fold decrease (35.4 to 31.2%) in 11Z-18:1 and 11cyc-19:0 (derived from 11Z-18:1) implies that a large fraction of the change in SFA:CUFA ratio is determined by FASII.

The average carbon chain length (ACCL) of wild-type fatty acids increased on entry to stationary phase, during growth (Figure 5.4). The degree and timing of this change in chain length differed between SFAs and CUFAs: the length of CUFAs increased during early stationary phase between OD2.5 and OD4.5, whereas the length of SFAs increased between early (OD4.5) and mid (OD6.5) stationary phase.

The cyclopropanated fatty acid (CPFA) content of was almost undetectable at OD1.5 and OD2.5, then increased during stationary phase to 7% at OD6.5 (Figure 5.5). Over the same time period, 16:0 and 18:0 were cyclopropanated to 9cyc-17:0 and 11cyc-19:0, respectively. The 35-fold increase in cis-11,12-methyleneoctadecadonic acid (11cyc19:0, 0.1% to 3.5%) and 11.7-fold increase in cis-9,10-methylenehexadecanoic acid (9cyc17:0, 0.3% to 3.5%) together accounted for 41% of the decrease in CUFAs.

These changes are similar to those reported previously to be associated with stationary phase adaptation (Dubois-Brissonnet et al. 2000, 2001; Härtig et al. 2005).

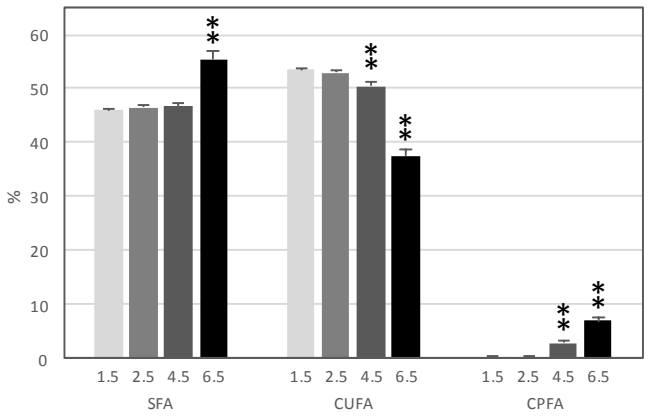

Figure 5.2 Saturated, *cis*-unsaturated and cyclopropane fatty acids in wild-type *P. aeruginosa* PAO1.

The percentage of saturated fatty acids (SFA) and cyclopropane fatty acids (CPFA) in *P. aeruginosa* increase as cultures enter stationary phase growth, while percentage of *cis*-unsaturated fatty acids (CUFA) decrease. Samples of bacterial cultures were analysed by FAME-GCMS at OD_{600} readings of 1.5 ( ), 2.5 ( ), 4.5 ( ) and 6.5 ( ). Error bars represent one standard deviation. Asterisks indicate significant differences (** P<=0.01, two-tailed Student's t test). Data are calculated from 6 biological replicates.

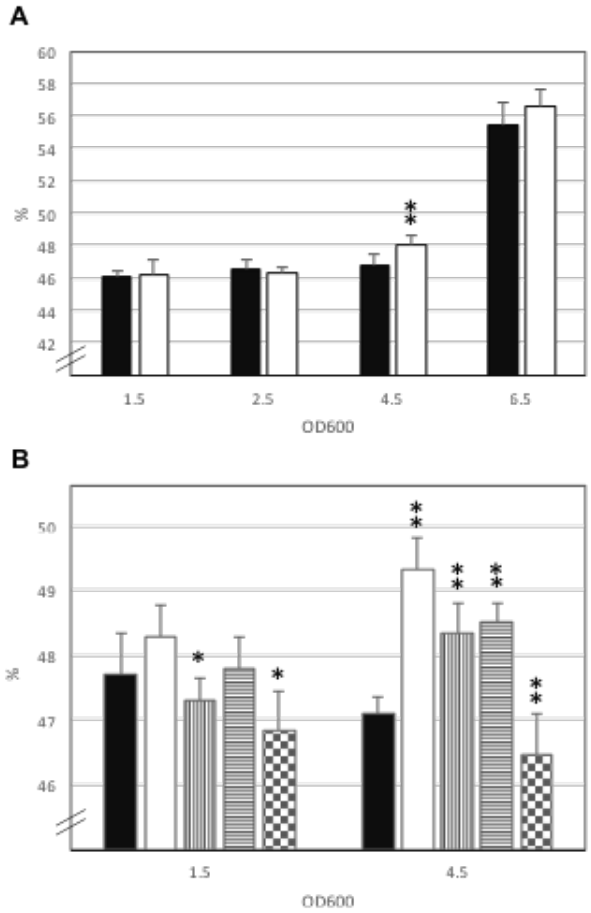

Figure 5.3 Stationary phase fatty acid saturation is repressed by QS.

Error bars represent one standard deviation. Asterisks indicate significant differences (* *P*<=0.05, ** *P*<=0.01, two-tailed Student's *t* test). A) *lasI rhlI* mutant (white bars) compared to wild-type PAO1 (black bars). B) Complementation of *lasI rhlI* mutant with 10 μM BHL (vertical stripes), 15 μM OdDHL (horizontal stripes) or both (chequered).

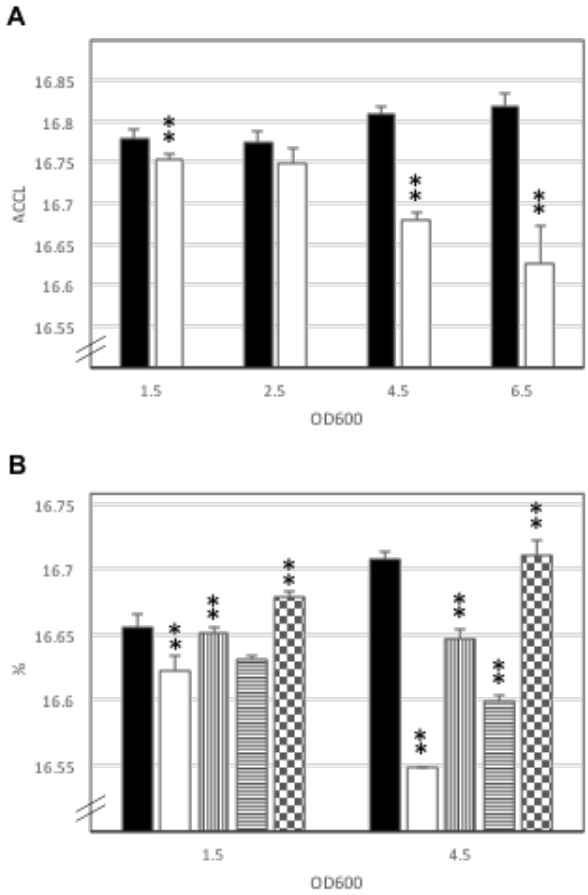

Figure 5.4 AHL Quorum Sensing induces a reduction in fatty acid chain length.

The average carbon chain length (ACCL) of fatty acids in the wild-type shortens during post-exponential growth, in contrast to the *lasI rhlI* mutant. Error bars represent one standard deviation. Asterisks indicate significant differences (* P<=0.05, ** P<=0.01, two-tailed Student's t test). A) *lasI rhlI* mutant (white bars) compared to wild-type PAO1 (black bars). B) Complementation of *lasI rhlI* mutant with 10 µM BHL (vertical stripes), 15 µM OdDHL (horizontal stripes) or both (chequered).

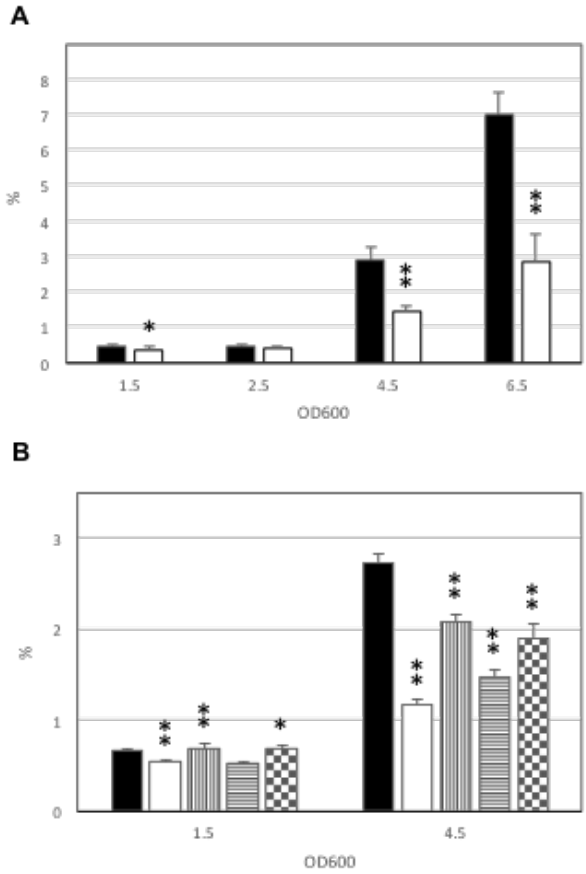

Figure 5.5 AHL Quorum Sensing increases cyclopropanation of fatty acids.

Error bars represent one standard deviation. Asterisks indicate significant differences (* *P*<=0.05, ** *P*<=0.01, two-tailed Student's *t* test). A) *lasI rhlI* mutant (white bars) compared to wild-type PAO1 (black bars). B) Complementation of *lasI rhlI* mutant with 10 μM BHL (vertical stripes), 15 μM OdDHL (horizontal stripes) or both (chequered).

5.2.4 The *lasI rhlI* mutant fatty acid profiles reveal reduced cyclopropanation and shorter acyl chain lengths

Consistent with data presented in Chapter 3, the wild-type and QS mutant fatty acid profiles were nearly identical during exponential growth, before diverging at the onset of stationary phase. From early stationary phase, there were differences in levels of 11 of 13 of the FAs detected (Table 5.1). In general, the *lasI rhlI* mutant showed a pattern of fatty acid saturation similar to that of the wild type, with the SFA:CUFA ratio increasing during early stationary phase. However, the degree of fatty acid cyclopropanation was less than half that of the wild type (Figure 5.4). The chain length of fatty acids in the mutant also differed from the wild-type: where FA chain length increased in the wild-type during early stationary phase growth, chain length of fatty acids in the QS mutant decreased. This shortening of FA length is driven by changes to the *cis*-unsaturated FA pool (principally a lower 18:1/16:1)

ratio; the length of saturated FAs increases in the mutant, albeit to a lesser degree than in the wild-type.

Chemical complementation of the *lasI rhlI* mutant with synthetic OdDHL and BHL was performed in order to examine the dependence of the observed phenotypes on AHL signalling (Table 5.1). Addition of both OdDHL and BHL returned levels of all 11 FAs modulated in the QS mutant towards or beyond wild-type levels. The same was true of composite variables including SFA levels and ACCL. In most cases, addition of the two AHLs in combination had a larger effect than either alone, with the notable exception of cyclopropanation, in which BHL alone had the greatest effect. More generally, BHL had greater effects than OdDHL on the FA profiles, suggesting that the *rhl* system is more intimately linked to fatty acid and membrane adaptation than is the *las* system.

5.3 Discussion

The lipid bilayers of bacterial membranes are crucial for cell integrity and survival as they act as partially-selective permeability barriers and house systems responsible for processes including nutrient acquisition, waste elimination, energy transduction and environmental sensing. Bacteria tune the properties of their lipid bilayers in order to maintain and adjust their function across diverse environments and physiological states. A key means by which bacteria achieve this is by controlling the fatty acid composition of their lipids.

Fatty acids are synthesised in the cytosol by FASII and though there are free FAs in the membrane envelope, they are for the most part incorporated into lipids. In Gram-negative bacteria such as *Pseudomonas* spp. the majority of fatty acyl chains are ester-linked to phospholipid head groups in the inner membrane bilayer and the inner leaflet of the outer membrane. These lipid acyl chains are major determinants of membrane physicochemistry, influencing bilayer fluidity, permeability and the activities of membrane proteins including nutrient permeases (Nikaido 2003; Vitrac et al. 2013).

The results presented here illustrate the fatty acid composition of wild-type PAO1 grown in AGSY medium changes during the transition from exponential to stationary phase growth, shifting towards higher levels of saturation, longer acyl chain lengths and higher levels of cyclopropanation. These trends are similar to those reported in other growth media (Hancock and Meadow 1969; Dubois-Brissonnet et al. 2000, 2001). Longer SFA fatty acyl chain lengths generally increase the rigidity of lipid bilayers, as longer chains have larger

non-polar surfaces in contact with adjacent acyl chains and also penetrate deeper into the membrane, increasing interactions between layers (Baysse and O'Gara 2007). By contrast cis C=C double bonds introduce a 30° kink into the acyl chain, disrupting the ordered packing of SFAs, thereby increasing bilayer fluidity. In addition, the cis double bond renders adjacent methylene (-CH_2-) groups vulnerable to peroxidation. By increasing the length and saturation of lipid acyl chains, bacteria increase their resistance to membrane stressors such as lipophilic solvents, acids, high temperatures and reactive oxygen species (Massa et al. 1988; Keweloh et al. 1991; Sikkema et al. 1995; Denich et al. 2003; Pesakhov et al. 2007).

Like other Gram-negative bacteria, *P. aeruginosa* can cyclopropanate cis-monounsaturated lipid acyl chains by inserting methylene groups across their C=C double bonds; this allows rapid adaptation of membrane properties without metabolically costly de novo fatty acid synthesis (Hancock and Meadow 1969; Grogan and Cronan 1997). In *P. aeruginosa* this cyclopropane-fatty-acyl-phospholipid synthase activity is likely encoded by hypothetical protein PA5546, which has 68% amino acid sequence identity to *cfaB* of *P. putida* KT2240 (Muñoz-Rojas et al. 2006). Wild-type PAO1 grown in AGSY showed 35-fold higher levels of cyclopropane fatty acids in mid-stationary compared to exponential phase growth. Cyclopropane fatty acids are thought to have effects on membrane fluidity intermediate to SFAs and CUFAs: they maintain the kink of CUFAs, but the introduction of a methylene group across the double bond is thought to enhance van der Waals interactions (Silvius and McElhaney 1979; Loffhagen et al. 2007). In addition, the absence of a C=C double bond reduces the vulnerability of the acyl chain to peroxidation. Cyclopropanation of unsaturated fatty acyl chains is especially associated with slowing growth rates in response to nutrient deprivation (Guckert et al. 1986; Dubois-Brissonnet et al. 2001; Loffhagen et al. 2007) and has been found to increase resistance to membrane stressors including reactive oxygen species and low pH (Grogan and Cronan 1997; Chang and Cronan 1999; Pradenas et al. 2013).

The transition to post-exponential growth corresponds to limitation of nutrients in the growth medium and a consequent reduction in growth rate. The consequences of growth rate perturbations on membrane metabolism of gram negative bacteria is best understood in *E. coli*, in which the reduction in growth rate at the onset of stationary phase is accompanied by inhibition of phospholipid synthesis. This is understood to be triggered by RelA- and SpoT- dependent increases in (p)ppGpp (Hengge 2011; Kanjee et al. 2012), which inhibits glycerol-3-phosphate acetyl transferase activity (PlsB) (Heath et al. 1994). Continued fatty acid synthesis results in accumulation of long chain acyl-ACP, which inhibits FASII via FabH, the type III beta-ketoacyl-ACP synthase responsible for initiating FASII by

condensation of acetyl-CoA with malonyl-ACP (Heath and Rock 1996*a*). ppGpp also modulates fatty acid metabolism by inhibiting expression of *accA*, *accB*, *fabB* and *fabZ* (Kanjee et al. 2012). The increase in ppGpp at the onset of stationary phase is a key inducer of the stationary phase sigma factor and general stress response regulator, RpoS. The regulatory scheme in *P. aeruginosa* is thought to be broadly similar to that in *E. coli*, including induction of RpoS expression by (p)ppGpp. As in *E. coli*, levels of RpoS increase at the onset of stationary phase growth of *P. aeruginosa*, conferring resistance to a number of stressors including heat, low pH, high osmolarity, H_2O_2 and ethanol (Jørgensen et al. 1999; Suh et al. 1999). This stationary-phase stress tolerance is conferred in part by modifications to the bacterial membranes such as those observed in the wildtype FA profiles in the present experiments.

The present FAME-GCMS analyses of the mutant and AHL-complemented mutants indicate that AHL signalling plays a significant role in increasing acyl-chain length and levels of cyclopropane fatty acids during entry to stationary phase. The mass spectrometric proteomic analysis described in Chapter 3 detected six proteins involved in fatty acid biosynthesis, of which two were downregulated in the wild-type relative to the *lasI rhlI* mutant during stationary phase: levels of FabG beta-ketoacyl-ACP reductase were 45% lower, levels of FabZ beta-hydroxyacyl-ACP dehydratase were 60% lower. Previous transcriptomic analyses have also identified genes involved in fatty acid and phospholipid metabolism to be modulated by AHL QS: across three independent microarray analyses, 26 genes were identified as modulated by AHL QS (Table 5.2) (Hentzer et al. 2003; Schuster et al. 2003; Wagner et al. 2003). It is striking that all 26 genes in Table 5.2 were identified as QS-modulated by Wagner et al., whereas Hentzer et al. and Schuster et al. identified only 6 of these genes. This suggests that the impact of fatty acid and phospholipid metabolism can vary widely and is sensitive to the prevailing growth conditions. The six genes modulated in all three transcriptomic studies include *fabH2* (PA3333, a beta-ketoacyl-ACP synthase III), *pqsD* (PA0999, a beta-ketoacyl-ACP synthase III, also called *fabH1*), PA1869 (a probable acyl carrier protein), PA3334 (probable acyl carrier protein) and PA3330 (probable short chain dehydrogenase).

FabG catalyses the first reductive step in the elongation cycle of fatty acid biosynthesis and is essential for fatty acid biosynthesis and cell growth (Zhang and Cronan 1998; Kutchma et al. 1999). Depressed levels of FabG therefore likely reflect a general slowing in fatty acid biosynthesis in the wild-type. Neither of the three transcriptomic studies found differences in fabG gene expression, suggesting that this is specific to our growth conditions and/or the timing of sampling.

Control of carbon chain length is exerted at multiple points in FASII. The only gene in Table 5.2 that is directly involved in FASII is *fabZ,* which was found to be downregulated 45% by QS in early stationary phase by (Wagner et al. 2003). Under the present condition of growth in AGSY, levels of the gene product FabZ beta-hydroxyacyl-ACP dehydratase were 60% lower in the wild-type than the *lasI rhlI* mutant during early post-exponential growth (Table 4.3). The influence of FabZ over the control of flux through FASII is not yet well-defined. The roles of FabA and FabZ beta-hydroxyacyl-ACP dehydratases have best been characterised in *E. coli*, in which both FabA and FabZ use saturated beta-hydroxyacyl-ACPs as substrates but only FabZ shows high dehydratase activity with unsaturated beta-hydroxyacyl-ACPs and so is considered the primary dehydratase for the CUFA branch of FASII. A reduction in FabZ activity might therefore be expected to decrease the overall rate of fatty acid biosynthesis and to increase the proportion of FA intermediates entering the SFA branch (Heath and Rock 1996*b*). However more recently researchers have observed that overexpression of FabZ can result in elevated proportions of SFAs (16:0 and 18:0) and an increase in the carbon chain length of SFAs in *E. coli* (Jeon 2012). It therefore seems plausible that depressed levels of FabZ in the present study contributed to the observed difference in chain length.

Wagner et al. also reported that levels of *plsY* transcripts, encoding a glycerol-3-phosphate acyltransferase, are two-fold repressed by *las-rhl* QS, implying that QS represses the rate of glycerolipid synthesis[4]. A QS-dependent decrease in PlsY activity would be consistent with the lower growth rate of the wild-type observed in the present conditions, though Wagner et al. did not report a QS-dependent growth effect under their growth conditions.

Interestingly *fabH2,* encoding the FabH2 beta-ketoacyl-ACP synthase III, was observed to be upregulated ~30-fold by QS in all three microarray studies (Table 5.2). (FabH2 was not detected in the proteomic analysis described in Chapter 4.) The physiological function of FabH2 is unknown. Whereas *E. coli* FASII is initiated with the condensation of acetyl-CoA with malonyl-ACP by the FabH beta-ketoacyl-ACP synthase III, the dominant FASII-initiating KAS in *P. aeruginosa* is FabY, a KASI/II enzyme (Yuan et al. 2012). *fabH2* is part of a predicted eight-gene operon all of whose members are predicted to be metabolic enzymes but whose physiological role is unknown. This suggests that FabH2 likely has a role in secondary metabolism rather than FASII.

[4] PlsY is thought to be the principle glycerol-3-phosphate acyltransferase in *P. aeruginosa*. PlsB is not essential (Yao and Rock 2013).

The genetic basis for cyclopropanation of fatty acid is well understood. PA5546 is a probable cyclopropane-fatty-acid-phospholipid synthase gene and was found to be upregulated 3.2-fold by AHL QS during early stationary phase by Wagner et al. (Table 5.2). PA5546 has a potential *las-rhl* box like sequence gaCtaggAGgTTTGGCAtG immediately upstream of its translational start site. This sequence has 11/19 sequence identity with the acCtgccAGaTTTGGCAgG putative rhl consensus sequence (uppercase letters match the rhl consensus, underlined letters are considered important in distinguishing *rhl* vs *las* regulation) (Schuster et al. 2004*a*; Schuster and Greenberg 2007). PA5546 is 3.7-fold repressed in a *rpoS* mutant during early stationary phase and has the likely RpoS -10 sequence CTATAgT (1 nt difference from the consensus CTATAcT) positioned 29 bp upstream of the ATG start codon (Schuster et al. 2004*b*). It therefore seems probable that transcription of PA5546 and hence cyclopropanation is directly regulated by both rhl QS and RpoS during the transition to early stationary phase. The present FAME analysis confirms that AHL QS plays a significant role in induction of FA cyclopropanation on entry to stationary phase growth and also indicates the rhl system has a greater degree of control than the *las* system. However, neither Hentzer et al. nor Schuster et al. observed changes in the transcript levels of PA5546 (Table 5.2). This could be due to differences in experimental setup, for example differences in growth conditions or the timing of sampling. The *E. coli* CFA synthase gene (also regulated by RpoS) is expressed transiently during entry to stationary phase, if the expression profile of PA5546 is similar then the power of microarray analyses to detect differential regulation will be highly dependent on the time of sampling (Wang and Cronan 1994; Chang et al. 2000).

Why might QS influence FA metabolism? There are a several mutually compatible explanations. First, changes to FA metabolism may be due to indirect effects of the global impact of AHL QS on *P. aeruginosa* physiology. AHL QS can modulate the expression of up to 12% of the *P. aeruginosa* genome (Wagner et al. 2003). As described in previous chapters, the global effects of AHL QS on gene expression shifts the demands placed on central metabolic functions and this could be expected to impinge on fatty acid metabolism. Indeed, a high proportion of these QS-regulated genes are involved in the synthesis of secondary metabolites from fatty acid metabolic intermediates, for example quinolones, rhamnolipids and AHLs themselves. QS-dependent changes to FA metabolism may therefore reflect indirect responses to shifting metabolic demand. In a similar fashion, many AHL QS-regulated secreted factors—including the quinolones, rhamnolipids and AHLs—are membrane-active and would be expected to trigger adaptive changes to membrane composition, including via fatty acid metabolism.

A second explanation for the influence of AHL QS on FA metabolism is that—because QS infers and communicates valuable information regarding the state of the cellular social and physical environment—*P. aeruginosa* AHL QS has evolved to directly regulate primary metabolic functions including FA metabolism. This is consistent with growing evidence that QS plays a role in stress signalling and that the rhl system in particular integrates metabolic regulatory cues (Baysse and O'Gara 2007; Mellbye and Schuster 2014). Both RelA and RpoS expression have been found to induce AHL QS in *P. aeruginosa* (Latifi et al. 1996; Van Delden et al. 2001; Schuster et al. 2004*b*; Khakimova et al. 2013). Likewise AHL QS induces RpoS expression, principally through the rhl system (Latifi et al. 1996; Schuster et al. 2004*b*). Like RpoS and RelA, AHL QS systems can confer increased resistance to oxidative, osmotic and thermal stressors (Hassett et al. 1999; García-Contreras 2016). The connectedness of these global regulators is illustrated by RpoS expression affecting 40% of the *las*-*rhl* regulon and 18% of the RpoS regulon being QS-regulated (Schuster et al. 2004*b*). This overlap has perhaps been best characterized with regard to resistance to oxidative stress by induction of catalase (CAT, via *katA* expression) and superoxide dismutase (SOD, via *sodA* expression) activities (Eichel et al. 1999; Schuster et al. 2004*b*; García-Contreras et al. 2014). Less is known about the relation of QS and stress signalling with regard to membrane adaptation. Previous work has shown that QS can be induced in response to membrane perturbations and that this is dependent on *relA* (Baysse et al. 2005). The present results demonstrate that the reverse is also true—QS can modulate membrane composition—and indicates QS is involved in development of stationary phase membrane stress tolerance, probably both directly via *rhl*-dependent regulation action at the PA5546 promoter, and indirectly via RpoS.

The impact of AHL QS on FA and membrane metabolism is likely a function of direct and indirect control via LuxR-type transcriptional regulators, as well as adaptive responses to to the wider regulatory effects of QS. Regardless of the mechanisms employed, the present results indicate that QS induces changes to FA and membrane metabolism consistent with stationary phase stress tolerance. Further experiments are needed to explore the physiological impact of these changes under conditions that represent the diverse ecology of *P. aeruginosa*. This will be important in understanding the role AHL QS plays in coordinating stress responses and in "competition sensing" (Cornforth and Foster 2013).

Table 5.2 QS-modulated genes involved in fatty acid and phospholipid metabolism.

Data was compiled from three independent studies: (Hentzer et al. 2003; Schuster et al. 2003; Wagner et al. 2003).

[a] Fold change was reported as the average fold induction in a *lasI rhlI* mutant when supplemented with 2 μM OdDHL and 5 μM BHL (average of samples collect at OD_{600} of 0.5, 1.3, 1.6, 2.0, 2.7). Bacteria were grown aerobically in ABt minimal medium with 0.5% casamino acids.

[b] Fold change was reported as the maximum fold induction in a *lasI rhlI* mutant when supplemented with 2 μM OdDHL and 10 μM BHL (maximum of samples collected at OD_{600} of 0.2, 0.4, 0.8, 1.4, 2.0, 3.0, and 4.0). Bacteria were grown aerobically in buffered Lysogeny Broth.

[c] Fold change was reported as the fold induction in a *lasI rhlI* mutant when supplemented with 1 μM OdDHL and 2 μM BHL. Values are reported for samples collected during early mid-logarithmic (ML) or stationary phase (ES) growth. The values are reported for the early stationary phase when differential expression was observed in both growth phases (B). Bacteria were grown aerobically in modified FAB medium.

		Fold modulation in *lasI rhlI* mutant			
PA number	Gene Name, synonyms	Hentzer et al. 2003[a]	Schuster et al. 2003[b]	Wagner et. al 2003[c]	Description / gene product
PA0228	*pcaF*			3.8 (ES)	beta-ketoadipyl CoA thiolase PcaF
PA0447	*gcdH*			7.8 (ML)	glutaryl-CoA dehydrogenase
PA0581	*plsY*			-2 (ML)	glycerol-3-phosphate acyltransferase
PA1869		57	41	79 (B)	probable acyl carrier protein
PA2001	*atoB*			23 (ML)	acetyl-CoA acetyltransferase
PA3300	*fadD2*			3.6 (ML)	long-chain-fatty-acid--CoA ligase
PA3333	*fabH2*	30	32	32 (B)	3-oxoacyl-[acyl-carrier-protein] synthase III
PA3334		30	49	23 (B)	probable acyl carrier protein
PA3645	*fabZ, sefA*			-1.8 (ES)	(3R)-hydroxymyristoyl-[acyl carrier protein] dehydratase

...Cont.

PA number	Gene Name, synonyms	Fold modulation in *lasI rhlI* mutant: Hentzer et al. 2003[a]	Fold modulation in *lasI rhlI* mutant: Schuster et al. 2003[b]	Fold modulation in *lasI rhlI* mutant: Wagner et. al 2003[c]	Description / gene product
PA3924				4.6 (ML)	probable medium-chain acyl-CoA ligase
PA4888	*desB*			-1.8 (B)	acyl-CoA delta-9-desaturase, DesB
PA0744				7 (ML)	probable enoyl-CoA hydratase/isomerase
PA0745				8.2 (ML)	probable enoyl-CoA hydratase/isomerase
PA0996	*pqsA*	9	90	4.7 (B)	probable coenzyme A ligase
PA0999	*pqsD, fabH1*	9	25	5.1 (B)	3-oxoacyl-[acyl-carrier-protein] synthase III
PA2552	*acdB*			10 (ML)	probable acyl-CoA dehydrogenase
PA2553				14 (ML)	probable acyl-CoA thiolase
PA2554				11 (ML)	probable short-chain dehydrogenase
PA2862	*lipA*			4 (ML)	lactonising lipase precursor
PA2889	*atuD*			2.8 (ML)	putative citronellyl-CoA dehydrogenase involved in catabolism of citronellol
PA3330		149	120	38 (ML)	probable short chain dehydrogenase
PA3924				4.6 (ML)	probable medium-chain acyl-CoA ligase
PA4907	*ydfG*			1.7 (ES)	probable short-chain dehydrogenase
PA4979				2.4 (ML)	probable acyl-CoA dehydrogenase
PA5521				1.9 (ML)	probable short-chain dehydrogenase
PA5546				3.2 (ES)	probable cyclopropane-fatty-acid-phospholipid synthase

Chapter 6

Focused metabolic profiling of amino acids and polyamines

6.1 Introduction

Experiments described in Chapter 4 found that the concentrations of several amino acids were perturbed in a *lasI rhlI* mutant. However, in many cases the detected levels of many of these metabolites was close to the limits of detection. Moreover, the GC-MS analysis performed in Chapter 4 was semi-quantitative, enabling comparison of the concentrations of individual analytes across conditions, but does not permit comparison of contributions to total metabolite pools by different component metabolites, or of changes to the size of such pools. Amino acids pools are known to change on entry to stationary phase and to be influenced by environmental factors.

A quantitative and more comprehensive analysis of amino acid metabolites will be valuable in evaluating QS-dependent changes to amino acid metabolism. This chapter describes efforts towards these aims, both developing and applying a liquid chromatography—tandem mass spectrometry (LC-MS/MS) method for the analysis of amino acids and polyamines.

A quantitative LC-MS/MS method was validated for the quantitative measurement of 40 compounds involved in amino acid and polyamines. This validated method was then applied to analysis of extracts from *P. aeruginosa* batch cultures to provide a more comprehensive and quantitative analysis of the impact of AHL QS on these branches of metabolism.

Aims and objectives:

- To establish and validate a quantitative LC-MS/MS method for analysis of amino acids and polyamines.

- To characterise the impact of *las* and *rhl* QS on amino acid and polyamine metabolites by comparing the profiles of amino acid and polyamine metabolites in wild-type PAO1 and a *lasI rhlI* mutant.

Outcomes:

- An LCMS-based method was validated for quantitative analysis of polyamines and agmatine.
- Quantitative measurements of all 39 metabolites were achieved with a 15 min runtime per sample.
- Lower limits of quantitation (LOQ) were 20–150 nM for putrescine, spermine, spermidine, cadaverine, agmatine, and below 5 μM for all analytes.
- Responses were linear for all analytes between 0.5 and 50 μM.
- The impact of AHL QS on amino acid and polyamines metabolism is discussed below.

Work presented here has been published in the Journal of Chromatography B (Ubhi et al. 2013). Development and validation of the EZ:faast LCMS method was conducted in collaboration with Baljit Ubhi. Peter Davenport was responsible for development of methods for measurement of analytes not previously validated for analysis using EZ:faast (personal communication with Phenomenex): agmatine, putrescine, spermidine, spermine, cadaverine. Baljit Ubhi was responsible for development of the methods for all other analytes.

6.2 Results

6.2.1 Development and validation of EZ:faast LC-MS method for analysis of amino acid and polyamine metabolites

Several methods have been reported that use MS in tandem with chromatographic separation to quantitate amino acids (Fonteh et al. 2006; Kaspar et al. 2008) or polyamines (Häkkinen et al. 2007) separately, or basic amino acids and polyamines simultaneously (Feistner 1994). Commercial kits provide convenient, high-throughput bioanalysis of amino acids and related metabolites (for example, Phenomenex EZ:faast, Waters Masstrak, AB Sciex aTRAQ, Perkin Elmer neogram AAAC kit).

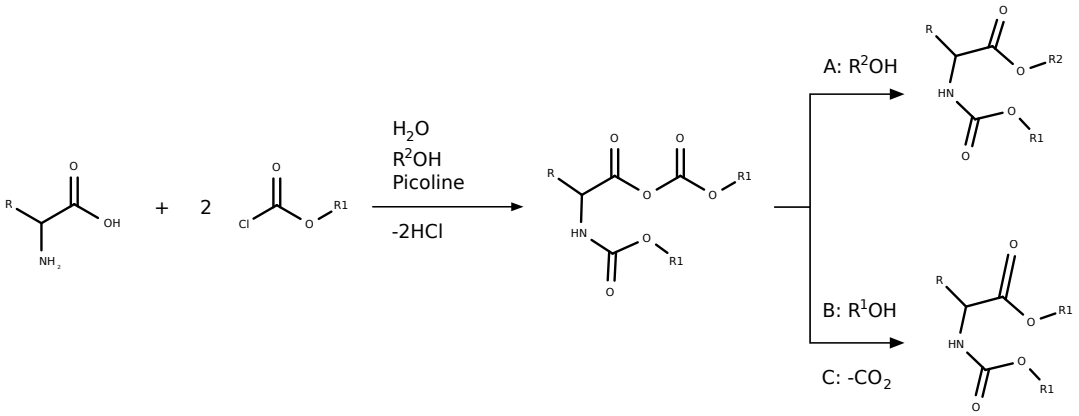

Figure 6.1 Reaction scheme for the derivatisation of amino acids to alkyl esters and alkyl carbamate esters by reaction with alkyl chloroformates and alcohols.

The esterification of carboxylic acids proceeds via either exchange with the dominant alcohol (A, the favoured pathway), exchange with alcohol derived from hydrolysis of the alkyl chloroformate (B), or decarboxylation of the intermediate carboxylic anhydride (C) (Wang et al. 1994); the EZ:faast (Phenomenex Inc., Torrence, CA, USA) derivitisation uses *n*-propyl chloroformate and *n*-propanol, thereby ensuring that all three pathways yield *n*-propyl esters.

The EZ:faast LC-MS and GC-MS methods (Phenomenex Inc., Torrence, CA, USA) comprise solid phase extraction and chloroformate derivatisation prior to chromatographic separation and MS analysis, and are notable for quick and quantitative measurement of over 40 amino acids and related metabolites in complex biological matrices (Fonteh et al. 2006; Kaspar et al. 2008). The EZ:faast preparation method involves i) a solid phase extraction, in which analytes are concentrated onto a cation exchange sorbent before wash and elution steps separate analytes from salts, proteins and other interfering matrix components, ii) a liquid phase derivatisation step with *n*-propyl chloroformate and *n*-propanol, using picoline as a catalyst, which converts carboxylic groups to n-propyl esters and amine groups to n-

propyl carbamate esters (see Figure 6.1), iii) a liquid/liquid aqueous/organic phase extraction step. Derivatisation improves separation of analystes by reverse-phase HPLC as well as aiding their purification.

The EZ:faast method was selected for evaluation due to its reported quick sample preparation (11 minutes) and analysis (15 mins), robustness to a variety of sample matrices and use of validated internal standards to account for absolute quantitation and to account for sample matrix effects. LC-MS/MS was chosen for the MS step on account of the relative ease of method development and validation, including unambiguous analyte identification, compared to typical GC-MS approaches. The EZ:faast method had been internally validated by Phenomenex for measurement of >40 amino acid metabolites, and the precision, linearity and other metrics have been independently assessed (data from a GCMS specific version of the kit) (Badawy et al. 2007).

The EZ:faast LC-MS/MS method used in this chapter was optimized and validated for use with the instrumentation described in the methods section. This involved assessing the analytical precision, recovery, linearity and stability in sample preparation and measurement of all analytes reported here. A calibration solution was prepared consisting of a mixture of all derivatised target analytes at 10 μM and internal standards homoarginine (HARG), methionine-d3 (MET-d3) and homophenylalanine (HPHE) at 2 μM. The 10 μM calibration solution was supplied to the mass spectrometer by continuous infusion driven by a syringe pump. For each analyte, the parent mass was detected to two decimal places, daughter ions were identified following fragmentation with collision gas and collision energies were optimised. Although the standard Phenomenex protocol recommends using internal standards (HARG, MET-d3 and HPHE) at 200 μM, this resulted in responses saturating the MS detector and so internal standards were subsequently used at 2 μM in all assays. Daughter scan experiments were then used to identify unique daughter ions for quantification of each amino acid, while additional daughter ions were used to confirm identification of analytes with reference with chemical standards. This process was repeated for each analyte and used to define a multiple reaction monitoring (MRM) method that specified transitions for each analyte and its unique fragment(s) across a chromatographic separation. The transitions specified in this MRM method are detailed in Table 6.1. The MRM method was divided into three time segments to increase the dwell time and decrease the cycle time per MRM scan, resulting high sensitivity and at least 15 data points per chromatographic peak of each analyte. Extracted ion chromatograms (XICs) based on this method are illustrated in Figure 6.2.

The linearity of each analyte response curve was assessed by measurement of calibration curves in which internal standards were constant at 2 μM whereas all target analytes were varied by serial dilution across a concentration range of 500 pM to 50 μM. Measurement of all analytes was linear within the range 500 nM to 50 μM, with R^2 values of >99.6%. The linearity of response across this range and the improvement in analytical precision following normalisation to the homophenylalanine internal standard is illustrated for analysis of spermidine in Figure 6.3.

Using linear models fitted to calibration curves of each analyte, measurements were assessed for precision across the full linear range for that analyte. Assay precision was assessed by intra-assay and inter-assay coefficients of variation (CVs). For each analyte, CVs were calculated for each concentration of the calibration standards within the linear range for that analyte. Intra-assay CVs were measured by injection of the derivatised sample of the 10 μM calibration solution ten times in succession and CVs were all below 15%, with a mean of 9%. Inter-assay CVs were calculated from four independent calibration solutions, prepared and analysed on separate days. Using raw response values, the mean inter-assay CV was ~30%. After normalisation to the internal homophenylalanine standard, all inter-assay CVs were >15% with a mean of 8%. This is illustrated for spermidine in Figure 6.3.

The lower limit of detection (LOD) for each analyte was calculated as the mean plus three times the standard deviation of signal in QC samples (Table 6.1). In accordance with the United States Federal Drug Administration guidance for quantitative biochemical assays the lower limit of quantitation was calculated as the lowest standard on the calibration curve that was i) greater than the LOD, ii) within the linear range of the calibration curve, iii) had a response CV of <15% (Food and Drug Administration 2001). LLOQ values were <=15 nM for putrescine, spermine, spermidine, cadaverine, agmatine, and <=500 nM for all analytes. Responses were linear for all analytes between 0.5μM and 50 μM. Repeat measurements of calibration curves over three days demonstrated that derivatised analytes were stable for at least 24 hours at 25 °C and 3 days at 4 °C: LLOQs were unchanged and inter-assay CVs were <15%.

Analyte recovery was assessed by first analysing five *P. aeruginosa* cell extracts both with and without addition of 15 μM calibration solutions. Recovery of all analytes was >96% and CVs of all target analytes after normalization to HPHE were all <7%. The only analyte measured with >7% precision was MET-d3, for which a CV of 40% was calculated. This is indicative of matrix effects interfering with measurement of MET-d3 (in the absence of cell extract the CV for MET-d3 was 7%).

This process of method development and optimization validated use of the EZ:faast method for quantitation of amino acid metabolites in *P. aeruginosa* cell extracts by LC-MS/MS and also validated the extended use of the method to quantify concentrations of agmatine, cadaverine, putrescine, spermidine and spermine: analytes not previously reported to have been measured using the EZ:faast method.

Table 6.1 Analytical parameters of the optimised LC-MS/MS method.

Analyte	Abbreviated name	Parent ion (m/z)	Product ion (m/z)	LOD (nM)	LLOQ (nM)	R^2
Arginine	ARG	303.23	156.04	11.2	15	0.989
Glutamine	GLN	275.27	172.1	13	15	0.987
Citrulline	CIT	304.8	287.1	3.4	5	0.99
Serine	SER	234.12	146.32	467.3	500	0.996
Asparagine	ASN	243.23	157.06	65.1	150	0.988
4-Hydroxyproline	HYP	260.02	171.97	74.7	150	0.9
3-Methylhistidine	3MIS	298.11	214.06	38.8	500	0.993
1-Methylhistidine	1MIS	298.11	210.08	1.9	5	0.998
Glycine	GLY	204.21	171.83	133.5	500	0.986
Glycine-proline	GPR	301.22	240.84	4.9	5	0.998
Threonine	THR	248.16	188	210.8	500	0.984
Alanine	ALA	217.98	130.4	21.9	500	0.983
Hydroxylysine	HYL	262.19	174.26	13.7	150	0.996
γ-Aminoisobutyric acid	GABA	232.02	172.03	5.7	15	0.997
Sarcosine	SAR	217.98	115.96	15.6	50	0.987
β-Aminoisobutyric acid	BAIBA	232.02	130	2.1	5	0.995
α-Aminobutyric acid	AABA	232.02	144.1	4.2	15	0.983
Ornithine	ORN	347.2	287.24	3.9	5	0.996
Methionine	MET	278.1	189.84	39.9	50	0.993

Proline	PRO	244.2	156.13	70.7	500	0.98
Lysine	LYS	361.21	170.07	10.3	50	0.992
Aspartic acid	ASP	304.08	216.21	124.4	150	0.989
Histidine	HIS	370.16	195.91	1.7	5	0.985
Thiaproline	TPR	262.19	174.26	216.5	500	0.972
Valine	VAL	256.13	115.94	330.5	500	0.988
Glutamic acid	GLU	318.25	172.16	62.9	150	0.995
Tryptophan	TRP	333.25	245.02	1.6	5	0.997
Aminoadipic acid	AAA	332.11	244.48	9.9	15	0.992
Leucine	LEU	260.7	172.07	0.8	5	0.983
Phenylalanine	PHE	294.18	206.16	16.4	50	0.994
Isoleucine	ILE	260.7	129.91	11.2	15	0.981
Aminopimelic acid	APA	346.2	286.06	0.6	5	0.998
Cystathionine	CTH	479.03	229.2	0.1	0.5	0.998
Cysteine	CYS	497	248.02	0.2	5	0.994
Tyrosine	TYR	396.17	308.15	6.2	15	0.995
Agmatine	AGM	303.44	243.31	15	15	0.987
Cadaverine	CAD	275.45	215.25	8.9	15	0.996
Putrescine	PUT	261.39	201.21	8.9	15	0.998
Spermine	SPM	461.53	155.31	0.8	15	0.996
Spermidine	SPD	461.52	284.29	0.2	1.5	0.998

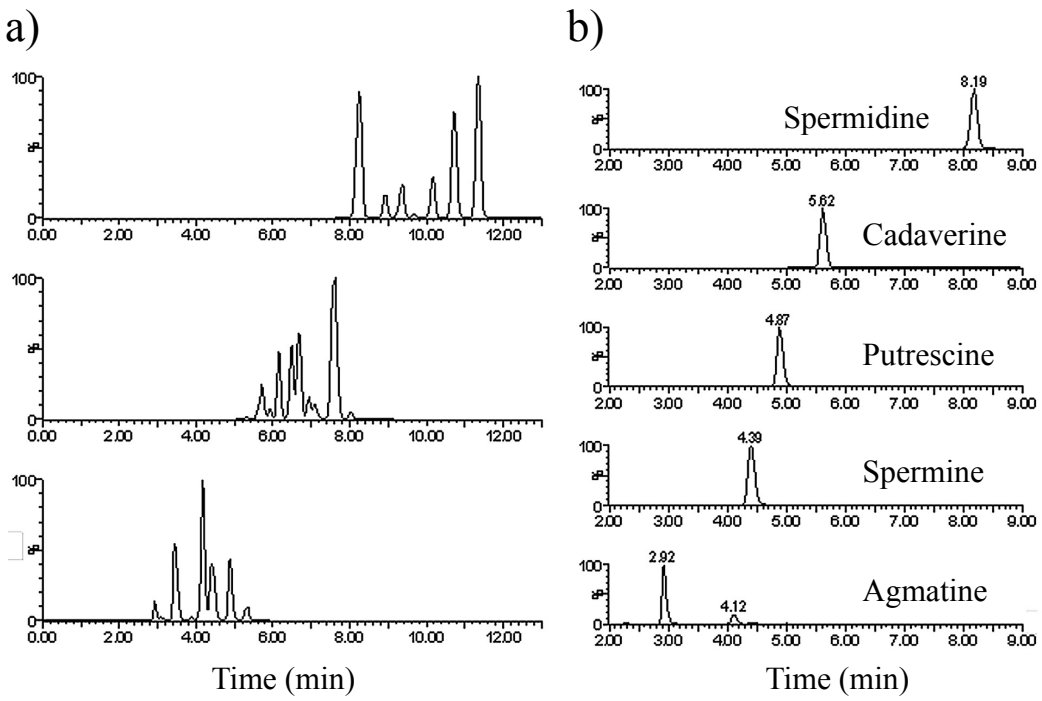

Figure 6.2 Total and extracted ion chromatograms from analysis of a standard mixture of amino acids, polyamines and dipeptides.

a) Total ion chromatograms (TICs): the MS/MS Multiple Reaction Monitoring (MRM) method was split into 3 three time segments to increase dwell time per analyte. b) Extracted ion chromatograms (XICs) of agmatine, spermine, putrescine, cadaverine and spermidine.

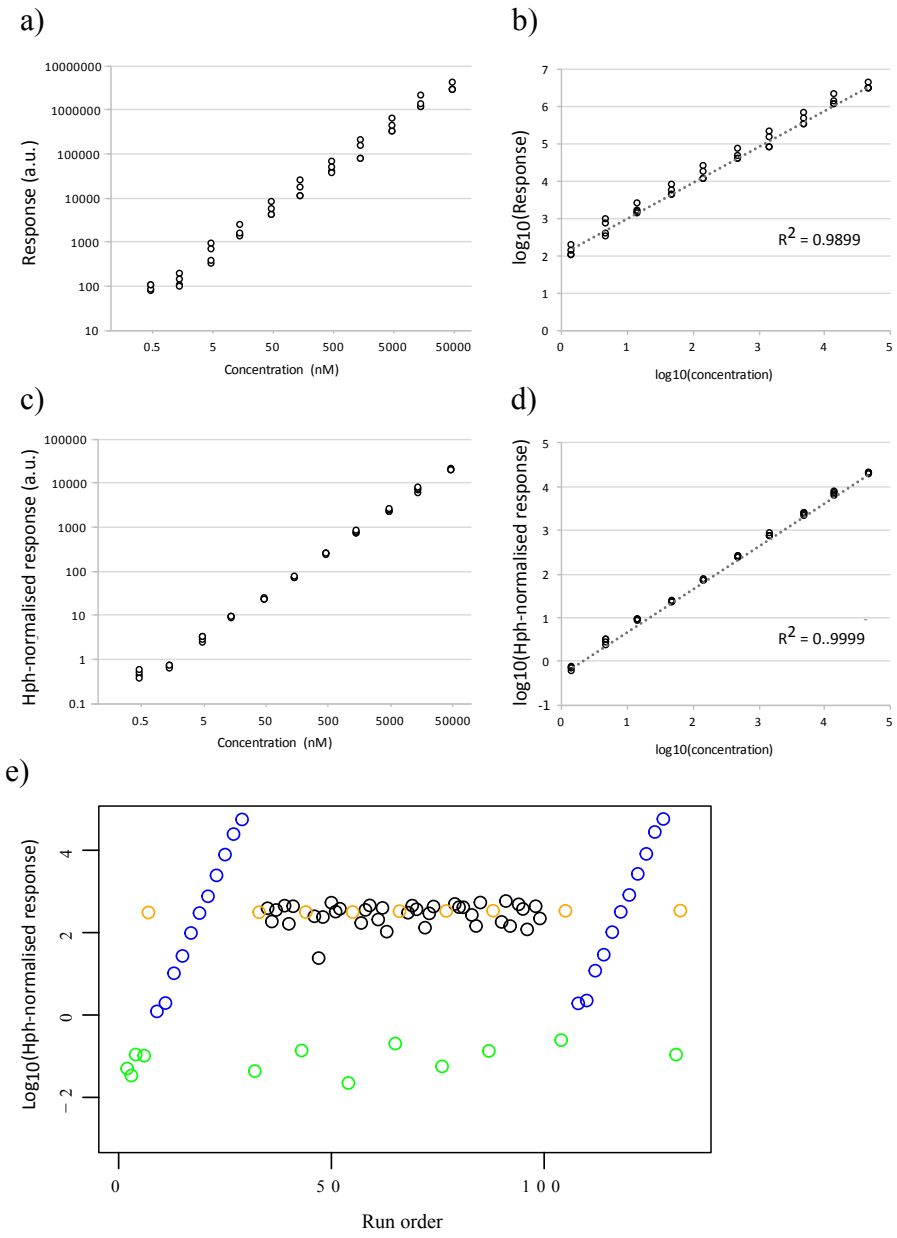

Figure 6.3 LC-MS/MS assays for spermidine show linear responses over a range of 1.5 nM to 15 µM.

The linearity of analyte responses of the optimised MRM method was evaluated by analysis of calibration standards in which internal standards (HARG, MET-d3 and HPHE) were kept constant at 2 µM while all target analytes were varied by serial dilution across a concentration range of 500 pM to 50 µM. Illustrative data for spermidine is shown in (a–e). Four calibration curves were prepared and analysed independently on different days, then analysed as either.raw response values (a–b) or homophenylalanine-normalised response values (c–d). Normalisation to the homophenylalanine internal standard improved inter-assay variability (compare a–b to c–d). Log-transformed data (b and d) was used to assess linearity. (e) illustrates homophenylalanine-normalised response values for spermidine in a typical LC-MS/MS run are depicted in (e): biological samples (black) are run in sets of <10, separated by blanks (green) and pooled QC (orange) samples; calibration curves (blue) are run before and after each run.

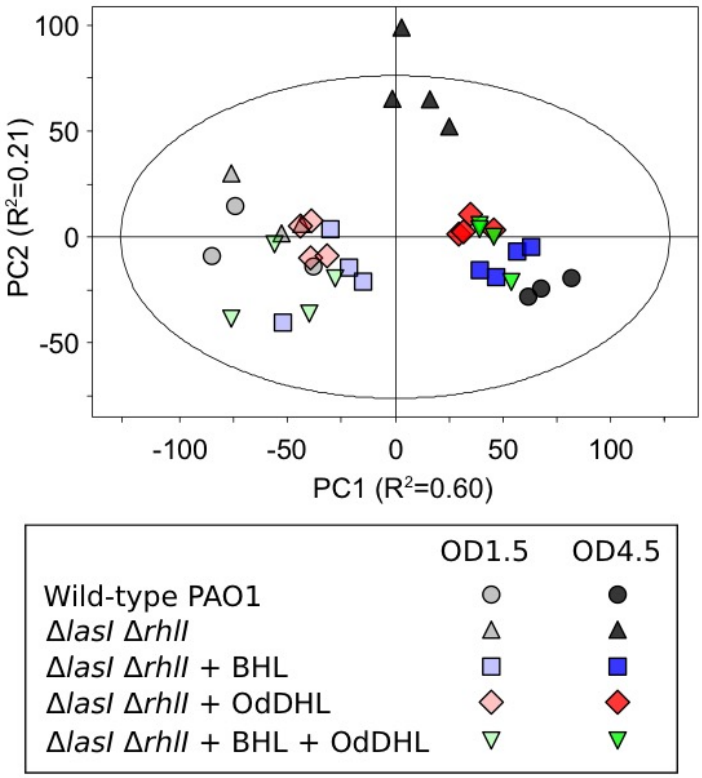

Figure 6.4 Global impression of impact of quorum sensing on amino acid metabolism.

Principle Components Analysis was used to analyse EZ:faast LC-MS/MS data. At a global level, addition of AHLs complements the *lasI rhlI* mutant towards a wild-type metabotype. Data was Pareto scaled prior to PCA analysis.

a) Agmatine

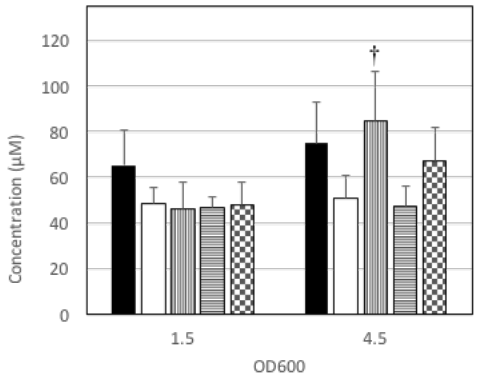

b) Arginine

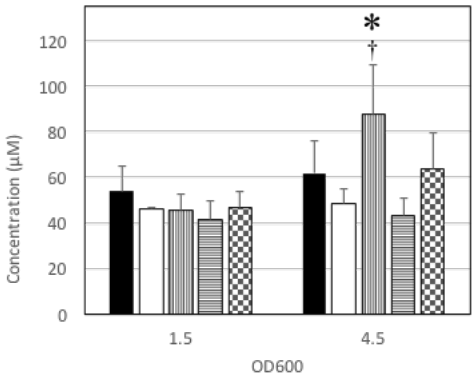

c) Aspartate

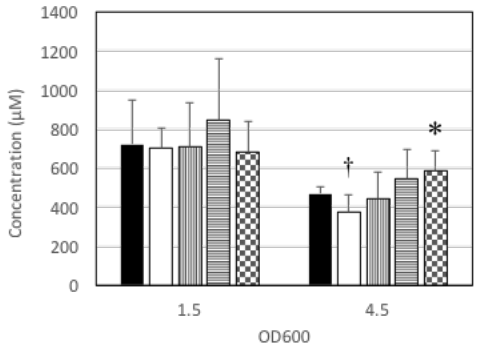

d) γ-Aminoisobutyric acid

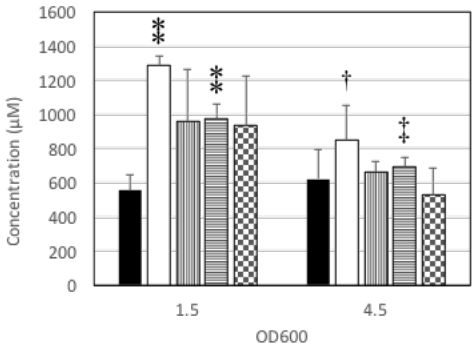

e) Cadaverine

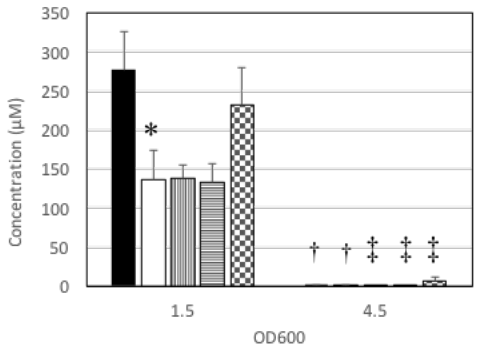

f) Glutamic acid

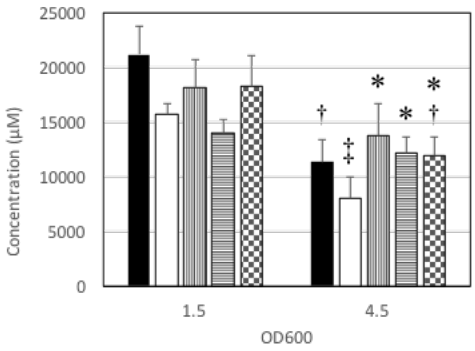

g) Glycine

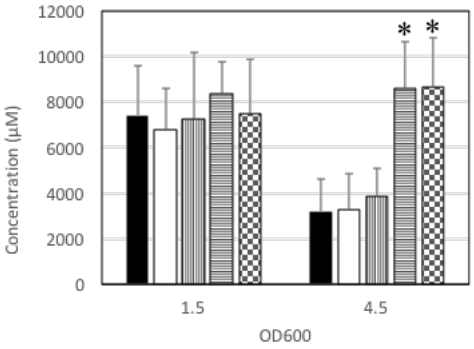

h) Lysine

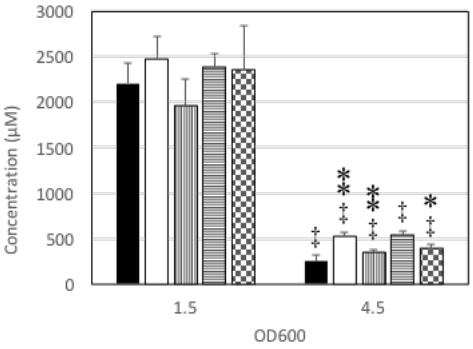

i) Methionine

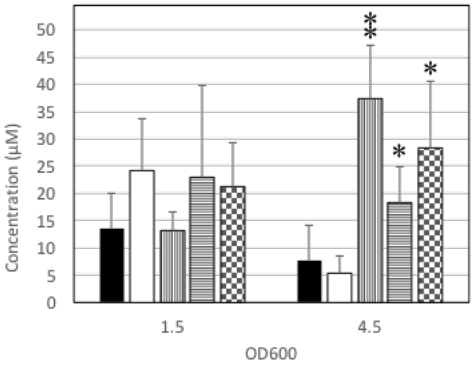

j) Ornithine

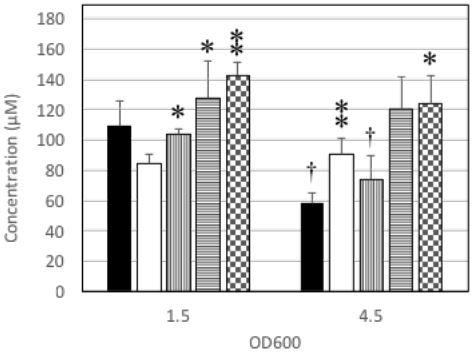

k) Phenylalanine

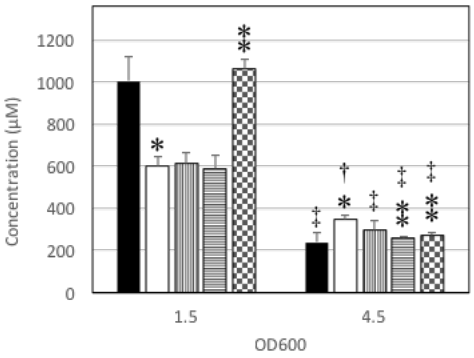

l) Putrescine

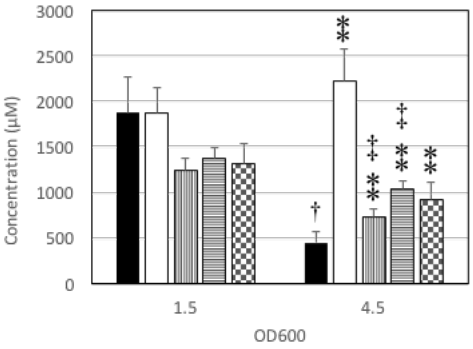

m) Spermidine

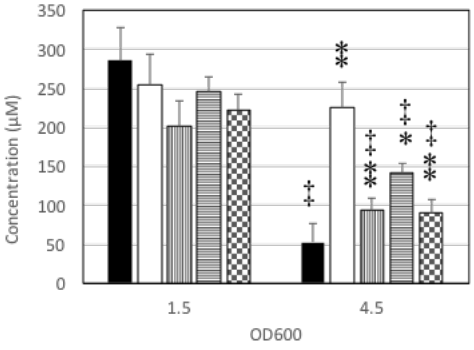

n) Tryptophan

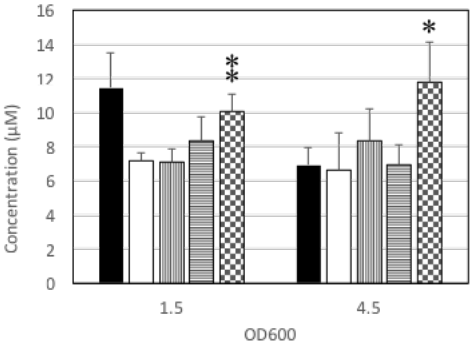

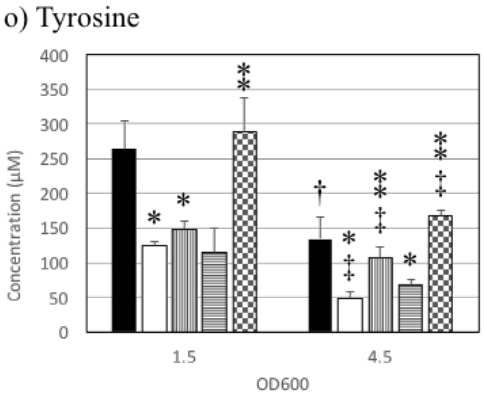

Figure 6.5 Concentrations of selected analytes as measured by EZ:faast LC-MS/MS.

Wild-type PAO1 (black bars), *lasI rhlI* mutant (white bars), *lasI rhlI* mutant complemented with 10 µM BHL (vertical stripes), 15 µM OdDHL (horizontal stripes) or both (chequered). Error bars represent one standard deviation. Asterisks indicate significant differences between lasI rhlI mutant and complementation with BHL, OdDHL or both (* *P*<=0.05, ** *P*<=0.01, two-tailed Student's *t* test). Daggers indicate significant differences between samples harvested at OD1.5 and OD4.5 for each growth condition († *P*<=0.05, ‡ *P*<=0.01, two-tailed Student's *t* test).

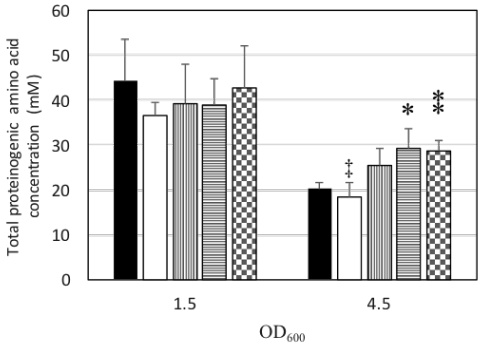

Figure 6.6 Total amino acid pools decline on entry to stationary phase.

Sum of analyte concentrations measured in cell extracts by LC-MS/MS. Component analytes are: arginine, aspartic acid, cysteine, glutamic acid, glutamine, glycine, histidine, isoleucine, leucine, lysine, methionine, ornithine, phenylalanine, proline, serine, threonine, tryptophan, tyrosine and valine. Wild-type PAO1 (black bars), *lasI rhlI* mutant (white bars), *lasI rhlI* mutant complemented with 10 µM BHL (vertical stripes), 15 µM OdDHL (horizontal stripes) or both (chequered). Error bars represent one standard deviation. Asterisks indicate significant differences between *lasI rhlI* mutant and complementation with BHL, OdDHL or both (* *P*<=0.05, ** *P*<=0.01, two-tailed Student's *t* test). Daggers indicate significant differences between samples harvested at OD1.5 and OD4.5 for each growth condition († *P*<=0.05, ‡ *P*<=0.01, two-tailed Student's *t* test).

6.2.2 QS-dependent impacts on amino acid and polyamine metabolism

Cell extracts were prepared from samples of the bacterial cultures using a methanol-chloroform method. Samples were collected at OD_{600} 1.5 and 4.5 in order bracket the divergence in cellular metabolism identified in Chapter 2. The validated EZ:faast LC-MS/MS method was then used to quantify amino acid and polyamine metabolites in the cell extracts.

Estimates of the cellular concentrations of amino acids, assuming a cytoplasmic volume of 2.2 fL (Cohen et al. 2015), indicate cellular concentrations similar to values previously reported for Gammaproteobacteria (Table 6.2). These estimated cellular concentrations offer reassurance that measurements are within expected ranges, but should be treated with caution since they assume a cell volume measured under different growth conditions. For example, estimated cellular concentrations at OD_{600}=1.5 for the two most abundant amino acids, glutamate and aspartate, were 100 mM and 3.4 mM respectively, similar to values of 96 mM and 4.3 mM reported for *E. coli* grown in a glucose minimal medium (Bennett et al. 2009). Estimated cellular concentrations of putrescine and spermidine during exponential growth are 8.8 mM and 1.3 mM, respectively, lower but within an order of magnitude of values reported for *E. coli* grown in nutrient broth (32.2 mM for putrescine and 6.88 mM for spermidine) (Miyamoto et al. 1993).

The PCA scores depicted in Figure 6.4 provides an overview of the relationships between the samples: in general, the concentrations of analytes in the wild-type and *lasI rhlI* mutant were similar at OD1.5, but became distinct by OD4.5. The PCA also illustrates that addition of exogenous OdDHL or BHL drives the analyte profiles of the *lasI rhlI* mutant towards those of the wild-type, confirming that both the *las* and *rhl* systems are involved in this composite metabolic phenotype.

Some of the more striking differences between the wild-type and mutant were in arginine and polyamine metabolism (Figure 6.5). Concentrations of putrescine, spermidine and their precursor ornithine were all lower in wild-type than in mutant cells during stationary phase (by 4, 5 and 1.8 fold, respectively): whereas wild-type concentrations decreased during post-exponential growth, the concentrations in *lasI rhlI* cells were more stable. Addition of BHL and to a lesser degree OdDHL decreased stationary phase concentrations of putrescine and spermidine towards wild-type levels. Surprisingly, supplementation of the mutant with BHL and OdDHL together resulted in higher in ornithine levels rather than complementation towards lower wild-type levels. Levels of a third polyamine, cadaverine, decreased from around 300 μM at OD 1.5 to negligible concentrations at OD 4.5 and parallel

a 5-fold drop in concentrations of lysine. Utilisation of L-lysine by *P. aeruginosa* PAO1 is dependent on the lysine decarboxylase pathway with cadaverine as an intermediate (Chou et al. 2010). This suggests that decreasing cadaverine concentrations reflect decreasing uptake and catabolism of lysine from the growth medium.

The size of free amino acid pools in bacteria (the combined concentration of proteinogenic amino acids) has long been observed to correlate strongly with bacterial growth rate. Under the present conditions, the size of the amino acid pool halved between OD 1.5 and OD 4.5 in both the wild-type and *lasI rhlI* mutant, consistent with studies in *E. coli* (Figure 6.6) (Mandelstam 1958). Despite marked shifts in the relative levels of amino acid analytes, the size of the amino acid pools of the wild-type and mutant were indistinguishable at both sampling points. However, the size of the amino acid pool in the *lasI rhlI* mutant at OD4.5 increased when cultures were supplemented with AHLs ($p<0.01$ for OdDHL, $p=0.051$ for BHL, Student's t-test). This was driven principally by higher levels of glycine and methionine in AHL-supplemented cultures. Despite the demand for SAM for AHL biosynthesis in the wild-type, levels of methionine were similar to those in the *lasI rhlI* mutant. Levels of methionine in the mutant were elevated >5-fold in response to supplementation with BHL and >3-fold in response to OdDHL. These low-micromolar increases in methionine may be due to metabolic assimilation of AHLs via SAM and suggest higher rates of assimilation of BHL than OdDHL. The millimolar increases in glycine concentrations in response to exogenous AHLs cannot be explained by assimilation of AHLs: a) there is no simple metabolic pathway or regulatory link that ties AHL catabolism to glycine concentrations, b) the concentrations of supplemented AHLs are insufficient to explain the increases in glycine (~1 µmole of AHL added to cultures compared to ~10 µmole increases in glycine, c) glycine concentrations responded only to OdDHL and not BHL.

Levels of several other amino acid metabolites were modulated in the mutant relative to the wild-type (Figure 6.5). Concentrations of lysine in the mutant during early post-exponential growth (OD 4.5) were twice those in the wild-type and this difference was complemented with exogenous BHL, suggesting that lysine metabolism is impacted by the rhl system. Glutamate concentrations were depressed by 40% in the mutant were increased to wild-type by addition of AHLs. Although measurements of γ-aminoisobutyric acid were noisy, they mirrored those of glutamate, suggesting that glutamate decarboxylase (GAD) activity is perturbed by QS. GAD activity is involved in several bacterial stress responses including acid shock, salt stress and stationary phase growth (De Biase et al. 1999; Feehily and Karatzas 2013).

Tyrosine concentrations in the *lasI rhlI* mutant were 60% lower than the wild-type in early post-exponential growth and increased to near wild-type levels in response to BHL. This may reflect diversion of flux from the shikimic acid pathway toward QS-induced exometabolites such as phenazines, however tyrosine concentrations correlated poorly with those of other aromatic amino acids.

Table 6.2 Estimated cellular concentrations of amino acid and polyamine metabolites.

Cellular concentrations are calculated based on data from Table 2, assuming a cell volume of 2.2 fL. Student's t-tests were calculated relative to the wild-type (WT, for the *lasI rhlI* mutant) or relative to the *lasI rhlI* mutant (LIRI, for chemical complementation(s)). Complementation values are shown where significant (p<=0.05). Asterisks indicate significant differences (*P<=0.05, ** P<=0.01, two-tailed Student's *t* test). "–" indicates no significant change relative to the non-complemented culture.

	Mean concentration (M)									
	OD600 = 1.5					OD600 = 4.5				
Metabolite	PAO1	*lasI rhlI*	BHL	OdDHL	BHL+OdDHL	PAO1	*lasI rhlI*	BHL	OdDHL	BHL+OdDHL
1-methyl histidine	2.20E-06	6.71E-07	—	—	—	8.35E-07	1.56E-06	—	—	—
3-methyl histidine	2.19E-06	7.35E-07	—	—	—	1.49E-05	5.07E-06	—	—	—
4-aminobutryic acid	2.61E-03	6.07E-03**	—	4.58E-03**	—	2.93E-03	3.98E-03	—	—	—
4-hydroxyproline	3.70E-04	3.43E-04	—	—	—	4.10E-04	1.64E-04	—	—	—
α-aminoadipic acid	3.50E-05	1.78E-05	—	—	—	7.34E-06	1.05E-05	—	—	—
α-aminobutyric acid	5.80E-04	5.41E-04	—	—	—	4.15E-04	6.04E-04	—	—	—
agmatine	3.07E-04	2.28E-04	—	—	—	3.57E-04	2.40E-04	—	—	—
aminopimelic acid	4.65E-06	2.12E-06	—	—	—	1.48E-06	1.90E-06	—	—	—
arginine	2.54E-04	2.17E-04	—	—	—	2.93E-04	2.30E-04	—	—	—
aspartic acid	3.39E-03	3.31E-03	—	—	—	2.20E-03	1.75E-03	—	—	2.77E-03*
β-aminoisobutyric acid	8.70E-06	9.67E-06	—	—	—	7.08E-06	1.05E-05	—	—	—
cadaverine	1.30E-03	6.38E-04*	—	—	—	3.23E-06	1.68E-06	—	—	—
citrulline	3.90E-03	2.87E-03	—	—	—	1.49E-03	1.86E-03	—	—	—
cystathionine	8.73E-05	8.36E-05	3.58E-05*	2.88E-05**	—	2.56E-05	4.42E-05	—	—	—
cysteine	2.19E-05	2.51E-05*	1.89E-05**	—	—	2.00E-05	2.75E-05	—	—	—
glutamic acid	9.97E-02	7.39E-02	—	—	—	5.35E-02	3.51E-02*	6.45E-02**	5.76E-02*	5.63E-02*
glutamine	6.47E-04	5.22E-04	—	—	—	5.19E-04	4.00E-04	—	—	—
glycine	2.50E-02	3.19E-02	—	—	—	1.50E-02	1.34E-02	—	4.30E-02**	4.12E-02*
glycine-proline	4.66E-05	2.50E-05	4.07E-05*	—	6.53E-05**	4.31E-05	2.81E-05	—	—	—
histidine	1.46E-03	6.65E-04	1.54E-03*	1.64E-03*	—	5.65E-04	1.04E-03	—	—	—
hydroxylysine	2.10E-04	1.46E-04	—	—	—	2.62E-04	1.82E-04	—	—	—
isoleucine	4.68E-03	4.30E-03	—	—	—	9.36E-04	1.03E-03	—	—	—
leucine	8.06E-03	6.18E-03	—	—	—	2.94E-03	4.44E-03	—	—	—
lysine	1.04E-02	1.17E-02	—	—	—	1.20E-03	2.47E-03**	1.63E-03**	—	1.85E-03*
methionine	2.47E-04	2.58E-04	—	—	—	3.59E-05	2.52E-05	—	8.58E-05*	-
ornithine	5.13E-04	3.97E-04	4.85E-04*	6.01E-04*	6.67E-04**	2.73E-04	4.25E-04**	—	—	5.84E-04*
phenylalanine	4.73E-03	2.82E-03*	—	—	5.01E-03**	1.12E-03	1.65E-03*	—	1.23E-03**	1.27E-03**
proline	2.86E-03	2.86E-03	—	—	—	1.56E-03	1.29E-03	—	—	—
putrescine	8.82E-03	8.83E-03	—	—	—	2.10E-03	1.04E-02**	3.44E-03**	4.90E-03**	4.32E-03**
sarcosine	3.95E-05	5.63E-05	—	—	—	5.84E-04	4.00E-04	—	—	—
serine	1.45E-02	1.66E-02	9.70E-03*	—	—	7.17E-03	8.91E-03	—	—	—
spermidine	1.34E-03	1.19E-03	—	—	—	2.47E-04	1.06E-03**	4.41E-04**	6.66E-04*	4.25E-04**
spermine	1.81E-07	4.53E-08	—	—	—	1.31E-07	2.72E-07	—	—	—
thiaproline	4.30E-04	1.09E-03	—	—	—	7.17E-04	7.36E-04	—	—	—
threonine	2.35E-03	3.12E-03	—	2.39E-03*	—	1.28E-03	1.34E-03	—	—	—
tryptophan	5.38E-05	3.36E-05	—	—	4.72E-05**	3.26E-05	3.13E-05	—	—	5.54E-05*
tyrosine	1.24E-03	5.83E-04*	7.00E-04*	—	1.36E-03**	6.31E-04	2.31E-04*	5.06E-04**	3.24E-04*	7.86E-04**
valine	1.77E-02	1.32E-02	—	—	—	6.26E-03	8.84E-03	—	—	—

6.3 Discussion

A rapid, reliable, high-throughput method was developed to simultaneously measure polyamine and amino acid metabolites with a large dynamic range. Detection limits were in the nM range for each analyte and responses were linear across the 0.5-50 μM range tested. Using this LC-MS/MS method, it was shown that *P. aeruginosa* has a marked impact on cellular concentrations of polyamine and amino acid metabolism.

Polyamines are multifunctional molecules associated with a variety of stress responses, notably against oxidative stress (Yoshida et al. 2004; Rhee et al. 2007). Polyamines execute these functions by diverse means, including modulating gene expression, modifying the activities of cell membrane components, and by scavenging free radicals. By sequestering free radicals, polyamines can protect cell components (especially GC-rich DNA) against reactive oxygen species (ROS)-induced stress. In the wild type, QS is known to elicit increased expression of enzymes involved in ROS detoxification, such as superoxide dismutases (Mn-SOD and Fe-SOD), the major catalase KatA (Hassett et al. 1999), and NADPH-generating glucose-6-phosphate dehydrogenase (NADPH is required for the synthesis of glutathione). Indeed, it has been suggested recently that because they are "private goods," the expression of these detoxification enzymes is another key factor suppressing the appearance of "social cheats" in the population (García-Contreras et al. 2014). Since these enzymes would no longer be upregulated in the *lasI rhlI* mutant, it is possible that the elevated levels of putrescine and spermidine reflect an alternative metabolic response to increased ROS-induced stress as the culture enters stationary phase.

The total concentration of free amino acids is closely linked to energy metabolism. Investigations in the 1950's demonstrated that inhibition of oxidative phosphorylation with azide, or dissipation of the proton motive force both lead to reductions in the total free amino acid pools. Similarly, the pool of free amino acids decreases as growth rate slows for example during the transition to stationary phase growth in batch culture, as rates of protein synthesis decrease (Mandelstam 1958; Tempest et al. 1970). The size and makeup of the free amino acids pool has long been known to vary with changes to a variety of environment conditions, for example rapid changes to amino acid pools in response to stresses such as mild changes in osmolarity. However, it is not clear why exogenously supplied AHLs should affect the total amino acid pool size and levels of glycine in particular, particularly as no difference was evident between the wild-type and *lasI rhlI* mutant cultures.

The QS-induced changes to amino acids suggest several avenues for further investigation. For example, aromatic amino acids including tyrosine are present at high concentrations in CF sputum and induce *P. aeruginosa* anti-microbial activity and synthesis of Pseudomonas quinolone signal (PQS) (Palmer et al. 2007, 2010). Tyrosine and tryptophan metabolism is also implicated in metabolic adaptation of *P. aeruginosa* to the CF lung (Behrends et al. 2013). Several gene products involved in aromatic amino acid metabolism have previously been shown to be induced by QS, including the anthranilate synthase genes *phnAB* (Table 4). The present data confirms that AHL QS can have a marked impact on cellular concentrations of free tyrosine.

Table 6.3 QS-modulated genes involved in amino acid metabolism.

Data was compiled from three independent studies: (Hentzer et al. 2003; Schuster et al. 2003; Wagner et al. 2003).

[a] Fold change was reported as the average fold induction in a *lasI rhlI* mutant when supplemented with 2 μM OdDHL and 5 μM BHL (average of samples collect at OD_{600} of 0.5, 1.3, 1.6, 2.0, 2.7). Bacteria were grown aerobically in ABt minimal medium with 0.5% casamino acids.

[b] Fold change was reported as the maximum fold induction in a *lasI rhlI* mutant when supplemented with 2 μM OdDHL and 10 μM BHL (maximum of samples collected at OD_{600} of 0.2, 0.4, 0.8, 1.4, 2.0, 3.0, and 4.0). Bacteria were grown aerobically in buffered Lysogeny Broth.

[c] Fold change was reported as the fold induction in a *lasI rhlI* mutant when supplemented with 1 μM OdDHL and 2 μM BHL. Values are reported for samples collected during early mid-logarithmic (ML) or stationary phase (ES) growth. The values are reported for the early stationary phase when differential expression was observed in both growth phases (B). Bacteria were grown aerobically in modified FAB medium.

		Fold modulation in *lasI rhlI* mutant			
PA number	Gene Name, synonyms	Hentzer et al. 2003[a]	Schuster et al. 2003[b]	Wagner et. al 2003[c]	Description
PA0228	pcaF			3.8 (ES)	beta-ketoadipyl CoA thiolase PcaF
PA0447	gcdH			7.8 (ML)	glutaryl-CoA dehydrogenase
PA0581	plsY			-2 (ML)	glycerol-3-phosphate acyltransferase
PA1869		57	41	79 (B)	probable acyl carrier protein
PA2001	atoB			23 (ML)	acetyl-CoA acetyltransferase
PA3300	fadD2			3.6 (ML)	long-chain-fatty-acid--CoA ligase
PA3333	fabH2	30	32	32 (B)	3-oxoacyl-[acyl-carrier-protein] synthase III
PA3334		30	49	23 (B)	probable acyl carrier protein
PA3645	fabZ, sefA			-1.8 (ES)	(3R)-hydroxymyristoyl-[acyl carrier protein] dehydratase
PA3924				4.6 (ML)	probable medium-chain acyl-CoA ligase

PA4888	desB, desB			-1.8 (B)	acyl-CoA delta-9-desaturase, DesB
PA0744				7 (ML)	probable enoyl-CoA hydratase/isomerase
PA0745				8.2 (ML)	probable enoyl-CoA hydratase/isomerase
PA0996	pqsA	9	90	4.7 (B)	probable coenzyme A ligase
PA0999	pqsD, fabH1	9	25	5.1 (B)	3-oxoacyl-[acyl-carrier-protein] synthase III
PA2552	acdB			10 (ML)	probable acyl-CoA dehydrogenase
PA2553				14 (ML)	probable acyl-CoA thiolase
PA2554				11 (ML)	probable short-chain dehydrogenase
PA2862	lipA			4 (ML)	lactonizing lipase precursor
PA2889	atuD			2.8 (ML)	putative citronellyl-CoA dehydrogenase involved in catabolism of citronellol
PA3330		149	120	38 (ML)	probable short chain dehydrogenase
PA3924				4.6 (ML)	probable medium-chain acyl-CoA ligase
PA4907	ydfG			1.7 (ES)	probable short-chain dehydrogenase
PA4979				2.4 (ML)	probable acyl-CoA dehydrogenase
PA5521				1.9 (ML)	probable short-chain dehydrogenase
PA5546				3.2 (ES)	conserved hypothetical protein

Chapter 7

Summary and General Discussion

AHL QS systems infer and convey valuable information about *P. aeruginosa*'s physical and social environment. They are intimately connected to a wider regulatory network that integrates cellular and environmental cues to determine the bacterium's growth strategy. Moreover, AHL regulatory systems regulate a large portion of the *P. aeruginosa* genome, including metabolically costly secreted factors. There is therefore good reason to expect QS systems to exert significant influence over primary metabolic functions. Indeed several lines of evidence from previous studies, including multiple independent transcriptomic studies, have suggested this might be the case (Hentzer et al. 2003; Schuster et al. 2003; Wagner et al. 2003). However, to my knowledge there has been no previous study of the global impact of AHL QS on the metabolome of *P. aeruginosa*, and so an important biochemical perspective on this relationship has been missing. The central aim of work presented in this dissertation was to conduct a systematic metabolomic investigation of the extent to which *P. aeruginosa*'s primary metabolism is coupled to AHL QS activity. This study has established that AHL QS has widespread effects on the small molecule primary metabolism of *P. aeruginosa* and that many of these changes are consistent with QS coordinating metabolic adaptation to stationary phase stresses.

Work described in Chapter 3 established that the *rhl*, *las* and PQS systems do indeed induce marked changes to the small molecule metabolism of *P. aeruginosa* and that these are apparent via ^{1}H-NMR metabolic footprinting. Mutants deficient in *lasI*, *rhlI* and *pqsR* were readily differentiated from wild-type *P. aeruginosa* PAO1. Fatty acid and amino acid profiles in particular were altered in all three QS mutants. The metabolic footprint of the *pqsR* mutant showed similar effects to the AHL QS mutants, although effect sizes were larger for the *lasI* and *rhl* mutants. This suggests that AHL signalling has a larger impact on primary metabolism than does alkyl quinolone signaling via *pqsR*, however further investigation is necessary to establish whether this holds true under other growth conditions and to assess the roles of the several AQ signals in modulating primary metabolism.

The pilot study prompted a systematic investigation of the impact of the *las* and *rhl* systems on primary metabolism, based on comparison of an "AHL signal-null" *lasI rhlI* mutant to wild-type *P. aeruginosa* PAO1. Time-resolved ^{1}H-NMR metabolic footprinting described in Chapter 4 proved valuable in identifying the timing of shifts in primary metabolism in the

mutant, revealing that rates of nutrient uptake and acetogenesis of the mutant diverge from that of wild-type *P. aeruginosa* during late exponential phase growth in AGSY medium. This divergence coincided with AHL accumulation in wild-type cultures, induction of *rhl*- and *las*-regulated gene expression and a small growth defect relative to the mutant. Complementary MS metabolomic and proteomic analyses were used to more precisely detail QS-dependent cellular metabolic changes during this transition to stationary phase growth, as described in Chapter 4, Chapter 5 and Chapter 6. These analyses revealed that AHL signalling has widespread effects on primary metabolism, including substantial impacts on central carbon metabolism, amino acid metabolism and fatty acid metabolism. Of the many QS-dependent effects on primary small molecule metabolism, perhaps the most compelling trend is that QS activity seems to induce metabolic adaptations to stationary phase stresses, particularly to oxidative stress and growth in oxygen-depleted environments. The slower growth of the wild-type was accompanied by repression of the oxidative CO_2-evolving portion of the TCA cycle, decreased acetogenesis and induction of the glyoxylate bypass. The glyoxylate shunt is has previously been shown to be induced in response to oxidative and antibiotic stress (Dunn et al. 2009; Ahn et al. 2016). Proteomic data indicated QS-induction of several other factors involved in adaptation to microaerobiosis, including arginine deiminase (ArcA), nitrite reductase (NirS, cytochrome cd1) and azurin (a nitrite reductase redox partner) (Schreiber et al. 2006; Trunk et al. 2010). Similarly, the fatty acid profiling revealed QS-dependent increases in cyclopropanation and longer acyl chain lengths, consistent with defense against stationary phase membrane stressors (including oxidative damage). In contrast, the *lasI rhlI* mutant—i.e. in the absence of AHL signalling—expressed lower levels of a variety of factors linked to protection against oxidative stress including catalase (KatA) and the siderophores pyoverdine and pyochelin. This may explain the elevated concentrations of the general stress-response molecules putrescine and spermidine seen in the mutant.

AHL QS has previously been shown to enhance the oxidative stress response: catalase and superoxide dismutase activities in *lasI*, *rhlI* and *lasI rhlI* mutants have been linked to increased sensitivity to oxidative stress (Hassett et al. 1999). More recently, a study of a *lasR rhlR* QS-deficient mutant demonstrated that QS confers resistance to osmotic, thermal and heavy metal stresses and exposure to oxidative stress (H_2O_2) can select for cells with active QS systems (García-Contreras et al. 2014). The present results suggest that QS-control of resistance to oxidative stress extends to protective modulation of primary metabolism. This implies there may be more general validity than realised to earlier hints that QS-dependent induction of primary metabolic processes serves protective roles, for example that AHL-induction of glucose-6-dehydrogenase in early stationary phase protects the cell from oxidative stress by supporting glutathione synthesis (Ma et al. 1998; Schuster et al. 2003).

The control of protective primary metabolic functions by QS in *P. aeruginosa* in the present study is consistent with growing evidence for similar functions in other bacteria. Environmental correlation between QS autoinducer concentrations, population cell density and resource competition means that QS may be used to infer the strength of ecological competition, and do so earlier than a stress responses system could allow (Cornforth and Foster 2013). More generally, stresses associated with crowded environments can be self-inflicted, for example via accumulation of toxic excretions. Work by (Goo et al. 2012) suggests that *Burkholderia* species use QS to perform "anticipatory" adaptation by inducing the excretion of oxalate as cultures approach carrying capacity, thereby protecting against ammonia-mediated alkaline toxicity in stationary phase. Similarly, QS-dependent repression of primary metabolic processes—including nutrient uptake and oxidative phosphorylation—in the rice pathogen *Burkholderia glumae* has been interpreted as a QS-controlled metabolic brake that supports metabolic homeostasis under crowded but cooperative conditions (An et al. 2014). QS-dependent induction of the glyoxylate cycle, arginine fermentation and protective fatty acid metabolism—as observed in the present study—suggest that QS may perform analagous anticipatory regulation of the primary metabolism of *P. aeruginosa*.

QS is one of several interlinked regulatory mechanisms determining stress responses in *P. aeruginosa*. QS-induced stress responses are mediated in part via regulators such as RpoS. The presence of putative RpoS and *rhl* boxes in the promoter region of PA5546 (a probable cyclopropane-fatty-acid-phospholipid synthase gene) suggests coordinate regulation of cyclopropanation. This expands the already extensive overlap in the RpoS and AHL QS regulons (Schuster et al. 2004*b*). The *las-rhl* box upstream of PA5546 points to direct regulation by QS, however it is likely that QS modulation of central metabolic processes is also a consequence of indirect regulation (via global regulators including RpoS) and adaptation to QS-induced perturbations to the cellular environment. AHL QS influences the cellular and environmental oxidative potential via expression of factors including rhamnolipid surfactants, phenazine redox shuttles, siderophores and catalase. For example oxygen availability can be modulated via secretion of rhamnolipid surfactants, as demonstrated by Sabra et al. (2002) and Kim et al. (2003). In a similar vein, AHL QS activity may increase the capacity for cellular oxidative phosphorylation via induction of AHL-regulated redox shuttles such as phenazines: pyocyanin regulates primary metabolism during stationary phase under conditions of low oxygen availability and lowers the intracellular NADH/NAD ratio (Price-Whelan et al. 2007). Such QS-mediated manipulations of the cellular and external environment could contribute to the changes in central carbon metabolism observed in the present study. Another consideration is that redirection of metabolic resources away from central metabolism and toward QS-dependent biosynthesis

public goods will itself result in adaptive metabolic responses, independent of any direct QS regulatory control. Metabolic supply-demand analysis illustrates that the control of flux through a supply pathway may reside outside that pathway, in downstream demand reactions (Hofmeyr and Cornish-Bowden 2000; Oliver 2002). This may contribute to depletion of TCA intermediates and amino acid precursors of secondary metabolites as well as the lower growth yield of the wild-type compared to the *lasI rhlI* mutant.

Defenses against biotic and abiotic stress play key roles in environmental persistance and virulence and, given the role of QS in stress tolerance, are probably also important in the evolution of QS systems. For example several of the QS-induced primary metabolic phenotypes are thought to play roles in host colonisation and disease. A recent analysis of genome-wide gene expression and mutant fitness profiles found metabolic phenotypes similar to those described here are implicated in fitness in a mouse acute wound model of infection: downregulation of the decarboxylating steps of the TCA cycle, upregulation of isocitrate lyase, and upregulation of a number of genes associated with growth under oxygen-limitation (Turner et al. 2014). The glyoxylate cycle and arginine deiminase are also induced in chronic lung infections (Son et al. 2007; Dunn et al. 2009).

To better understand the mechanisms connecting QS and metabolic changes, it will be important to distinguish the direct from the indirect consequences of QS, for example between direct regulation of primary metabolic enzymes and indirect regulation of metabolism via modulation of metabolic demand (synthesis of secondary metabolites and secreted factors), cellular physiology (membrane composition) and environmental conditions (environmental oxidative potential). Using chromatin immunoprecipitation in conjunction with DNA microarray analysis (ChIP-chip), Gilbert et al. (2009) assessed direct transcriptional regulation, observing that only a small fraction of las-induced transciptional regulation could be ascribed to direct promoter-binding by LasR. Given the apparent interdependency of multiple regulators in mediating QS responses, it would be useful to extend this line of investigation to examine coordination between LasR, RhlR and their regulatory partners, using metabolomic, gene expression and ChIP-chip data obtained under common conditions.

Understanding the various indirect mechanisms by which QS controls primary metabolism will require careful experimental control of nutrient composition, environmental conditions and QS-dependent gene expression (ideally exogenous, QS-indpendent control). Chemostat fermentation would be a particularly attactive approach, affording independent control of environmental conditions, bacterial cell density and exogenous inducers of gene expression. Ideally, such experiments would be desinged to allow for analysis of population

heterogeneity, for example using single-cell measurement of gene expression using fluorescent reporters and high-resolution microscopy. Such approaches offer the exciting prospect of unravelling the fundamental metabolic adaptive functions of QS in terms of true quorum sensing (population density), diffusion sensing (mass transfer environment), competition sensing (ecological competition) and metabolic prudence.

It is important to note that only a portion of the *P. aeruginosa* metabolome was assayed in the present study and so the data inevitably provides a partial view of the role of QS in regulating small molecules metabolism. Moreover, the analyses were conducted on cells grown in batch culture in rich medium at a single temperature, with an emphasis on the transition from exponential to stationary phase growth. It is certainly the case that QS has many effects on primary metabolism not yet identified and that these are highly dependent on prevailing growth conditions. There is also scope for optimising the sampling protocols used. For example the sampling protocol used for cellular metabolic profiling in Chapters 4–6 consisted of quenching by cooling and washing with cold saline, following by snap freezing and methanol-chloroform extraction. Quenching with cold saline and centrifugation was performed so as to avoid the high rates of cell leakage observed with direct injection into solvents (Bolten et al. 2007). However, some reactions will continue at significant rates for several minutes prior to snap freezing in liquid nitrogen. This could be addressed by applying rapid sampling techniques, for example fast filtration methods or direct injection techniques optimised so as to minimise cell leakage (Faijes et al. 2007; Canelas et al. 2009). Stable isotope labelling for metabolic flux analysis would be valuable in supplementing the present current metabolite concentation data, particularly in examining the effects of QS on central carbon metabolism.

To conclude, the present work provides a missing perspective on the relationship between QS and small molecule metabolism—that of a broad analysis of the QS-modulated metabolome—and in doing so identifies QS-regulated primary metabolic traits with implications for the evolutionary stability of *P. aeruginosa* QS systems and their adaptive functions in the environment and during infection.

References

Ahn, S., Jung, J., Jang, I.-A., Madsen, E.L. and Park, W. 2016. Role of glyoxylate shunt in oxidative stress response. *Journal of Biological Chemistry* 291 (22): 11928–11938.

Albus, A.M., Pesci, E.C., Runyen-Janecky, L.J., West, S.E. and Iglewski, B.H. 1997. Vfr controls quorum sensing in *Pseudomonas aeruginosa*. *Journal of Bacteriology* 179 (12): 3928–3935.

Alhede, M., Bjarnsholt, T., Jensen, P.Ø., Phipps, R.K., Moser, C., Christophersen, L., Christensen, L.D., van Gennip, M., Parsek, M., Høiby, N., Rasmussen, T.B. and Givskov, M. 2009. *Pseudomonas aeruginosa* recognizes and responds aggressively to the presence of polymorphonuclear leukocytes. *Microbiology* 155 (11): 3500–3508.

Allen, J., Davey, H.M., Broadhurst, D., Rowland, J.J., Oliver, S.G. and Kell, D.B. 2004. Discrimination of modes of action of antifungal substances by use of metabolic footprinting. *Applied and Environmental Microbiology* 70 (10): 6157–6165.

Allen, J., Davey, H.M., Broadhurst, D., Heald, J.K., Rowland, J.J., Oliver, S.G. and Kell, D.B. 2003. High-throughput classification of yeast mutants for functional genomics using metabolic footprinting. *Nature Biotechnology* 21 (6): 692–696.

Allen, R.C., McNally, L., Popat, R. and Brown, S.P. 2016. Quorum sensing protects bacterial co-operation from exploitation by cheats. *The ISME Journal*.

Alvarez-Ortega, C. and Harwood, C.S. 2007. Responses of *Pseudomonas aeruginosa* to low oxygen indicate that growth in the cystic fibrosis lung is by aerobic respiration. *Molecular Microbiology* 65 (1): 153–165.

An, J.H., Goo, E., Kim, H., Seo, Y.-S. and Hwang, I. 2014. Bacterial quorum sensing and metabolic slowing in a cooperative population. *Proceedings of the National Academy of Sciences* 111 (41): 14912–14917.

Arai, H. 2011. Regulation and function of versatile aerobic and anaerobic respiratory metabolism in *Pseudomonas aeruginosa*. *Frontiers in Microbiology* 2.

Arevalo-Ferro, C., Hentzer, M., Reil, G., Görg, A., Kjelleberg, S., Givskov, M., Riedel, K. and Eberl, L. 2003. Identification of quorum-sensing regulated proteins in the opportunistic pathogen *Pseudomonas aeruginosa* by proteomics. *Environmental Microbiology* 5 (12): 1350–1369.

Ashby, M.K. 2004. Survey of the number of two-component response regulator genes in the complete and annotated genome sequences of prokaryotes. *FEMS Microbiology Letters* 231 (2): 277–281.

Atherton, H.J., Bailey, N.J., Zhang, W., Taylor, J., Major, H., Shockcor, J., Clarke, K. and Griffin, J.L. 2006. A combined ^{1}H-NMR spectroscopy- and mass spectrometry-based metabolomic study of the PPAR-α null mutant mouse defines profound systemic changes in metabolism linked to the metabolic syndrome. *Physiological Genomics* 27 (2): 178–186.

Badawy, A. a.-B., Morgan, C.J. and Turner, J.A. 2007. Application of the Phenomenex EZ:faast™ amino acid analysis kit for rapid gas-chromatographic determination of concentrations of plasma tryptophan and its brain uptake competitors. *Amino Acids* 34 (4): 587–596.

Balasubramanian, D., Schneper, L., Kumari, H. and Mathee, K. 2013. A dynamic and intricate regulatory network determines *Pseudomonas aeruginosa* virulence. *Nucleic Acids Research* 41 (1): 1–20.

Baumann, U., King, M., App, E.M., Tai, S., Konig, A., Fischer, J.J., Zimmermann, T., Sextro, W. and von der Hardt, H. 2004. Long term azithromycin therapy in cystic fibrosis patients: a study on drug levels and sputum properties. *Can Respir J* 11 (2): 151–155.

Baysse, C. and O'Gara, F. 2007. Role of membrane structure during stress signalling and adaptation in *Pseudomonas*. *In*: Ramos, J.-L. and Filloux, A. (eds.), *Pseudomonas*, 193–224. Springer Netherlands.

Baysse, C., Cullinane, M., Denervaud, V., Burrowes, E., Dow, J.M., Morrissey, J.P., Tam, L., Trevors, J.T. and O'Gara, F. 2005. Modulation of quorum sensing in *Pseudomonas aeruginosa* through alteration of membrane properties. *Microbiology* 151 (8): 2529–2542.

Beatson, S.A., Whitchurch, C.B., Semmler, A.B.T. and Mattick, J.S. 2002. Quorum sensing is not required for twitching motility in *Pseudomonas aeruginosa*. *Journal of Bacteriology* 184 (13): 3598–3604.

Behrends, V., Ryall, B., Zlosnik, J.E.A., Speert, D.P., Bundy, J.G. and Williams, H.D. 2013. Metabolic adaptations of *Pseudomonas aeruginosa* during cystic fibrosis chronic lung infections: Metabolomic adaptations of cystic fibrosis isolates. *Environmental Microbiology* 15 (2): 398–408.

Belle, J.E.L., Harris, N.G., Williams, S.R. and Bhakoo, K.K. 2002. A comparison of cell and tissue extraction techniques using high-resolution ^{<FONT SIZE='-1'>1</FONT>}H-NMR spectroscopy. *NMR in Biomedicine* 15 (1): 37–44.

Benjamini, Y. and Hochberg, Y. 1995. Controlling the false discovery rate: a practical and powerful approach to multiple testing. *Journal of the Royal Statistical Society. Series B, Statistical methodology* 57 (1): 289–300.

Benjamini, Y. and Yekutieli, D. 2001. The control of the false discovery rate in multiple testing under dependency. *The Annals of Statistics* 29 (4): 1165–1188.

Bennett, B.D., Kimball, E.H., Gao, M., Osterhout, R., Van Dien, S.J. and Rabinowitz, J.D. 2009. Absolute metabolite concentrations and implied enzyme active site occupancy in *Escherichia coli*. *Nature chemical biology* 5 (8): 593–599.

Boles, B.R., Thoendel, M. and Singh, P.K. 2005. Rhamnolipids mediate detachment of *Pseudomonas aeruginosa* from biofilms. *Mol Microbiol* 57 (5): 1210–1223.

Bollinger, N., Hassett, D.J., Iglewski, B.H., Costerton, J.W. and McDermott, T.R. 2001. Gene expression in *Pseudomonas aeruginosa*: evidence of iron override effects on quorum sensing and biofilm-specific gene regulation. *Journal of Bacteriology* 183 (6): 1990–1996.

Bolten, C.J., Kiefer, P., Letisse, F., Portais, J.-C. and Wittmann, C. 2007. Sampling for Metabolome Analysis of Microorganisms. *Analytical Chemistry* 79 (10): 3843–3849.

Botzenhart, K. and Döring, G. 1993. Ecology and epidemiology of *Pseudomonas aeruginosa*. *In*: Campa, M., Bendinelli, M. and Friedman, H. (eds.), *Pseudomonas Aeruginosa as an Opportunistic Pathogen*, 1–18. Springer US.

Boucher, R.C. 2004. New concepts of the pathogenesis of cystic fibrosis lung disease. *European Respiratory Journal* 23: 146–158.

Bredenbruch, F., Geffers, R., Nimtz, M., Buer, J. and Häussler, S. 2006. The *Pseudomonas aeruginosa* quinolone signal (PQS) has an iron-chelating activity. *Environmental Microbiology* 8 (8): 1318–1329.

Brencic, A., McFarland, K.A., McManus, H.R., Castang, S., Mogno, I., Dove, S.L., Lory, S., Brencic, A., McFarland, K.A., McManus, H.R., Castang, S., Mogno, I., Dove, S.L. and Lory, S. 2009. The GacS/GacA signal transduction system of *Pseudomonas aeruginosa* acts exclusively through its control over the transcription of the RsmY and RsmZ regulatory small RNAs. *Molecular Microbiology, Molecular Microbiology* 73, 73 (3, 3): 434, 434–445, 445.

Brint, J. and Ohman, D. 1995. Synthesis of multiple exoproducts in *Pseudomonas aeruginosa* is under the control of RhlR-RhlI, another set of regulators in strain PAO1 with homology to the autoinducer-responsive LuxR-LuxI family. *J. Bacteriol.* 177 (24): 7155–7163.

Bruger, E.L. and Waters, C.M. 2016. Bacterial quorum sensing stabilizes cooperation by optimizing growth strategies. *Applied and Environmental Microbiology* 82 (22): 6498–6506.

Cabrol, S., Olliver, A., Pier, G.B., Andremont, A. and Ruimy, R. 2003. Transcription of quorum-sensing system genes in clinical and environmental isolates of *Pseudomonas aeruginosa*. *J. Bacteriol.* 185 (24): 7222–7230.

Canelas, A.B., ten Pierick, A., Ras, C., Seifar, R.M., van Dam, J.C., van Gulik, W.M. and Heijnen, J.J. 2009. Quantitative Evaluation of Intracellular Metabolite Extraction Techniques for Yeast Metabolomics. *Analytical Chemistry* 81 (17): 7379–7389.

Chang, Y.-Y. and Cronan, J.E. 1999. Membrane cyclopropane fatty acid content is a major factor in acid resistance of *Escherichia coli*. *Molecular Microbiology* 33 (2): 249–259.

Chang, Y.-Y., Eichel, J. and Cronan, J.E. 2000. Metabolic instability of *Escherichia coli* cyclopropane fatty acid synthase is due to Rpoh-dependent proteolysis. *J. Bacteriol.* 182 (15): 4288–4294.

Choi, K.-H., Kumar, A. and Schweizer, H.P. 2006. A 10-min method for preparation of highly electrocompetent *Pseudomonas aeruginosa* cells: Application for DNA fragment transfer between chromosomes and plasmid transformation. *Journal of Microbiological Methods* 64 (3): 391–397.

Cholley, P., Thouverez, M., Floret, N., Bertrand, X. and Talon, D. 2008. The role of water fittings in intensive care rooms as reservoirs for the colonization of patients with *Pseudomonas aeruginosa*. *Intensive Care Medicine* 34 (8): 1428.

Chou, H.T., Hegazy, M. and Lu, C.-D. 2010. l-Lysine Catabolism Is Controlled by l-Arginine and ArgR in Pseudomonas aeruginosa PAO1. *Journal of Bacteriology* 192 (22): 5874–5880.

Coggan, K.A. and Wolfgang, M.C. 2012. Global regulatory pathways and cross-talk control *Pseudomonas aeruginosa* environmental lifestyle and virulence phenotype. *Current issues in molecular biology* 14 (2): 47.

Cohen, D., Mechold, U., Nevenzal, H., Yarmiyhu, Y., Randall, T.E., Bay, D.C., Rich, J.D., Parsek, M.R., Kaever, V., Harrison, J.J. and Banin, E. 2015. Oligoribonuclease is a central

feature of cyclic diguanylate signaling in *Pseudomonas aeruginosa*. *Proceedings of the National Academy of Sciences* 112 (36): 11359–11364.

Cornelis, P., Wei, Q., C. Andrews, S. and Vinckx, T. 2011. Iron homeostasis and management of oxidative stress response in bacteria. *Metallomics* 3 (6): 540–549.

Cornforth, D.M. and Foster, K.R. 2013. Competition sensing: the social side of bacterial stress responses. *Nature Reviews Microbiology* 11 (4): 285–293.

Cosson, P., Zulianello, L., Join-Lambert, O., Faurisson, F., Gebbie, L., Benghezal, M., Delden, C. van, Curty, L.K. and Köhler, T. 2002. *Pseudomonas aeruginosa* virulence analyzed in a *Dictyostelium discoideum* host system. *Journal of Bacteriology* 184 (11): 3027–3033.

Costerton, J.W. and Anwar, H. 1994. *Pseudomonas aeruginosa*: the microbe and pathogen. *In*: *Infectious Disease and Therapy Series*, Vol. 12, 1–1. Marcel Dekker, New York, NY.

Cozzone, A.J. 1998. Regulation of acetate metabolism by protein phosphorylation in enteric bacteria. *Annual Reviews in Microbiology* 52 (1): 127–164.

Damron, F.H., Owings, J.P., Okkotsu, Y., Varga, J.J., Schurr, J.R., Goldberg, J.B., Schurr, M.J. and Yu, H.D. 2012. Analysis of the *Pseudomonas aeruginosa* regulon controlled by the sensor kinase KinB and sigma factor RpoN. *Journal of Bacteriology* 194 (6): 1317–1330.

Dandekar, A.A., Chugani, S. and Greenberg, E.P. 2012. Bacterial quorum sensing and metabolic incentives to cooperate. *Science* 338 (6104): 264–266.

Darch, S.E., West, S.A., Winzer, K. and Diggle, S.P. 2012. Density-dependent fitness benefits in quorum-sensing bacterial populations. *Proceedings of the National Academy of Sciences*.

Davenport, P.W., Griffin, J.L. and Welch, M. 2015. Quorum sensing is accompanied by global metabolic changes in the opportunistic human pathogen *Pseudomonas aeruginosa*. *Journal of Bacteriology* 197 (12): 2072–2082.

De Biase, D., Tramonti, A., Bossa, F. and Visca, P. 1999. The response to stationary-phase stress conditions in *Escherichia coli*: role and regulation of the glutamic acid decarboxylase system. *Molecular Microbiology* 32 (6): 1198–1211.

Dekimpe, V. and Déziel, E. 2009. Revisiting the quorum-sensing hierarchy in *Pseudomonas aeruginosa*: the transcriptional regulator RhlR regulates LasR-specific factors. *Microbiology (Reading, England)* 155 (Pt 3): 712–723.

Dénervaud, V., TuQuoc, P., Blanc, D., Favre-Bonte, S., Krishnapillai, V., Reimmann, C., Haas, D. and van Delden, C. 2004. Characterization of cell-to-cell signaling-deficient *Pseudomonas aeruginosa* strains colonizing intubated patients. *J Clin Microbiol* 42 (2): 554–562.

Denich, T.J., Beaudette, L.A., Lee, H. and Trevors, J.T. 2003. Effect of selected environmental and physico-chemical factors on bacterial cytoplasmic membranes. *Journal of Microbiological Methods* 52 (2): 149–182.

Déziel, E., Lépine, F., Milot, S., He, J., Mindrinos, M.N., Tompkins, R.G. and Rahme, L.G. 2004. Analysis of *Pseudomonas aeruginosa* 4-hydroxy-2-alkylquinolines (HAQs) reveals a role for 4-hydroxy-2-heptylquinoline in cell-to-cell communication. *Proceedings of the National Academy of Sciences of the United States of America* 101 (5): 1339–1344.

Diggle, S.P., Cornelis, P., Williams, P. and Camara, M. 2006. 4-quinolone signalling in *Pseudomonas aeruginosa*: old molecules, new perspectives. *Int J Med Microbiol* 296 (2–3): 83–91.

Diggle, S.P., Winzer, K., Lazdunski, A., Williams, P. and Cámara, M. 2002. Advancing the quorum in *Pseudomonas aeruginosa*: MvaT and the regulation of *N*-acylhomoserine lactone production and virulence gene expression. *Journal of Bacteriology* 184 (10): 2576–2586.

Diggle, S.P., Matthijs, S., Wright, V.J., Fletcher, M.P., Chhabra, S.R., Lamont, I.L., Kong, X., Hider, R.C., Cornelis, P., Cámara, M. and Williams, P. 2007. The *Pseudomonas aeruginosa* 4-quinolone signal molecules HHQ and PQS play multifunctional roles in quorum sensing and iron entrapment. *Chemistry & Biology* 14 (1): 87–96.

Dubois-Brissonnet, F., Malgrange, C., Guérin-Méchin, L., Heyd, B. and Leveau, J.. 2000. Effect of temperature and physiological state on the fatty acid composition of *Pseudomonas aeruginosa*. *International Journal of Food Microbiology* 55 (1–3): 79–81.

Dubois-Brissonnet, F., Malgrange, C., Guérin-Méchin, L., Heyd, B. and Leveau, J.Y. 2001. Changes in fatty acid composition of *Pseudomonas aeruginosa* ATCC 15442 induced by growth conditions: consequences of resistance to quaternary ammonium compounds. *Microbios* 106 (414): 97–110.

Dunn, M.F., Ramírez-Trujillo, J.A. and Hernández-Lucas, I. 2009. Major roles of isocitrate lyase and malate synthase in bacterial and fungal pathogenesis. *Microbiology* 155 (10): 3166–3175.

Dunn, O.J. 1958. Estimation of the Means of Dependent Variables. *The Annals of Mathematical Statistics* 29 (4): 1095–1111.

Dunn, O.J. 1961. Multiple Comparisons among Means. *Journal of the American Statistical Association* 56 (293): 52–64.

Durbin, B.P., Hardin, J.S., Hawkins, D.M. and Rocke, D.M. 2002. A variance-stabilizing transformation for gene-expression microarray data. *Bioinformatics* 18 (suppl_1): S105–S110.

Eberhard, A. 1972. Inhibition and activation of bacterial luciferase synthesis. *Journal of Bacteriology* 109 (3): 1101–1105.

Eder, K. 1995. Gas chromatographic analysis of fatty acid methyl esters. *Journal of Chromatography B: Biomedical Sciences and Applications* 671 (1–2): 113–131.

Eichel, J., Chang, Y.-Y., Riesenberg, D. and Cronan, J.E. 1999. Effect of ppGpp on *Escherichia coli* cyclopropane fatty acid synthesis is mediated through the RpoS sigma factor. *Journal of Bacteriology* 181 (2): 572–576.

El-Mansi, M. 2004. Flux to acetate and lactate excretions in industrial fermentations: physiological and biochemical implications. *Journal of Industrial Microbiology & Biotechnology* 31 (7).

Faijes, M., Mars, A. and Smid, E. 2007. Comparison of quenching and extraction methodologies for metabolome analysis of Lactobacillus plantarum. *Microbial Cell Factories* 6 (1): 27.

Farinha, M.A. and Kropinski, A.M. 1990. Construction of broad-host-range plasmid vectors for easy visible selection and analysis of promoters. *Journal of Bacteriology* 172 (6): 3496–3499.

Favre-Bonté, S., Köhler, T. and Van Delden, C. 2003. Biofilm formation by *Pseudomonas aeruginosa*: role of the C4-HSL cell-to-cell signal and inhibition by azithromycin. *Journal of Antimicrobial Chemotherapy* 52 (4): 598–604.

Feehily, C. and Karatzas, K. a. g. 2013. Role of glutamate metabolism in bacterial responses towards acid and other stresses. *Journal of Applied Microbiology* 114 (1): 11–24.

Feistner, G.J. 1994. Profiling of basic amino acids and polyamines in microbial culture supernatants by electrospray mass spectrometry. *Biological Mass Spectrometry* 23 (12): 784–792.

Fonteh, A.N., Harrington, R.J. and Harrington, M.G. 2006. Quantification of free amino acids and dipeptides using isotope dilution liquid chromatography and electrospray ionization tandem mass spectrometry. *Amino Acids* 32 (2): 203–212.

Food and Drug Administration. 2001. *Guidance for Industry: Bioanalytical Method Validation*. Food and Drug Administration, .

Fujitani, S., Sun, H.-Y., Yu, V.L. and Weingarten, J.A. 2011. Pneumonia due to *Pseudomonas aeruginosa*: Part i: epidemiology, clinical diagnosis, and source. *Chest* 139 (4): 909–919.

Fuqua, W.C., Winans, S.C. and Greenberg, E.P. 1994. Quorum sensing in bacteria: the LuxR-LuxI family of cell density-responsive transcriptional regulators. *Journal of Bacteriology* 176 (2): 269–275.

Gales, A.C., Jones, R.N., Turnidge, J., Rennie, R. and Ramphal, R. 2001. Characterization of *Pseudomonas aeruginosa* isolates: occurrence rates, antimicrobial susceptibility patterns, and molecular typing in the global SENTRY Antimicrobial Surveillance Program, 1997-1999. *Clin Infect Dis* 32 Suppl 2: S146-55.

Gallagher, L.A. and Manoil, C. 2001. *Pseudomonas aeruginosa* PAO1 kills *Caenorhabditis elegans* by cyanide poisoning. *J Bacteriol* 183 (21): 6207–6214.

Gallagher, L.A., McKnight, S.L., Kuznetsova, M.S., Pesci, E.C. and Manoil, C. 2002. Functions Required for Extracellular Quinolone Signaling by *Pseudomonas aeruginosa*. *Journal of Bacteriology* 184 (23): 6472–6480.

Gambello, M.J. and Iglewski, B.H. 1991. Cloning and characterization of the *Pseudomonas aeruginosa lasR* gene, a transcriptional activator of elastase expression. *Journal of Bacteriology* 173 (9): 3000–3009.

Gambello, M.J., Kaye, S. and Iglewski, B.H. 1993. LasR of *Pseudomonas aeruginosa* is a transcriptional activator of the alkaline protease gene (*apr*) and an enhancer of exotoxin A expression. *Infection and Immunity* 61 (4): 1180–1184.

García-Contreras, R. 2016. Is quorum sensing interference a viable alternative to treat *Pseudomonas aeruginosa* infections? *Frontiers in Microbiology* 7.

García-Contreras, R., Nuñez-López, L., Jasso-Chávez, R., Kwan, B.W., Belmont, J.A., Rangel-Vega, A., Maeda, T. and Wood, T.K. 2014. Quorum sensing enhancement of the stress response promotes resistance to quorum quenching and prevents social cheating. *The ISME Journal*.

Geller, S.C., Gregg, J.P., Hagerman, P. and Rocke, D.M. 2003. Transformation and normalization of oligonucleotide microarray data. *Bioinformatics* 19 (14): 1817–1823.

Gilbert, K.B., Kim, T.H., Gupta, R., Greenberg, E.P. and Schuster, M. 2009. Global position analysis of the *Pseudomonas aeruginosa* quorum-sensing transcription factor LasR. *Molecular Microbiology* 73 (6): 1072–1085.

Gillis, R.J. and Iglewski, B.H. 2004. Azithromycin retards *Pseudomonas aeruginosa* biofilm formation. *Journal of Clinical Microbiology* 42 (12): 5842–5845.

Goo, E., Majerczyk, C.D., An, J.H., Chandler, J.R., Seo, Y.-S., Ham, H., Lim, J.Y., Kim, H., Lee, B., Jang, M.S., Greenberg, E.P. and Hwang, I. 2012. Bacterial quorum sensing, cooperativity, and anticipation of stationary-phase stress. *Proceedings of the National Academy of Sciences of the United States of America* 109 (48): 19775–19780.

Graf, J. and Ruby, E.G. 1998. Host-derived amino acids support the proliferation of symbiotic bacteria. *Proceedings of the National Academy of Sciences of the United States of America* 95 (4): 1818–1822.

Grogan, D. and Cronan, J. 1997. Cyclopropane ring formation in membrane lipids of bacteria. *Microbiology and molecular biology reviews* 61 (4): 429–441.

Grosso-Becerra, M.-V., Santos-Medellín, C., González-Valdez, A., Méndez, J.-L., Delgado, G., Morales-Espinosa, R., Servín-González, L., Alcaraz, L.-D. and Soberón-Chávez, G. 2014. *Pseudomonas aeruginosa* clinical and environmental isolates constitute a single population with high phenotypic diversity. *BMC Genomics* 15: 318.

Guckert, J.B., Hood, M.A. and White, D.C. 1986. Phospholipid ester-linked fatty acid profile changes during nutrient deprivation of *Vibrio cholerae*: increases in the *trans*/*cis* ratio and proportions of cyclopropyl fatty acids. *Applied and environmental microbiology* 52 (4): 794–801.

Hagins, J.M., Scoffield, J.A., Suh, S.-J. and Silo-Suh, L. 2010. Influence of RpoN on isocitrate lyase activity in *Pseudomonas aeruginosa*. *Microbiology* 156 (4): 1201–1210.

Häkkinen, M.R., Keinänen, T.A., Vepsäläinen, J., Khomutov, A.R., Alhonen, L., Jänne, J. and Auriola, S. 2007. Analysis of underivatized polyamines by reversed phase liquid chromatography with electrospray tandem mass spectrometry. *Journal of Pharmaceutical and Biomedical Analysis* 45 (4): 625–634.

Hancock, I.C. and Meadow, P.M. 1969. The extractable lipids of *Pseudomonas aeruginosa*. *Biochimica et biophysica acta.* 187 (3): 366–379.

Hansen, C.R., Pressler, T., Koch, C. and Hoiby, N. 2005. Long-term azitromycin treatment of cystic fibrosis patients with chronic *Pseudomonas aeruginosa* infection; an observational cohort study. *J Cyst Fibros* 4 (1): 35–40.

Härtig, C., Loffhagen, N. and Harms, H. 2005. Formation of *trans* fatty acids is not involved in growth-linked membrane adaptation of *Pseudomonas putida*. *Applied and Environmental Microbiology* 71 (4): 1915–1922.

Hassett, D.J., Ma, J.-F., Elkins, J.G., McDermott, T.R., Ochsner, U.A., West, S.E.H., Huang, C.-T., Fredericks, J., Burnett, S., Stewart, P.S., McFeters, G., Passador, L. and Iglewski, B.H. 1999. Quorum sensing in *Pseudomonas aeruginosa* controls expression of catalase

and superoxide dismutase genes and mediates biofilm susceptibility to hydrogen peroxide. *Molecular microbiology* 34 (5): 1082–1093.

Hazan, R., He, J., Xiao, G., Dekimpe, V., Apidianakis, Y., Lesic, B., Astrakas, C., Déziel, E., Lépine, F. and Rahme, L.G. 2010. Homeostatic interplay between bacterial cell-cell signaling and iron in virulence. *PLOS Pathogens* 6 (3): e1000810.

Heath, R.J. and Rock, C.O. 1996a. Inhibition of beta-ketoacyl-acyl carrier protein synthase III (FabH) by acyl-acyl carrier protein in *Escherichia coli*. *The Journal of Biological Chemistry* 271 (18): 10996–11000.

Heath, R.J. and Rock, C.O. 1996b. Roles of the FabA and FabZ beta-hydroxyacyl-acyl carrier protein dehydratases in *Escherichia coli* fatty acid biosynthesis. *The Journal of Biological Chemistry* 271 (44): 27795–27801.

Heath, R.J., Jackowski, S. and Rock, C.O. 1994. Guanosine tetraphosphate inhibition of fatty acid and phospholipid synthesis in *Escherichia coli* is relieved by overexpression of glycerol-3-phosphate acyltransferase (*plsB*). *Journal of Biological Chemistry* 269 (42): 26584–26590.

Hengge, R. 2011. Stationary-phase gene regulation in *Escherichia coli*. *EcoSal Plus* 4 (2).

Hentzer, M., Wu, H., Andersen, J.B., Riedel, K., Rasmussen, T.B., Bagge, N., Kumar, N., Schembri, M.A., Song, Z., Kristoffersen, P., Manefield, M., Costerton, J.W., Molin, S., Eberl, L., Steinberg, P., Kjelleberg, S., Høiby, N. and Givskov, M. 2003. Attenuation of *Pseudomonas aeruginosa* virulence by quorum sensing inhibitors. *The EMBO Journal* 22 (15): 3803–3815.

Heurlier, K., Dénervaud, V. and Haas, D. 2006. Impact of quorum sensing on fitness of *Pseudomonas aeruginosa*. *International Journal of Medical Microbiology* 296 (2–3): 93–102.

Heurlier, K., Dénervaud, V., Pessi, G., Reimmann, C. and Haas, D. 2003. Negative control of quorum sensing by RpoN (σ54) in *Pseudomonas aeruginosa* PAO1. *Journal of Bacteriology* 185 (7): 2227–2235.

Heurlier, K., Dénervaud, V., Haenni, M., Guy, L., Krishnapillai, V. and Haas, D. 2005. Quorum-sensing-negative (*lasR*) mutants of *Pseudomonas aeruginosa* avoid cell lysis and death. *Journal of bacteriology* 187 (14): 4875–4883.

Heurlier, K., Williams, F., Heeb, S., Dormond, C., Pessi, G., Singer, D., Cámara, M., Williams, P. and Haas, D. 2004. Positive control of swarming, rhamnolipid synthesis, and lipase production by the posttranscriptional RsmA/RsmZ system in *Pseudomonas aeruginosa* PAO1. *Journal of Bacteriology* 186 (10): 2936–2945.

Hoffmann, N., Lee, B., Hentzer, M., Rasmussen, T.B., Song, Z., Johansen, H.K., Givskov, M. and Høiby, N. 2007. Azithromycin blocks quorum sensing and alginate polymer formation and increases the sensitivity to serum and stationary-growth-phase killing of *Pseudomonas aeruginosa* and attenuates chronic *P. aeruginosa* lung infection in Cftr−/− mice. *Antimicrobial Agents and Chemotherapy* 51 (10): 3677–3687.

Hofmeyr, J.-H.S. and Cornish-Bowden, A. 2000. Regulating the cellular economy of supply and demand. *FEBS Letters* 476 (1–2): 47–51.

Holloway, B.W. 1969. Genetics of Pseudomonas. *Bacteriological Reviews* 33 (3): 419–443.

Howe, R.A. and Spencer, R.C. 1997. Macrolides for the treatment of *Pseudomonas aeruginosa* infections? *J Antimicrob Chemother* 40 (2): 153–155.

Huber, W., von Heydebreck, A., Sültmann, H., Poustka, A. and Vingron, M. 2002. Variance stabilization applied to microarray data calibration and to the quantification of differential expression. *Bioinformatics* 18 (suppl_1): S96–S104.

Ikeda, T., Kajiyama, K., Kita, T., Takiguchi, N., Kuroda, A., Kato, J. and Ohtake, H. 2001. The synthesis of optically pure enantiomers of *N*-acyl-homoserine lactone autoinducers and their analogues. *Chemistry Letters* 30 (4): 314–315.

Jensen, P.Ø., Bjarnsholt, T., Phipps, R., Rasmussen, T.B., Calum, H., Christoffersen, L., Moser, C., Williams, P., Pressler, T., Givskov, M. and Høiby, N. 2007. Rapid necrotic killing of polymorphonuclear leukocytes is caused by quorum-sensing-controlled production of rhamnolipid by *Pseudomonas aeruginosa*. *Microbiology* 153 (5): 1329–1338.

Jeon, E. 2012. Improved production of long-chain fatty acid in *Escherichia coli* by an engineering elongation cycle during fatty acid synthesis (FAS) through genetic manipulation. *Journal of Microbiology and Biotechnology* 22 (7): 990–999.

Jones, B.W. and Nishiguchi, M.K. 2004. Counterillumination in the Hawaiian bobtail squid, *Euprymna scolopes* Berry (Mollusca: Cephalopoda). *Marine Biology* 144 (6): 1151–1155.

Jørgensen, F., Bally, M., Chapon-Herve, V., Michel, G., Lazdunski, A., Williams, P. and Stewart, G. 1999. RpoS-dependent stress tolerance in *Pseudomonas aeruginosa*. *Microbiology* 145 (4): 835–844.

Juhas, M., Eberl, L. and Tümmler, B. 2005. Quorum sensing: the power of cooperation in the world of Pseudomonas. *Environmental Microbiology* 7 (4): 459–471.

Kaderbhai, N.N., Broadhurst, D.I., Ellis, D.I., Goodacre, R. and Kell, D.B. 2003. Functional genomics via metabolic footprinting: monitoring metabolite secretion by *Escherichia coli* tryptophan metabolism mutants using FT–IR and direct injection electrospray mass spectrometry. *Comparative and Functional Genomics* 4 (4): 376–391.

Kai, T., Tateda, K., Kimura, S., Ishii, Y., Ito, H., Yoshida, H., Kimura, T. and Yamaguchi, K. 2009. A low concentration of azithromycin inhibits the mRNA expression of *N*-acyl homoserine lactone synthesis enzymes, upstream of *lasI* or *rhlI*, in *Pseudomonas aeruginosa*. *Pulmonary Pharmacology & Therapeutics* 22 (6): 483–486.

Kanjee, U., Ogata, K. and Houry, W.A. 2012. Direct binding targets of the stringent response alarmone (p)ppGpp. *Molecular Microbiology* 85 (6): 1029–1043.

Kaplan, H.B. and Greenberg, E.P. 1985. Diffusion of autoinducer is involved in regulation of the *Vibrio fischeri* luminescence system. *J. Bacteriol.* 163 (3): 1210–1214.

Kaspar, H., Dettmer, K., Gronwald, W. and Oefner, P.J. 2008. Automated GC–MS analysis of free amino acids in biological fluids. *Journal of Chromatography B* 870 (2): 222–232.

Kay, E., Humair, B., Denervaud, V., Riedel, K., Spahr, S., Eberl, L., Valverde, C. and Haas, D. 2006. Two gaca-dependent small rnas modulate the quorum-sensing response in *Pseudomonas aeruginosa*. *J. Bacteriol.* 188 (16): 6026–6033.

Kell, D.B., Brown, M., Davey, H.M., Dunn, W.B., Spasic, I. and Oliver, S.G. 2005. Metabolic footprinting and systems biology: the medium is the message. *Nature Reviews. Microbiology* 3 (7): 557–565.

Keweloh, H., Diefenbach, R. and Rehm, H.-J. 1991. Increase of phenol tolerance of *Escherichia coli* by alterations of the fatty acid composition of the membrane lipids. *Archives of Microbiology* 157 (1): 49–53.

Khakimova, M., Ahlgren, H.G., Harrison, J.J., English, A.M. and Nguyen, D. 2013. The stringent response controls catalases in *Pseudomonas aeruginosa* and is required for hydrogen peroxide and antibiotic tolerance. *Journal of Bacteriology* 195 (9): 2011–2020.

Kim, E.-J., Sabra, W. and Zeng, A.-P. 2003. Iron deficiency leads to inhibition of oxygen transfer and enhanced formation of virulence factors in cultures of *Pseudomonas aeruginosa* PAO1. *Microbiology* 149 (9): 2627–2634.

Kim, E.-J., Wang, W., Deckwer, W.-D. and Zeng, A.-P. 2005. Expression of the quorum-sensing regulatory protein LasR is strongly affected by iron and oxygen concentrations in cultures of *Pseudomonas aeruginosa* irrespective of cell density. *Microbiology* 151 (4): 1127–1138.

Klockgether, J., Cramer, N., Wiehlmann, L., Davenport, C.F. and Tümmler, B. 2011. *Pseudomonas aeruginosa* genomic structure and diversity. *Frontiers in Microbiology* 2.

Kulasekara, B.R. and Lory, S. 2004. The genome of *Pseudomonas aeruginosa*. *In*: Ramos, J.-L. (ed.), *Pseudomonas*, 47–75. Springer US.

Kung, V.L., Ozer, E.A. and Hauser, A.R. 2010. The accessory genome of *Pseudomonas aeruginosa*. *Microbiology and Molecular Biology Reviews* 74 (4): 621–641.

Kuroki, M., Igarashi, Y., Ishii, M. and Arai, H. 2014. Fine-tuned regulation of the dissimilatory nitrite reductase gene by oxygen and nitric oxide in *Pseudomonas aeruginosa*. *Environmental Microbiology Reports* 6 (6): 792–801.

Kutchma, A.J., Hoang, T.T. and Schweizer, H.P. 1999. Characterization of a *Pseudomonas aeruginosa* fatty acid biosynthetic gene cluster: purification of acyl carrier protein (ACP) and malonyl-coenzyme A:ACP transacylase (FabD). *J. Bacteriol.* 181 (17): 5498–5504.

Laing, R.B. 1999. Nosocomial infections in patients with HIV disease. *J Hosp Infect* 43 (3): 179–185.

Latifi, A., Foglino, M., Tanaka, K., Williams, P. and Lazdunski, A. 1996. A hierarchical quorum-sensing cascade in *Pseudomonas aeruginosa* links the transcriptional activators LasR and RhIR (VsmR) to expression of the stationary-phase sigma factor RpoS. *Molecular Microbiology* 21 (6): 1137–1146.

Lee, J.-H., Lequette, Y. and Greenberg, E.P. 2006. Activity of purified QscR, a *Pseudomonas aeruginosa* orphan quorum-sensing transcription factor. *Molecular Microbiology* 59 (2): 602–609.

Lee, K.-H. and Ruby, E.G. 1994. Effect of the squid host on the abundance and distribution of symbiotic *Vibrio fischeri* in nature. *Appl. Environ. Microbiol.* 60 (5): 1565–1571.

Lépine, F., Milot, S., Déziel, E., He, J. and Rahme, L.G. 2004. Electrospray/mass spectrometric identification and analysis of 4-hydroxy-2-alkylquinolines (HAQs) produced by *Pseudomonas aeruginosa*. *Journal of the American Society for Mass Spectrometry* 15 (6): 862–869.

Lequette, Y., Lee, J.H., Ledgham, F., Lazdunski, A. and Greenberg, E.P. 2006. A distinct QscR regulon in the *Pseudomonas aeruginosa* quorum-sensing circuit. *J Bacteriol* 188 (9): 3365–3370.

Loewen, P.C., Hu, B., Strutinsky, J. and Sparling, R. 1998. Regulation in the *rpoS* regulon of *Escherichia coli*. *Canadian Journal of Microbiology* 44 (8): 707–717.

Loffhagen, N., Härtig, C., Geyer, W., Voyevoda, M. and Harms, H. 2007. Competition between *cis*, *trans* and cyclopropane fatty acid formation and its impact on membrane fluidity. *Engineering in Life Sciences* 7 (1): 67–74.

Lupp, C. and Ruby, E.G. 2005. *Vibrio fischeri* uses two quorum-sensing systems for the regulation of early and late colonization factors. *J. Bacteriol.* 187 (11): 3620–3629.

Lüthi, E., Baur, H., Gamper, M., Brunner, F., Villeval, D., Mercemier, A. and Haas, D. 1990. The *arc* operon for anaerobic arginine catabolism in *Pseudomonas aeruginosa* contains an additional gene, *arcD*, encoding a membrane protein. *Gene* 87 (1): 37–43.

Ma, J.-F., Hager, P.W., Howell, M.L., Phibbs, P.V. and Hassett, D.J. 1998. Cloning and Characterization of the Pseudomonas aeruginosa zwf Gene Encoding Glucose-6-Phosphate Dehydrogenase, an Enzyme Important in Resistance to Methyl Viologen (Paraquat). *Journal of Bacteriology* 180 (7): 1741–1749.

Mahajan-Miklos, S., Rahme, L.G. and Ausubel, F.M. 2000. Elucidating the molecular mechanisms of bacterial virulence using non-mammalian hosts. *Molecular Microbiology* 37 (5): 981–988.

Maharjan, R.P. and Ferenci, T. 2003. Global metabolite analysis: the influence of extraction methodology on metabolome profiles of Escherichia coli. *Analytical Biochemistry* 313 (1): 145–154.

Mandelstam, J. 1958. The free amino acids in growing and non-growing populations of *Escherichia coli*. *Biochemical Journal* 69 (1): 103–110.

Martínez-Gómez, K., Flores, N., Castañeda, H.M., Martínez-Batallar, G., Hernández-Chávez, G., Ramírez, O.T., Gosset, G., Encarnación, S. and Bolivar, F. 2012. New insights into *Escherichia coli* metabolism: carbon scavenging, acetate metabolism and carbon recycling responses during growth on glycerol. *Microbial Cell Factories* 11: 46.

Marvig, R.L., Søndergaard, M.S.R., Damkiær, S., Høiby, N., Johansen, H.K., Molin, S. and Jelsbak, L. 2012. Mutations in 23S rRNA confer resistance against azithromycin in *Pseudomonas aeruginosa*. *Antimicrobial Agents and Chemotherapy* 56 (8): 4519–4521.

Massa, E.M., Viñals, A.L. and Farías, R.N. 1988. Influence of unsaturated fatty acid membrane component on sensitivity of an *Escherichia coli* fatty acid auxotroph to conditions of nutrient depletion. *Applied and Environmental Microbiology* 54 (8): 2107–2111.

Mellbye, B. and Schuster, M. 2014. Physiological framework for the regulation of quorum sensing-dependent public goods in *Pseudomonas aeruginosa*. *Journal of Bacteriology* 196 (6): 1155–1164.

Mendelson, M.H., Gurtman, A., Szabo, S., Neibart, E., Meyers, B.R., Policar, M., Cheung, T.W., Lillienfeld, D., Hammer, G., Reddy, S. and et al. 1994. *Pseudomonas aeruginosa* bacteremia in patients with AIDS. *Clin Infect Dis* 18 (6): 886–895.

Migula, W. 1900. Pseudomonas aeruginosa (Schröter) Migula. System der Bakterien. Handbuch der Morphologie, Entwicklungsgeschichte und Systematik der Bakterien. Gustav Fischer, Jena: 884–885.

Mikkelsen, H., Duck, Z., Lilley, K.S. and Welch, M. 2007. Interrelationships between colonies, biofilms, and Planktonic cells of *Pseudomonas aeruginosa*. *Journal of bacteriology* 189 (6): 2411–2416.

Miyamoto, S., Kashiwagi, K., Ito, K., Watanabe, S. and Igarashi, K. 1993. Estimation of polyamine distribution and polyamine stimulation of protein synthesis in *Escherichia coli*. *Archives of Biochemistry and Biophysics* 300 (1): 63–68.

Molinari, G., Guzmán, C.A., Pesce, A. and Schito, G.C. 1993. Inhibition of *Pseudomonas aeruginosa* virulence factors by subinhibitory concentrations of azithromycin and other macrolide antibiotics. *Journal of Antimicrobial Chemotherapy* 31 (5): 681–688.

Monson, R., Foulds, I., Foweraker, J., Welch, M. and Salmond, G.P.C. 2011. The *Pseudomonas aeruginosa* generalized transducing phage φPA3 is a new member of the φKZ-like Groupg of 'jumbo' phages, and infects model laboratory strains and clinical isolates from cystic fibrosis patients. *Microbiology (Reading, England)* 157 (3): 859–867.

Montgomery, M.K. and McFall-Ngai, M.J. 1998. Late postembryonic development of the symbiotic light organ of *Euprymna scolopes* (Cephalopoda: Sepiolidae). *Biol Bull* 195 (3): 326–336.

Morrison, W.R. and Smith, L.M. 1964. Preparation of fatty acid methyl esters and dimethylacetals from lipids with boron fluoride–methanol. *Journal of Lipid Research* 5 (4): 600–608.

Muñoz-Rojas, J., Bernal, P., Duque, E., Godoy, P., Segura, A. and Ramos, J.-L. 2006. Involvement of cyclopropane fatty acids in the response of *Pseudomonas putida* KT2440 to freeze-drying. *Applied and Environmental Microbiology* 72 (1): 472–477.

Munson, P. 2001. A 'consistency'test for determining the significance of gene expression changes on replicate samples and two convenient variance-stabilizing transformations. *GeneLogic workshop on low level analysis of Affymetrix GeneChip data*.

Nalca, Y., Jänsch, L., Bredenbruch, F., Geffers, R., Buer, J. and Häussler, S. 2006. Quorum-sensing antagonistic activities of azithromycin in *Pseudomonas aeruginosa* PAO1: a global approach. *Antimicrobial Agents and Chemotherapy* 50 (5): 1680–1688.

Nealson, K.H., Platt, T. and Hastings, J.W. 1970. Cellular control of the synthesis and activity of the bacterial luminescent system. *Journal of Bacteriology* 104 (1): 313–322.

Nikaido, H. 2003. Molecular basis of bacterial outer membrane permeability revisited. *Microbiol. Mol. Biol. Rev.* 67 (4): 593–656.

Nikiforova, V.J., Kopka, J., Tolstikov, V., Fiehn, O., Hopkins, L., Hawkesford, M.J., Hesse, H. and Hoefgen, R. 2005. Systems rebalancing of metabolism in response to sulfur deprivation, as revealed by metabolome analysis of arabidopsis plants. *Plant Physiology* 138 (1): 304–318.

Nouwens, A.S., Beatson, S.A., Whitchurch, C.B., Walsh, B.J., Schweizer, H.P., Mattick, J.S. and Cordwell, S.J. 2003. Proteome analysis of extracellular proteins regulated by the *las* and *rhl* quorum sensing systems in *Pseudomonas aeruginosa* PAO1. *Microbiology (Reading, England)* 149 (5): 1311–1322.

Ochsner, U.A. and Reiser, J. 1995. Autoinducer-mediated regulation of rhamnolipid biosurfactant synthesis in *Pseudomonas aeruginosa*. *Proceedings of the National Academy of Sciences* 92 (14): 6424–6428.

Ochsner, U.A., Koch, A.K., Fiechter, A. and Reiser, J. 1994. Isolation and characterization of a regulatory gene affecting rhamnolipid biosurfactant synthesis in *Pseudomonas aeruginosa*. *Journal of Bacteriology* 176 (7): 2044–2054.

Oldiges, M. and Takors, R. 2005. Applying metabolic profiling techniques for stimulus-response experiments: chances and pitfalls. *Adv Biochem Eng Biotechnol* 92: 173–196.

Oliver, S. 2002. Metabolism: Demand management in cells. *Nature* 418 (6893): 33–34.

Pai, A., Tanouchi, Y. and You, L. 2012. Optimality and robustness in quorum sensing (QS)-mediated regulation of a costly public good enzyme. *Proceedings of the National Academy of Sciences* 109 (48): 19810–19815.

Palleroni, N.J. 2010. The *Pseudomonas* story. *Environmental Microbiology* 12 (6): 1377–1383.

Palmer, G.C., Palmer, K.L., Jorth, P.A. and Whiteley, M. 2010. Characterization of the *Pseudomonas aeruginosa* transcriptional response to phenylalanine and tyrosine. *J. Bacteriol.* 192 (11): 2722–2728.

Palmer, K.L., Aye, L.M. and Whiteley, M. 2007. Nutritional Cues Control *Pseudomonas aeruginosa* Multicellular Behavior in Cystic Fibrosis Sputum. *Journal of Bacteriology* 189 (22): 8079–8087.

Pappas, G., Saplaoura, K. and Falagas, M.E. 2009. Current treatment of Pseudomonal infections in the elderly. *Drugs & Aging* 26 (5): 363–379.

Passador, L., Cook, J.M., Gambello, M.J., Rust, L. and Iglewski, B.H. 1993. Expression of *Pseudomonas aeruginosa* virulence genes requires cell-to-cell communication. *Science* 260 (5111): 1127–1130.

Pears, M.R., Cooper, J.D., Mitchison, H.M., Mortishire-Smith, R.J., Pearce, D.A. and Griffin, J.L. 2005. High resolution ^{1}H NMR-based metabolomics indicates a neurotransmitter cycling deficit in cerebral tissue from a mouse model of Batten Disease. *Journal of Biological Chemistry* 280 (52): 42508–42514.

Pearson, J.P., Pesci, E.C. and Iglewski, B.H. 1997. Roles of *Pseudomonas aeruginosa las* and *rhl* quorum-sensing systems in control of elastase and rhamnolipid biosynthesis genes. *Journal of Bacteriology* 179 (18): 5756–5767.

Pearson, J.P., Passador, L., Iglewski, B.H. and Greenberg, E.P. 1995. A second *N*-acylhomoserine lactone signal produced by *Pseudomonas aeruginosa*. *Proceedings of the National Academy of Sciences* 92 (5): 1490–1494.

Pearson, J.P., Gray, K.M., Passador, L., Tucker, K.D., Eberhard, A., Iglewski, B.H. and Greenberg, E.P. 1994. Structure of the autoinducer required for expression of

Pseudomonas aeruginosa virulence genes. *Proceedings of the National Academy of Sciences* 91 (1): 197–201.

Pesakhov, S., Benisty, R., Sikron, N., Cohen, Z., Gomelsky, P., Khozin-Goldberg, I., Dagan, R. and Porat, N. 2007. Effect of hydrogen peroxide production and the Fenton reaction on membrane composition of *Streptococcus pneumoniae*. *Biochimica Et Biophysica Acta* 1768 (3): 590–597.

Pessi, G., Williams, F., Hindle, Z., Heurlier, K., Holden, M.T.G., Camara, M., Haas, D. and Williams, P. 2001. The global posttranscriptional regulator RsmA modulates production of virulence determinants and *N*-acylhomoserine lactones in *Pseudomonas aeruginosa*. *J. Bacteriol.* 183 (22): 6676–6683.

Pfeiffer, T., Rutte, C., Killingback, T., Taborsky, M. and Bonhoeffer, S. 2005. Evolution of cooperation by generalized reciprocity. *Proceedings of the Royal Society of London B: Biological Sciences* 272 (1568): 1115–1120.

Polack, B., Dacheux, D., Delic-Attree, I., Toussaint, B. and Vignais, P.M. 1996. The *Pseudomonas aeruginosa fumC* and *sodA* genes belong to an iron-responsive operon. *Biochemical and biophysical research communications* 226 (2): 555–560.

Pradenas, G.A., Díaz-Vásquez, W.A., Pérez-Donoso, J.M. and Vásquez, C.C. 2013. Monounsaturated fatty acids are substrates for aldehyde generation in tellurite-exposed *Escherichia coli*. *Biomed Research International* 2013.

Price-Whelan, A., Dietrich, L.E.P. and Newman, D.K. 2007. Pyocyanin Alters Redox Homeostasis and Carbon Flux Through Central Metabolic Pathways in Pseudomonas Aeruginosa PA14. *Journal of Bacteriology* 189 (17): 6372–6381.

R Development Core Team. 2008. *R: A Language and Environment for Statistical Computing*. R Foundation for Statistical Computing, Vienna, Austria, .

Rampioni, G., Schuster, M., Greenberg, E.P., Bertani, I., Grasso, M., Venturi, V., Zennaro, E. and Leoni, L. 2007. RsaL provides quorum sensing homeostasis and functions as a global regulator of gene expression in *Pseudomonas aeruginosa*. *Molecular Microbiology* 66 (6): 1557–1565.

Rampioni, G., Pustelny, C., Fletcher, M.P., Wright, V.J., Bruce, M., Rumbaugh, K.P., Heeb, S., Cámara, M. and Williams, P. 2010. Transcriptomic analysis reveals a global alkyl-quinolone-independent regulatory role for PqsE in facilitating the environmental adaptation of *Pseudomonas aeruginosa* to plant and animal hosts. 12 (6): 1659–1673.

Ramsay, J. 2013. High-throughput β-galactosidase and β-glucuronidase assays using fluorogenic substrates. *Bio-protocol* 3:e827.

Redfield, R.J. 2002. Is quorum sensing a side effect of diffusion sensing? *Trends in Microbiology* 10 (8): 365–370.

Rhee, H.J., Kim, E.-J. and Lee, J.K. 2007. Physiological polyamines: simple primordial stress molecules. *Journal of cellular and molecular medicine* 11 (4): 685–703.

Rocke, D., Lee, G.C., Tillinghast, J., Durbin-Johnson, B. and Wu, S. 2013. LMGene: LMGene Software for Data Transformation and Identification of Differentially Expressed Genes in Gene Expression Arrays. .

Sabra, W., Kim, E.-J. and Zeng, A.-P. 2002. Physiological responses of *Pseudomonas aeruginosa* PAO1 to oxidative stress in controlled microaerobic and aerobic cultures. *Microbiology* 148 (10): 3195–3202.

Sadowski, P.G., Dunkley, T.P., Shadforth, I.P., Dupree, P., Bessant, C., Griffin, J.L. and Lilley, K.S. 2006. Quantitative proteomic approach to study subcellular localization of membrane proteins. *Nature Protocols* 1 (4): 1778–1789.

Salunkhe, P., Smart, C.H., Morgan, J.A., Panagea, S., Walshaw, M.J., Hart, C.A., Geffers, R., Tummler, B. and Winstanley, C. 2005. A cystic fibrosis epidemic strain of *Pseudomonas aeruginosa* displays enhanced virulence and antimicrobial resistance. *J Bacteriol* 187 (14): 4908–4920.

Sandoz, K.M., Mitzimberg, S.M. and Schuster, M. 2007. Social cheating in *Pseudomonas aeruginosa* quorum sensing. *Proceedings of the National Academy of Sciences* 104 (40): 15876–15881.

Schaefer, A.L., Val, D.L., Hanzelka, B.L., Cronan, J.E. and Greenberg, E.P. 1996. Generation of cell-to-cell signals in quorum sensing: acyl homoserine lactone synthase activity of a purified *Vibrio fischeri* LuxI protein. *Proceedings of the National Academy of Sciences of the United States of America* 93 (18): 9505–9509.

Schreiber, K., Boes, N., Eschbach, M., Jaensch, L., Wehland, J., Bjarnsholt, T., Givskov, M., Hentzer, M. and Schobert, M. 2006. Anaerobic survival of *Pseudomonas aeruginosa* by pyruvate fermentation requires an Usp-type stress protein. *Journal of Bacteriology* 188 (2): 659–668.

Schröter. 1872. Ueber einige durch Bakterien gebildete Pigmente. *In*: *Cohn, Beiträge Zur Biologie Der Pflanzen, 1, Heft 2.*, 122–123. Max Muller, Breslau.

Schuster, M. and Peter Greenberg, E. 2006. A network of networks: Quorum-sensing gene regulation in *Pseudomonas aeruginosa*. *International Journal of Medical Microbiology* 296 (2–3): 73–81.

Schuster, M. and Greenberg, E.P. 2007. Early activation of quorum sensing in *Pseudomonas aeruginosa* reveals the architecture of a complex regulon. *BMC Genomics* 8 (1): 287.

Schuster, M., Urbanowski, M.L. and Greenberg, E.P. 2004a. Promoter specificity in *Pseudomonas aeruginosa* quorum sensing revealed by DNA binding of purified LasR. *Proceedings of the National Academy of Sciences of the United States of America* 101 (45): 15833–15839.

Schuster, M., Lostroh, C.P., Ogi, T. and Greenberg, E.P. 2003. Identification, timing, and signal specificity of *Pseudomonas aeruginosa* quorum-controlled genes: a transcriptome analysis. *Journal of Bacteriology* 185 (7): 2066–2079.

Schuster, M., Hawkins, A.C., Harwood, C.S. and Greenberg, E.P. 2004b. The *Pseudomonas aeruginosa* RpoS regulon and its relationship to quorum sensing. *Molecular Microbiology* 51 (4): 973–985.

Scoffield, J.A. and Wu, H. 2016. Nitrite reductase is critical for *Pseudomonas aeruginosa* survival during co-infection with the oral commensal *Streptococcus parasanguinis*. *Microbiology* 162 (Pt 2): 376–383.

Shadforth, I., Xu, W., Crowther, D. and Bessant, C. 2006. GAPP: a fully automated software for the confident identification of human peptides from tandem mass spectra. *Journal of Proteome Research* 5 (10): 2849–2852.

Shadforth, I.P., Dunkley, T.P., Lilley, K.S. and Bessant, C. 2005. i-Tracker: For quantitative proteomics using iTRAQ™. *BMC Genomics* 6: 145.

Sikkema, J., Bont, J.A. de and Poolman, B. 1995. Mechanisms of membrane toxicity of hydrocarbons. *Microbiological Reviews* 59 (2): 201–222.

Silvius, J.R. and McElhaney, R.N. 1979. Effects of phospholipid acylchain structure on thermotropic phase properties. 2: Phosphatidylcholines with unsaturated or cyclopropane acyl chains. *Chemistry and Physics of Lipids* 25 (2): 125–134.

Smith, R.S. and Iglewski, B.H. 2003. *P. aeruginosa* quorum-sensing systems and virulence. *Current Opinion in Microbiology* 6 (1): 56–60.

Soberón-Chávez, G., Lépine, F. and Déziel, E. 2005. Production of rhamnolipids by *Pseudomonas aeruginosa*. *Applied Microbiology and Biotechnology* 68 (6): 718–725.

Son, M.S., Jr, W.J.M., Kang, Y., Nguyen, D.T. and Hoang, T.T. 2007. In vivo evidence of *Pseudomonas aeruginosa* nutrient acquisition and pathogenesis in the lungs of Cystic Fibrosis patients. *Infection and Immunity* 75 (11): 5313–5324.

Storey, J.D. 2002. A Direct Approach to False Discovery Rates. *Journal of the Royal Statistical Society. Series B (Statistical Methodology)* 64 (3): 479–498.

Storey, J.D., Taylor, J.E. and Siegmund, D. 2004. Strong control, conservative point estimation and simultaneous conservative consistency of false discovery rates: a unified approach. *Journal of the Royal Statistical Society: Series B (Statistical Methodology)* 66 (1): 187–205.

Storey, J.D., Bass, A.J., Dabney, A. and Robinson, D. 2015. qvalue: Q-value estimation for false discovery rate control. R package version 2.6.0. .

Stover, C.K., Pham, X.Q., Erwin, A.L., Mizoguchi, S.D., Warrener, P., Hickey, M.J., Brinkman, F.S.L., Hufnagle, W.O., Kowalik, D.J., Lagrou, M., Garber, R.L., Goltry, L., Tolentino, E., Westbrock-Wadman, S., Yuan, Y., Brody, L.L., Coulter, S.N., Folger, K.R., Kas, A., Larbig, K., Lim, R., Smith, K., Spencer, D., Wong, G.K.-S., Wu, Z., Paulsen, I.T., Reizer, J., Saier, M.H., Hancock, R.E.W., Lory, S. and Olson, M.V. 2000. Complete genome sequence of *Pseudomonas aeruginosa* PAO1, an opportunistic pathogen. *Nature* 406 (6799): 959–964.

Su, S., Panmanee, W., Wilson, J.J., Mahtani, H.K., Li, Q., VanderWielen, B.D., Makris, T.M., Rogers, M., McDaniel, C., Lipscomb, J.D., Irvin, R.T., Schurr, M.J., Jr, J.R.L., Kovall, R.A. and Hassett, D.J. 2014. Catalase (KatA) plays a role in protection against anaerobic nitric oxide in *Pseudomonas aeruginosa*. *PLOS ONE* 9 (3): e91813.

Suh, S.J., Silo-Suh, L., Woods, D.E., Hassett, D.J., West, S.E. and Ohman, D.E. 1999. Effect of *rpoS* mutation on the stress response and expression of virulence factors in *Pseudomonas aeruginosa*. *Journal of Bacteriology* 181 (13): 3890–3897.

Swatton, J.E., Davenport, P.W., Maunders, E.A., Griffin, J.L., Lilley, K.S. and Welch, M. 2016. Impact of azithromycin on the quorum sensing-controlled proteome of *Pseudomonas aeruginosa*. *PLOS ONE* 11 (1): e0147698.

Swift, S., Karlyshev, A.V., Fish, L., Durant, E.L., Winson, M.K., Chhabra, S.R., Williams, P., Macintyre, S. and Stewart, G.S. 1997. Quorum sensing in *Aeromonas hydrophila* and *Aeromonas salmonicida*: identification of the LuxRI homologs AhyRI and AsaRI and their cognate *N*-acylhomoserine lactone signal molecules. *Journal of Bacteriology* 179 (17): 5271–5281.

Szalewska-Palasz, A., Johansson, L.U.M., Bernardo, L.M.D., Skärfstad, E., Stec, E., Brännström, K. and Shingler, V. 2007. Properties of RNA polymerase bypass mutants: Implications for the role of ppGpp and its co-factor DksA in controlling transcription dependent on σ54. *Journal of Biological Chemistry* 282 (25): 18046–18056.

Tateda, K., Comte, R., Pechere, J.-C., Köhler, T., Yamaguchi, K. and Delden, C.V. 2001. Azithromycin inhibits quorum sensing in *Pseudomonas aeruginosa*. *Antimicrobial Agents and Chemotherapy* 45 (6): 1930–1933.

Tempest, D.W., Meers, J.L. and Brown, C.M. 1970. Influence of environment on the content and composition of microbial free amino acid pools. *J Gen Microbiol* 64 (2): 171–185.

Toder, D.S., Gambello, M.J. and Iglewski, B.H. 1991. *Pseudomonas aeruginosa* LasA: a second elastase under the transcriptional control of *lasR*. *Molecular Microbiology* 5 (8): 2003–2010.

Trunk, K., Benkert, B., Quäck, N., Münch, R., Scheer, M., Garbe, J., Jänsch, L., Trost, M., Wehland, J., Buer, J., Jahn, M., Schobert, M. and Jahn, D. 2010. Anaerobic adaptation in *Pseudomonas aeruginosa*: definition of the Anr and Dnr regulons. *Environmental Microbiology* 12 (6): 1719–1733.

Tsai, W.C., Hershenson, M.B., Zhou, Y. and Sajjan, U. 2009. Azithromycin increases survival and reduces lung inflammation in cystic fibrosis mice. *Inflammation Research* 58 (8): 491–501.

Turner, K.H., Everett, J., Trivedi, U., Rumbaugh, K.P. and Whiteley, M. 2014. Requirements for Pseudomonas aeruginosa Acute Burn and Chronic Surgical Wound Infection. *PLoS Genetics* 10 (7): e1004518.

Ubhi, B.K., Davenport, P.W., Welch, M., Riley, J., Griffin, J.L. and Connor, S.C. 2013. Analysis of chloroformate-derivatised amino acids, dipeptides and polyamines by LC–MS/MS. *Journal of Chromatography B* 934: 79–88.

Val, D.L. and Cronan, J.E. 1998. In vivo evidence that *S*-adenosylmethionine and fatty acid synthesis intermediates are the substrates for the LuxI family of autoinducer synthases. *J. Bacteriol.* 180 (10): 2644–2651.

Van Delden, C., Comte, R. and Bally, A.M. 2001. Stringent response activates quorum sensing and modulates cell density-dependent gene expression in *Pseudomonas aeruginosa*. *Journal of Bacteriology* 183 (18): 5376–5384.

Viducic, D., Ono, T., Murakami, K., Katakami, M., Susilowati, H. and Miyake, Y. 2007. *rpoN* gene of *Pseudomonas aeruginosa* alters its susceptibility to quinolones and carbapenems. *Antimicrobial Agents and Chemotherapy* 51 (4): 1455–1462.

Vinckx, T., Wei, Q., Matthijs, S., Noben, J.-P., Daniels, R. and Cornelis, P. 2011. A proteome analysis of the response of a *Pseudomonas aeruginosa oxyR* mutant to iron limitation. *BioMetals* 24 (3): 523–532.

Vitrac, H., Bogdanov, M. and Dowhan, W. 2013. Proper fatty acid composition rather than an ionizable lipid amine is required for full transport function of lactose permease from *Escherichia coli*. *Journal of Biological Chemistry* 288 (8): 5873–5885.

Wagner, V.E., Bushnell, D., Passador, L., Brooks, A.I. and Iglewski, B.H. 2003. Microarray analysis of *Pseudomonas aeruginosa* quorum-sensing regulons: effects of growth phase and environment. *Journal of Bacteriology* 185 (7): 2080–2095.

Wang, A.-Y. and Cronan, J.E. 1994. The growth phase-dependent synthesis of cyclopropane fatty acids in *Escherichia coli* is the result of an RpoS(KatF)-dependent promoter plus enzyme instability. *Molecular Microbiology* 11 (6): 1009–1017.

Wang, J., Huang, Z.-H., Gage, D.A. and Watson, J.T. 1994. Analysis of amino acids by gas chromatography—flame ionization detection and gas chromatography—mass spectrometry: Simultaneous derivatization of functional groups by an aqueous-phase chloroformate-mediated reaction. *Journal of Chromatography A* 663 (1): 71–78.

Waters, C.M. and Bassler, B.L. 2005. Quorum sensing: cell-to-cell communication in bacteria. *Annual Review of Cell and Developmental Biology* 21 (1): 319–346.

Weiner, L.M., Webb, A.K., Limbago, B., Dudeck, M.A., Patel, J., Kallen, A.J., Edwards, J.R. and Sievert, D.M. 2016. Antimicrobial-resistant pathogens associated with healthcare-associated infections: summary of data reported to the national healthcare safety network at the centers for disease control and prevention, 2011–2014. *Infection Control & Hospital Epidemiology* 37 (11): 1288–1301.

Welch, B.L. 1947. The Generalization of 'Student's' Problem When Several Different Population Varlances Are Involved. *Biometrika* 34 (1–2): 28–35.

West, S.A., Winzer, K., Gardner, A. and Diggle, S.P. 2012. Quorum sensing and the confusion about diffusion. *Trends in Microbiology* 20 (12): 586–594.

Whiteley, M. and Greenberg, E.P. 2001. Promoter specificity elements in *Pseudomonas aeruginosa* quorum-sensing-controlled genes. *J. Bacteriol.* 183 (19): 5529–5534.

Whiteley, M., Parsek, M.R. and Greenberg, E.P. 2000. Regulation of quorum sensing by RpoS in *Pseudomonas aeruginosa*. *J. Bacteriol.* 182 (15): 4356–4360.

Winson, M.K., Swift, S., Fish, L., Throup, J.P., Jørgensen, F., Chhabra, S.R., Bycroft, B.W., Williams, P. and Stewart, G.S.A.B. 1998. Construction and analysis of *luxCDABE*-based plasmid sensors for investigating *N*-acyl homoserine lactone-mediated quorum sensing. *FEMS Microbiology Letters* 163 (2): 185–192.

Winson, M.K., Camara, M., Latifi, A., Foglino, M., Chhabra, S.R., Daykin, M., Bally, M., Chapon, V., Salmond, G.P. and Bycroft, B.W. 1995. Multiple *N*-acyl-L-homoserine lactone signal molecules regulate production of virulence determinants and secondary metabolites in *Pseudomonas aeruginosa*. *Proceedings of the National Academy of Sciences of the United States of America* 92 (20): 9427–9431.

Winsor, G.L., Van Rossum, T., Lo, R., Khaira, B., Whiteside, M.D., Hancock, R.E.W. and Brinkman, F.S.L. 2009. *Pseudomonas* Genome Database: facilitating user-friendly, comprehensive comparisons of microbial genomes. *Nucleic Acids Research* 37 (suppl_1): D483–D488.

Wolfe, A.J. 2005. The acetate switch. *Microbiology and Molecular Biology Reviews* 69 (1): 12–50.

Wolfgang, M.C., Kulasekara, B.R., Liang, X., Boyd, D., Wu, K., Yang, Q., Miyada, C.G. and Lory, S. 2003. Conservation of genome content and virulence determinants among clinical and environmental isolates of *Pseudomonas aeruginosa*. *Proc Natl Acad Sci U S A* 100 (14): 8484–8489.

Xavier, J.B., Kim, W. and Foster, K.R. 2011. A molecular mechanism that stabilizes cooperative secretions in *Pseudomonas aeruginosa*. *Molecular microbiology* 79 (1): 166–179.

Yao, J. and Rock, C.O. 2013. Phosphatidic acid synthesis in bacteria. *Biochimica et biophysica acta* 1831 (3): 495–502.

Yates, E.A., Philipp, B., Buckley, C., Atkinson, S., Chhabra, S.R., Sockett, R.E., Goldner, M., Dessaux, Y., Cámara, M., Smith, H. and Williams, P. 2002. *N*-Acylhomoserine Lactones Undergo Lactonolysis in a pH-, Temperature-, and Acyl Chain Length-Dependent Manner during Growth of *Yersinia pseudotuberculosis* and *Pseudomonas aeruginosa*. *Infection and Immunity* 70 (10): 5635–5646.

Yoshida, M., Kashiwagi, K., Shigemasa, A., Taniguchi, S., Yamamoto, K., Makinoshima, H., Ishihama, A. and Igarashi, K. 2004. A unifying model for the role of polyamines in bacterial cell growth, the polyamine modulon. *The journal of biological chemistry* 279 (44): 46008–46013.

Yuan, Y., Sachdeva, M., Leeds, J.A. and Meredith, T.C. 2012. Fatty acid biosynthesis in *Pseudomonas aeruginosa* is initiated by the FabY class of β-ketoacyl acyl carrier protein synthases. *Journal of Bacteriology* 194 (19): 5171–5184.

Zhang, Y. and Cronan, J.E. 1998. Transcriptional analysis of essential genes of the *Escherichia coli* fatty acid biosynthesis gene cluster by functional replacement with the analogous *Salmonella typhimurium* gene cluster. *Journal of Bacteriology* 180 (13): 3295–3303.

Zhu, K., Choi, K.-H., Schweizer, H.P., Rock, C.O. and Zhang, Y.-M. 2006. Two aerobic pathways for the formation of unsaturated fatty acids in *Pseudomonas aeruginosa*. *Molecular Microbiology* 60 (2): 260–273.

Zumft, W.G. 1997. Cell biology and molecular basis of denitrification. *Microbiology and Molecular Biology Reviews* 61 (4): 533–616.